WESTERN SYDNEY
UNIVERSITY

Hawkesbury Institute
for the Environment

Non-invasive imaging of drought-induced cavitation in plants

By

Alice Gauthey (BSc, MSc)

A thesis submitted in fulfilment of requirements for the award of the degree of Doctor of Philosophy

Hawkesbury Institute for the Environment

Western Sydney University

March 2021

Acknowledgements

First, I would like to thank my principal supervisor Brendan Choat for being so available through the completion of this work, for not minding me dropping by unannounced to your office and for the fascinating work discussions. I would also like to thank my co-supervisors David Tissue and Belinda Medlyn, thank you for your permanent good mood, your kind words and for helping me think outside the box.

I was lucky to be hosted and collaborate with Tim Brodribb, Lucas Cernusak, Damien Maher, Sylvain Delzon, Jordi Martinez-Vilalta and Maurizo Mencuccini. Thank you all for the great opportunities to share my work with you.

I would like to thank my colleagues Jen Peters, Ximeng Li and Leah Koladin that provided amazing guidance, Diana Backes, Jeff Balland, Russell Alam and Anthea Challis for the fieldwork help and all the great conversations during those long drives, my M14 team, Coline Deveautour, Elisa Stefaniak, Julia Ryland, Desi Quintans, Chathurika Daulagala and Kate Fuller (last both absolutely incredible housemates too), Victoria Perez Martinez and Scott Nacko for the support and the fun lunch breaks, and my colleague and friend Adriano Losso who helped me survive this Covid-crazy last year. I would also like to thank my friends from back home, for their constant care and support, you made being away from home bearable.

I want to express my gratitude for the technical assistance of Burhan Amiji, Craig Barton, Gavin McKenzie and Marcus Klein and the administrative support of David Harland, Patricia Hellier, Jenny Harvey and Lisa Davison, thank you for sorting out all my last-minute TEMS requests.

Last but not least, I would like to dedicate this thesis to my family, for always encouraging me, from the other side of the world and to Alex, I cannot thank you enough for your love, your endless ‘joie de vivre’ and your unconditional support.

Statement of authentication

The work presented in this thesis is, to the best of my knowledge and belief, original except as acknowledged in the text. I hereby declare that I have not submitted this material, either in full or in part, for a degree at this or any other institution.

.....

Table of contents

Acknowledgements ..... **i**

Statement of authentication ..... **ii**

Table of contents ..... **iii**

List of figures ..... **v**

List of tables ..... **vii**

List of abbreviations ..... **viii**

Abstract ..... **ix**

Chapter 1: General introduction **1**

1.1. Literature review 1

1.2. Research objectives 9

1.3. References 12

Chapter 2: Visual and hydraulic techniques produce similar estimates of cavitation resistance in woody species **22**

2.1. Abstract 22

2.2. Introduction 23

2.3. Materials and methods 27

2.4. Results 37

2.5. Discussion 45

2.6. Conclusions 49

2.7. Supplementary figures 51

2.8. References 54

Chapter 3: Absence of embolism repair after long-term drought recovery observed with micro-computed tomography in *Eucalyptus saligna* **60**

3.1. Abstract 60

3.2. Introduction 61

3.3. Materials and methods 64

3.4. Results 70

3.5. Discussion 77

3.6. Conclusions 82

3.7. Supplementary figures 83

3.8. References 85

Chapter 4: The role of hydraulic failure in a massive mangrove die off event **91**

4.1. Abstract 91

4.2. Introduction 92

4.3. Materials and methods 95

4.4. Results 100

4.5. Discussion 103

4.6. References 109

Chapter 5: Summary and synthesis **114**

5.1. Synthesis of experimental chapters 115

5.2. Conclusion and future directions 121

5.3. References 125

List of figures

Chapter 2

Fig. 2-1 Visualization of embolism in stems of *Wisteria brachybotrys* during dehydration by microcomputed tomography (microCT) and the optical vulnerability (OV) technique. **38**

Fig. 2-2 Vulnerability curves for three diffuse porous angiosperm species produced using visual and hydraulic techniques. **40**

Fig. 2-3 Vulnerability curves for three diffuse porous angiosperm species produced using visual and hydraulic techniques. **41**

Fig. 2-4 Vulnerability curves for one ring porous and one liana angiosperm species produced using visual and hydraulic techniques. **42**

Fig. 2-5 Vulnerability curves for two conifer species produced using visual and hydraulic techniques. **43**

Fig. 2-6 Correlations between P50 values obtained with microcomputed tomography (CT), optical vulnerability (OV) and hydraulic methods (HM) across seven species. **44**

Figure S2-1 Example of stem reconstruction for four species with different xylem anatomy using the software DRISHTI **51**

Figure S2-2 Relationship between the bagged leaf water potential measured using a Scholander chamber and the stem water potential measured using a psychrometer across three species with different xylem anatomy. **51**

Figure S2- 1 Transverse surfaces of *Cedrus deodara* visualized by SEM and X-ray microCT. **52**

Figure S2- 2 Transverse slices produced with the OV technique for *Acacia aneura.* **52**

Figure S2- 5 P50 with CIs for the three different techniques and across seven species. **53**

Chapter 3

Figure 3- 1 Mean water potential (-MPa) and transpiration rate per plant (g h-1) according to the treatment and the time of measurement. **71**

Figure 3- 2 Mean percentage loss of vessels (PLV) at different time points during two treatments. **72**

Figure 3- 3 Micro-CT scans of *Eucalyptus saligna* at different times during dry down and recovery. **73**

Figure 3- 4 Micro-CT scan of *Eucalyptus saligna* after 6 months recovery from severe drought stress. **74**

Figure 3- 5 MicroCT scans along the plant axis of an individual after 6 months of recovery. In this individual, the upper stem died after severe drought and a new shoot was regrown after rewatering. **76**

Figure 3- 6 Percentage loss of vessels as a function of (stem water potential) at different time points. **77**

Figure S3-7 Description of the experimental timeline of the watering treatments throughout the different stages of the experiment. **83**

Figure 3- 8 Transpiration rate on leaf area basis (mmol m-2 s1) at different timepoints during medium drought and severe drought. **84**

Chapter 4

Figure 4-1 Map showing the field site in Queensland (A) and a detail of transects and sampling sites (B). **96**

Figure 4- 2 Effect of the degree of impact (MI minimal impact, II intermediate impact and SI severe impact) on water potential (-MPa) (A) and percentage of loss of conductivity (B). **100**

Figure 4- 3 Vulnerability curve (VC) from *Avicennia marina* trees sampled on the sites of minimal impact **101**

Figure 4- 4 Native embolism measurements with percentage of loss of conductivity in function of the water potential in branches sampled in sites of different impact. **102**

Chapter 5

Figure 5- 1 Conceptual framework of the thesis highlighting the dynamics of xylem embolism during a cycle of drought and recovery **115**

List of tables

Chapter 2

Table S2-1 P_{50} (in bold characters) with confidence intervals for the three different techniques and across seven species. **53**

List of abbreviations

BD	Bench dehydration
CA	Cavitron
ENSO	El-Niño Southern Oscillation
K (kg m^{-1} s^{-1} MPa^{-1})	Stem specific conductivity
MD	Medium drought
Micro CT	Micro-computated tomography
NSW	New South Wales
OV	Optical vulnerability technique
PLC (%)	Percentage of loss of conductivity
QLD	Queensland
$\mathbf{R_x}$	Recovery x time after rewatering
SD	Severe drought
VC(s)	Vulnerability curve(s)
WP (-MPa)	Water potential
WW	Well-water
Ψ	Stem water potential
Ψ_{12}	Ψ causing 12% of loss of conductivity in the xylem
Ψ_{50}	Ψ causing 50% of loss of conductivity in the xylem
Ψ_{88}	Ψ causing 88% of loss of conductivity in the xylem

Abstract

The increased frequency of extreme events, associated with climate change, can lead to loss of biodiversity and forest dieback. Intense drought has disastrous effects on plants growth and physiology and maintaining hydraulic conductivity during time of water stress is necessary for plants survival. However, during drought, the blockage of the hydraulic pathway by air-seeding results in the loss of conductivity by embolism formation. Therefore, it is essential to be able to accurately measure the conductivity, leading to a better prediction of species vulnerability through vulnerability curves (VCs). The measure of vulnerability thresholds is necessary in order to evaluate the causes of forests dieback. Moreover, understanding the mechanisms behind drought-recovery and embolism repair can contribute to the advance of models used to predict the impact of drought on vegetation dynamics. This PhD was designed to test the accuracy and applicability of new visual techniques and aim to provide alternatives to invasive methods for measure of VCs.

While invasive techniques measure conductivity on cut samples, visual techniques allow for measurements on intact samples. However, the question of the accuracy of visual methods are still discussed on the ground that they do not provide a direct measurement of conductivity (PLC) but instead use a proxy through the measurements of loss of vessels (PLV). In the first experimental chapter (chapter 2), we build vulnerability curves for 7 species with different xylem anatomy (diffuse-porous, ring-porous, liana and conifer) using two visual techniques (micro-computated tomography -microCT- and the optical vulnerability -OV- technique) and one invasive technique (bench dehydration or centrifuge-flow technique). Through the comparison of their Ψ_{50} (i.e. water potential at which the plant loses of 50% of conductivity) and their vulnerability curves, the methods were found to be non-significant from one another. In addition, a strong relationship between PLC and PLV was obtained. These results provided

further confirmation for the validation of visual techniques and aimed to valorise these methods as they can present interesting insight in the visualisation of embolism dynamics.

Following the validation of visual methods, microCT was used to investigate drought recovery in *Eucalyptus saligna*. Embolism repair via refilling (i.e. refill of gas-filled vessels) has been proposed as a possible mechanism to restore hydraulic conductivity after water-stress. However, this mechanism may be impossible while plants are still under tension due to thermodynamics constraints. In the second experimental chapter (chapter 3), *E. saligna* was submitted to a cycle of drought of different intensity (mild and severe) and recovery during which transpiration rate (E), water potential (Ψ_x) and PLV were monitored. Both droughts led to an increase in PLV, with severe drought driving a higher PLV than mild drought. During long-term recovery (1 to 3 weeks after rewatering), PLV was observed the be higher than at the peak of drought. Embolism repair via refilling was not observed in either treatments but, after 6 months of recovery, growth of new vessels was found to be the main mechanism allowing the restoration of conductivity through the xylem. This study provided further evidence that refilling may not be a common mechanism for drought recovery in plants. Furthermore, these results showed that lagged mortality in forests may be the result of an intense drought, emerging from a fragility of the xylem resistance by embolism accumulation.

While controlled experimental works are necessary for the understanding of specific mechanisms, the study of natural events is often complicated as multiple uncontrolled factors are present. In the third experimental chapter (chapter 4), we investigated a natural dieback event that occurred during the summer 2015/2016 and led to the mortality of 7400 ha of mangrove vegetation in the Gulf of Carpentaria (Queensland). This event was suspected to be the result of an intense ENSO (El-Niño Southern Oscillation) event that generated a drop in sea level, high temperatures and low precipitation rates in northern Australia. On this coastline, a natural gradient of impact (severely impacted on the saltpan, minimally impacted close to the

sea) provided a good platform to study the causes of this mortality. For this study, we used another visual technique, the OV technique, that provides a portable and effective alternative to other methods for field-based studies. We measured native embolism along this gradient in the dominant mangrove species, *Avicennia marina* and we generated a vulnerability curve for this species to test its vulnerability to drought-induced embolism. The results of this study showed that trees growing on the saltpan experienced very high water stress that led to a high proportion of embolised vessels in their xylem, compared to trees growing on the edge of the water where native embolism values were very low and were associated with high predawn water potentials. Even though this species exhibited a low P50 (-9.6MPa), mangroves growing on the saltpan experienced predawn water potentials that were able to generate up to 12% of embolism. This study showed that, as a result of intense drought, hydraulic failure, in combination with other factors, was responsible for this massive dieback event.

In conclusion, my PhD research addresses the use of visual techniques as an accurate alternative for invasive methods and aims to provide further knowledge concerning mechanisms that regulates drought-induced embolism and recovery, under controlled conditions as well as in field-based studies. The results of this research suggest that (1) visual techniques may be used with all xylem anatomy, but need precise implementation in order to avoid erroneous results, (2) embolism repair via refilling is not a common for *E. saligna* and severe drought may be responsible for lagged-mortality also observed in the field and that (3) hydraulic failure driven by drought-induced embolism was one of the factors that contributed to the massive dieback of *A. marina* in northern Australia. Overall, drought-induced embolism may lead to forest mortality and lagged-mortality in many ecosystems, and the understanding of species-dependant embolism recovery responses is necessary to determine species resistance and resilience to extreme events and climate change.

Chapter 1: General introduction

1.1. Literature review

Forest mortality

Trees are incredible organisms that provide the main pathway of water movement from soil to atmosphere (Meinzer *et al.*, 2001). Each year forests store approximately 30% of the global carbon and redistribute almost 40% of the rainfall to the environment (Canadell & Raupach, 2008; Ent *et al.*, 2010; Schlesinger & Jasechko, 2014; Ellison *et al.*, 2017; Pugh *et al.*, 2019). Unfortunately, these delicate cycles are perturbed by human activities and are part of a feedback system that strongly influences global climate change (Saxe *et al.*, 2001; Curtis *et al.*, 2018). As climate change is predicted to increase the severity and frequency of extreme natural events (Cook *et al.*, 2018; Mukherjee *et al.*, 2018; Madakumbura *et al.*, 2020), drought-induced mortality has been observed more frequently in the past few decades, leading to massive forest dieback (e.g. in Australia, Duke *et al.*, 2017, Nolan *et al.*, 2021; in California, Fettig *et al.*, 2019; in Canada, Michaelian *et al.*, 2011; in Europe, Senf *et al.*, 2020) and ecosystem shifts (Allen & Breshears, 1998; Mueller *et al.*, 2005; Martínez-Vilalta & Lloret, 2016; Liu *et al.*, 2018). A striking example of this process is the increased occurrence of the extreme climatic ENSO events (El-Niño Southern Oscillation) (Wang *et al.*, 2019), with local shifts induced by ENSO driving reductions in forest biomass (Rolim *et al.*, 2005; Riascos *et al.*, 2018). ENSO coincides with periods of low sea level in the Indo-Pacific region and vulnerable coastal ecosystems, such as mangrove forests and wetlands, are directly impacted by these changes (Drexler & Ewel, 2001; Duke *et al.*, 2017; Lovelock *et al.*, 2017).

Drought-induced mortality can be explained by three main non-exclusive mechanisms: (1) carbon starvation, (2) hydraulic failure and (3) biotic attack (McDowell *et al.*, 2008; Adams *et al.*, 2017). Although carbon starvation and hydraulic failure are believed to be intertwined mechanisms responsible of tree dieback during drought (Yoshimura *et al.*, 2016; Tomasella *et al.*, 2017; Kono *et al.*, 2019; Savi *et al.*, 2020), recent studies have minimized the importance of carbon starvation in drought-induced mortality (Camisón *et al.*, 2020; Arend *et al.*, 2021). The loss of hydraulic efficiency during drought is considered to be the main mechanism that lead to widespread forest mortality while carbon status is more often associated with recovery from drought (Trifilò *et al.*, 2017; Savi *et al.*, 2020). Carbon pools are used during recovery to repair embolised conduits (refilling or regrowth, see chapter 3) but might be depleted during drought, thus accelerating mortality and reducing recovery rates.

The carbon starvation mechanism advances as water-stress progresses, signals associated with leaf cell turgor loss and soil drying cause plants to close their stomata to reduce water loss through the leaves (Rodriguez-Dominguez *et al.*, 2016). Consequently, access to atmospheric carbon dioxide is restricted, and plants must survive the drought by relying primarily on their internal carbon storage (Breshears *et al.*, 2009; Adams *et al.*, 2013). In more anisohydric species (i.e. species maintaining high photosynthetic rates during water stress), photosynthetic carbon gain is often favoured over regulation of water loss and could accelerate hydraulic failure during drought (Kumagai & Porporato, 2012; Li *et al.*, 2020b). While stomata remain open, the tension in the water column increases proportionally to the intensity of drought, thus increasing the chances of the rupture of the water column by cavitation (Barigah *et al.*, 2013; Rowland *et al.*, 2015). Although it is important to mention that most species will regulate their stomata so minimal embolism is formed in the xylem. These two mechanisms (i.e. carbon starvation and hydraulic failure) can occur simultaneously and are interdependent to a large degree (Sevanto *et al.*, 2014; Trifilò *et al.*, 2017; Kono *et al.*, 2019). The third hypothesis is biotic attack by

insects and pathogens. However, in most cases, biotic attacks become more likely to cause mortality when trees are already stressed (Anderegg *et al.*, 2015; Das *et al.*, 2016). In this thesis, I will focus on drought-induced mortality by hydraulic failure.

Drought and cohesion-tension theory

Drought is a major limitation for plant growth as water is required for photosynthesis, nutrient uptake, temperature regulation and other metabolic processes. In higher plants, the cohesion-tension theory proposes that water is transported from the roots to the shoots through the conductive tissue (i.e. xylem) following a pressure gradient (Dixon & Joly, 1894). Because the pressure is usually quite high in the soil (~0MPa) and low in the atmosphere is (~-100MPa), it creates a natural gradient by which water can be "pulled up" even through the tallest trees. The energy required to transport water up the plant against gravitational gradient is supplied by the sun and surrounding air; as water evaporates from the interior of leaves, a negative pressure develops behind air-water menisci in the pores of leaf cell walls. Because the osmotic potential (Ψs, -MPa) is very low in xylem sap, the pressure potential (Ψp, -MPa), physically equivalent to a tension, is comparable to xylem water potential (Ψx= Ψp+ Ψs, -MPa). This continuous water-flow through the plant is known as the soil-plant-atmosphere continuum (SPAC) (Sperry *et al.*, 2003; Zimmermann *et al.*, 2004).

However, this mechanism comes with a cost. To be able to undergo such pressures without turning into gas, water has to be in a metastable state. Water must remain liquid at sub-atmospheric pressures below its vapor pressure (Tyree & Sperry, 1989). This phenomenon is possible because of the strong bonding between water molecules and the lack of suitable nucleation sites within the xylem conduits. As long as the intermolecular force holds, the negative pressures allows the liquid sap to be pulled to the leaves through the water column

(Domec, 2011; Denny, 2012). Thus, as drought intensifies, the tension in the xylem increases, eventually leading to the formation of gas bubbles (i.e. emboli) inside the vessels and/or tracheids. Embolism can spread through the conductive system, leading to the obstruction of the water transport and a decline in xylem hydraulic conductivity (Tyree & Sperry, 1989; Sperry & Tyree, 1990). The spread of emboli through the xylem is thought to occur by a process known as "air-seeding", in which air enters the vessels and/or tracheids from neighbouring xylem elements via bordered pits (Jarbeau *et al.*, 1995; Zimmermann, 2013). Increasing amounts of embolism in the xylem is associated with declining rates of photosynthesis (Hubbard *et al.*, 2001; Nardini *et al.*, 2001; Cochard *et al.*, 2002; Ennajeh *et al.*, 2008), branch and leaf shedding (Rood *et al.*, 2000; Li *et al.*, 2018; Cardoso *et al.*, 2020), frost damage (Maruta *et al.*, 2020), gene regulation (Secchi & Zwieniecki, 2011; Secchi *et al.*, 2011),S as well as whole plant mortality (Venturas *et al.*, 2016; Nolan *et al.*, 2021). Hydraulic failure by drought-induced embolism is considered to be one of the primary mechanisms causing tree mortality and forest dieback (Anderegg *et al.*, 2012).

Assessment of hydraulic vulnerability

The measure of the quotient of the flow rate and pressure gradient is called hydraulic conductivity (K_h). Its value is often correlated to xylem and wood traits (Steppe & Lemeur, 2007; Zanne *et al.*, 2010), photosynthetic rates (Santiago *et al.*, 2004), as well as the environment (Atkinson & Taylor, 1996; Brodribb & Feild, 2000; Zach *et al.*, 2010; Lens *et al.*, 2011). The vulnerability of plants to embolism is usually assessed through analysis of vulnerability curves (VCs), which measure the percentage of loss of conductivity (PLC) (i.e. the amount of embolism in the plant) as a function of the water potential. Vulnerability curves follow a sigmoid shape characterised by a slow increase of PLC as the water potential becomes

more negative until a critical threshold value of water potential is reached, after which a steep increase in embolism occurs, leading finally to another slow plateau corresponding to the last phase before plant death (Cochard *et al.*, 2013). Typically, the curves are used to estimate three parameters: (1) Ψ_{12} (i.e. water potential at which 12% of the conductivity is lost) is often associated with stomatal closure, although depending on the species, this point can be closer to Ψ_{50} (Brodribb *et al.*, 2010; Martin-StPaul *et al.*, 2017) or before any embolism occurs (Creek *et al.*, 2020). (2) Ψ_{88} is considered to be the threshold of a plant survival, the point of no-return (Choat *et al.*, 2012; Urli *et al.*, 2013). (3) Ψ_{50} is used to compare vulnerability across species, biomes (Nardini & Luglio, 2014; Anderegg, 2015) or among organs (Nolf *et al.*, 2015; Zhu *et al.*, 2016; Johnson *et al.*, 2016; Rodriguez-Dominguez *et al.*, 2018; Losso *et al.*, 2019). Variation in Ψ_{50} is correlated to climate and precipitation regime where a lower Ψ_{50} corresponds to a higher resistance to drought-induced embolism and can be found in species growing under arid and mesic climates; on the other hand, species in tropical ecosystems usually have a higher Ψ_{50} as the water is not a constraint (Trueba *et al.*, 2017; Oyanoghafo *et al.*, 2020). As studies usually focus on one particular organ (i.e. stem, leaf or roots), it is important to recognise that cavitation resistance may differ between organs within a plant. This idea comes from the hydraulic segmentation hypothesis (Zimmermann, 2013) that proposes that organs representing lower carbon investment (i.e. leaf, branch) will be isolated during drought stress in order to reduce water loss from transpiration and protect proximal organs (i.e. stem, trunk) (Tyree & Ewers, 1991). Although recent studies showed that segmentation seems to be a species-specific trait (Nardini *et al.*, 2001; Li *et al.*, 2020a), it was believed that leaves and stems were more resistant than roots (Sperry & Ikeda, 1997) and petioles were the most vulnerable organ (Tsuda & Tyree, 1997; Hochberg *et al.*, 2016) and would work as “hydraulic fuses” slowing the spread of cavitation through the plant (Nardini & Luglio, 2014).

Methods of assessment

The capacity to accurately measure Ψ_{50} is essential to predict forest mortality. Methods that were originally developed to measure hydraulic conductivity required samples (branches, leaves, roots) to be excised from the plant and increasing the possibility of artefacts related to destructive sampling (Choat *et al.*, 2010; Cochard *et al.*, 2010; Wheeler *et al.*, 2013). As water is transported in a metastable state, disturbance could rupture the hydrogen bonding between water molecules and create embolisms inside the plant. Although cutting a branch or a stem could introduce embolisms and lead to erroneous results, requirements such as cutting and keeping segments under water for 30 min to 1 hour have been established in order to reduce the artificial formation of embolisms (Wheeler *et al.*, 2013; Torres-Ruiz *et al.*, 2017; López *et al.*, 2019).

Among the "destructive" techniques, bench dehydration (Sperry & Tyree, 1988) is the most commonly used. It uses gravitational force to measure conductivity inside a living wood segment. Hydraulic conductivity (K, kg s^{-1} m^{-1} MPa^{-1}) is calculated following equation (1):

$$K = \frac{Q \,.\, l}{A \,.\, \Delta P'} \qquad (1)$$

Where Q, sap flow rate (kg s^{-1}); l, segment length (m); A, xylem cross- sectional area (m^2); and ΔP, pressure drops across a segment of conducting tissue (MPa).

Another common invasive method, the centrifuge technique (Holbrook *et al.*, 1995), was popularised by development of the Cavitron (Cochard, 2002). This method has been shown to be very accurate with tracheid-bearing species (Cochard *et al.*, 2005, 2010), but might be prone to the "open-vessel" artefact in angiosperms leading to an overestimation of vulnerability (López *et al.*, 2019). The principle of this method is to measure the sample conductivity while generating a known water potential using centrifugal force.

Although these methods provide direct evaluation of how embolism reduces xylem hydraulic conductivity, samples need to be cut (with precautions) in order to be measured. In the past decade, new non-destructive imaging methods such as microCT (Cochard *et al.*, 2015) and the optical technique (Brodribb *et al.*, 2016) have been developed and provide a measure of percentage of loss of vessels (PLV) for microCT or percent loss of area (PLA) for OV. Although, PLV and PLC show good agreement (Li *et al.*, 2020a), these techniques are often criticised on the basis that they are not measuring an actual conductivity. This argument rests on the fact that the xylem network is complex, and measures of conductivity need to account for pit membrane resistance, the complexity of conduit connectivity ,as well as the vessels length and diameter, that will not be captured by counts of embolised vessels or of area embolised in cross section (Mrad *et al.*, 2018; Venturas *et al.*, 2019).

Among imaging methods, micro-computated tomography (microCT) and the optical vulnerability techniques have been widely used in the past years. MicroCT was first developed for medical applications and has recently been applied to plant physiology (Pajor *et al.*, 2013; McElrone *et al.*, 2013). The principle of this method is to use X-rays to visualise a three-dimensional volume of a segment of an intact plant. Water-filled and air-filled vessels can be easily differentiated in reconstructed images due to high contrasts between regions of differing density. Through image analysis, PLV can be calculated at each targeted water potential. Although this method assesses PLV, a theoretical PLC can be calculated with the Poiseuille-Hagen law as:

$$K_h = \frac{\pi\rho}{128\eta}\sum_{i-1}^{n}(d_i^4) \quad (2)$$

With η the coefficient of viscosity of water, d the conduit diameter (m) and ρ the density of water.

On the other hand, the optical technique (Brodribb *et al.*, 2016, 2017) does not allow a calculation of PLC. This technique uses differences in transmitted or reflected light between embolised and water-filled conduits to detect embolism when it occurs in a stem, leaf or root. To proceed, a window is gently cut into the bark of the intact sample and the exposed xylem is placed under a camera. As the reflectance is higher in embolised vessels than in water-filled conduits, embolism events can be measured by recording the changes in the transmission of light through the xylem (Brodribb *et al.*, 2016). Through image analysis, these events can be isolated and translated in percent of loss of area (PLA).

While debate exists concerning their accuracy (Venturas *et al.*, 2019; Pratt *et al.*, 2019), these imaging methods have been widely used in the last few years to examine the impact of drought (Cochard *et al.*, 2015; Choat *et al.*, 2016; Hochberg *et al.*, 2016; Brodribb *et al.*, 2017; Losso *et al.*, 2019; Creek *et al.*, 2020) and drought recovery (Lee & Kim, 2008; Brodersen *et al.*, 2010, 2018; Choat *et al.*, 2015) on plant vulnerability and mortality.

Recovery of hydraulic conductance after drought

Recovery of hydraulic conductance following drought is necessary for plant survival. Depending on the drought magnitude (length and intensity), the plant might be severely impacted in terms of loss of hydraulic capacity. So, in order to restore hydraulic conductivity through the xylem, two main strategies have been proposed: (1) growing new xylem tissue (Brodribb *et al.*, 2010) and/or (2) repairing embolised conduits (i.e. refilling) (Tyree & Yang, 1992; Tyree *et al.*, 1999). Refilling appears to be possible in species that are able to create positive pressure within the xylem via the establishment of a strong root pressure, leaf water uptake, low transpiration and/or unlimited water supply (Sperry *et al.*, 1987; Cochard *et al.*, 1994; Hacke & Sauter, 1995; Hao *et al.*, 2013; Mayr *et al.*, 2014; Charrier *et al.*, 2016; Gleason

et al., 2017; Miller, 2020). This mechanism is often reported for winter embolism after freeze-thaw events (Utsumi *et al.*, 1998; Cobb *et al.*, 2007). While this mechanism is well documented under positive pressures (Schenk *et al.*, 2020), refilling under tension goes against the laws of thermodynamics. Despite this paradigm, several studies have reported occurrence of embolism repair under negative pressures in herbaceous species or in trees (Stiller *et al.*, 2005; Nardini *et al.*, 2008; Taneda & Sperry, 2008), although recent studies question still this mechanism. In order to recover from drought, some species might adopt a different strategy such as growing new conduits (vessels and/or tracheids) (Ameglio *et al.*, 2002; Brodribb *et al.*, 2010; Christensen-Dalsgaard & Tyree, 2014). However, this strategy takes longer to be effective and the cost of carbon is likely to be higher.

1.2. Research objectives

The use of non-invasive techniques was a primary objective of this dissertation. After checking for their accuracy, these methods are used to explore hydraulic vulnerability and recovery strategies of different species.

Are new non-invasive methods accurate to measure hydraulic vulnerability?

The main criticism directed towards non-destructive techniques is the absence of direct measurements of hydraulic conductivity (i.e. PLC vs PLV/PLA) (Jacobsen *et al.*, 2015). Since their establishment, many studies have provided evidence to support (Nardini *et al.*, 2017; Nolf *et al.*, 2017; Brodribb *et al.*, 2017; Savi *et al.*, 2017) or evidence against (Venturas *et al.*, 2019; Pratt *et al.*, 2019) the accuracy of non-destructive methods. However, the debate is still ongoing. In chapter 2, we investigate this controversy by comparing the two newer non-destructive

techniques (CT and OV) with the most commonly used invasive one (BD). We hypothesised that different techniques would give similar results and that the VCs would be similar. In order to analyse the VCs, we used Ψ_{50} as an indicator. Xylem anatomy has been found to be a problem implementing some techniques, so we measured seven plant species with different xylem anatomy (Cochard *et al.*, 2005, 2010; Ennajeh *et al.*, 2011).

What happens to the hydraulic pathway after drought? Use of micro computated-tomography in a controlled experiment.

After drought, it is critical for trees that have survived to be able to restore their hydraulic conductivity in order to live. Understanding the processes leading to recovery of the hydraulic pathway is therefore essential. Two main strategies have been discussed in the past few years: (1) embolism repair (i.e. refilling) and/or (2) growth of new xylem. In chapter 3, we use microCT to investigate the strategy used by *Eucalyptus saligna*, a common species growing in the Sydney Basin, to recover after drought. We subjected potted saplings of *E. saligna* to a cycle of mild and severe drought, and subsequent rewatering, and monitored the transpiration rate over ~6 months (few days of drought and 6 months recovery). The same plants were also scanned at regular intervals during dry down and recovery. Following a previous study on the same species (Choat *et al.*, 2019), we hypothesised that refilling might happen if positive pressures were generated through the xylem (i.e. unlimited water availability and limited transpiration rate); otherwise, growing new xylem would be the preferred strategy.

Can intense drought lead to extreme mangroves dieback? Use of the optical technique in the field.

The use of non-destructive techniques was explored in chapters 2 and 3. In chapter 4, we investigated the cause(s) of a massive mangrove dieback in the gulf of Carpentaria, QLD, using the optical technique (OV). This dieback was linked to an strong El-Niño event and represented an important mangrove mortality event due to the magnitude of its spread and its short timeline (Duke *et al.*, 2017). We hypothesised that the environmental conditions at the time of El-Niño (e.g. low sea level, high temperatures) might have been responsible for hydraulic failure in a dominant mangrove species in the gulf, *Avicennia marina,* thus facilitating the intense mortality event.

1.3. References

Adams HD, Germino MJ, Breshears DD, Barron-Gafford GA, Guardiola-Claramonte M, Zou CB, Huxman TE. 2013. Nonstructural leaf carbohydrate dynamics of Pinus edulis during drought-induced tree mortality reveal role for carbon metabolism in mortality mechanism. *New Phytologist* **197**: 1142–1151.

Adams HD, Zeppel MJB, Anderegg WRL, Hartmann H, Landhäusser SM, Tissue DT, Huxman TE, Hudson PJ, Franz TE, Allen CD, *et al.* 2017. A multi-species synthesis of physiological mechanisms in drought-induced tree mortality. *Nature Ecology & Evolution* **1**: 1285–1291.

Allen CD, Breshears DD. 1998. Drought-induced shift of a forest–woodland ecotone: Rapid landscape response to climate variation. *Proc. Natl. Acad. Sci. USA*: 4.

Ameglio T, Bodet C, Lacointe A, Cochard H. 2002. Winter embolism, mechanisms of xylem hydraulic conductivity recovery and springtime growth patterns in walnut and peach trees. *Tree Physiology* **22**: 1211–1220.

Anderegg WRL. 2015. Spatial and temporal variation in plant hydraulic traits and their relevance for climate change impacts on vegetation. *New Phytologist* **205**: 1008–1014.

Anderegg WRL, Berry JA, Smith DD, Sperry JS, Anderegg LDL, Field CB. 2012. The roles of hydraulic and carbon stress in a widespread climate-induced forest die-off. *Proceedings of the National Academy of Sciences* **109**: 233–237.

Anderegg WRL, Hicke JA, Fisher RA, Allen CD, Aukema J, Bentz B, Hood S, Lichstein JW, Macalady AK, McDowell N, *et al.* 2015. Tree mortality from drought, insects, and their interactions in a changing climate. *New Phytologist* **208**: 674–683.

Arend M, Link RM, Patthey R, Hoch G, Schuldt B, Kahmen A. 2021. Rapid hydraulic collapse as cause of drought-induced mortality in conifers. *Proceedings of the National Academy of Sciences* **118**: e2025251118.

Atkinson CJ, Taylor JM. 1996. Effects of elevated CO2 on stem growth, vessel area and hydraulic conductivity of oak and cherry seedlings. *New Phytologist* **133**: 617–626.

Barigah TS, Charrier O, Douris M, Bonhomme M, Herbette S, Améglio T, Fichot R, Brignolas F, Cochard H. 2013. Water stress-induced xylem hydraulic failure is a causal factor of tree mortality in beech and poplar. *Annals of Botany* **112**: 1431–1437.

Breshears DD, Myers OB, Meyer CW, Barnes FJ, Zou CB, Allen CD, McDowell NG, Pockman WT. 2009. Tree die-off in response to global change-type drought: mortality insights from a decade of plant water potential measurements. *Frontiers in Ecology and the Environment* **7**: 185–189.

Brodersen CR, Knipfer T, McElrone AJ. 2018. In vivo visualization of the final stages of xylem vessel refilling in grapevine (Vitis vinifera) stems. *New Phytologist* **217**: 117–126.

Brodersen CR, McElrone AJ, Choat B, Matthews MA, Shackel KA. 2010. The Dynamics of Embolism Repair in Xylem: In Vivo Visualizations Using High-Resolution Computed Tomography. *PLANT PHYSIOLOGY* **154**: 1088–1095.

Brodribb TJ, Bowman DJMS, Nichols S, Delzon S, Burlett R. **2010**. Xylem function and growth rate interact to determine recovery rates after exposure to extreme water deficit. *New Phytologist* **188**: 533–542.

Brodribb TJ, Carriqui M, Delzon S, Lucani C. **2017**. Optical Measurement of Stem Xylem Vulnerability. *Plant Physiology* **174**: 2054–2061.

Brodribb TJ, Feild TS. **2000**. Stem hydraulic supply is linked to leaf photosynthetic capacity: evidence from New Caledonian and Tasmanian rainforests. *Plant, Cell & Environment* **23**: 1381–1388.

Brodribb TJ, Skelton RP, McAdam SAM, Bienaimé D, Lucani CJ, Marmottant P. **2016**. Visual quantification of embolism reveals leaf vulnerability to hydraulic failure. *New Phytologist* **209**: 1403–1409.

Camisón Á, Ángela Martín M, Dorado FJ, Moreno G, Solla A. **2020**. Changes in carbohydrates induced by drought and waterlogging in Castanea sativa. *Trees* **34**: 579–591.

Canadell JG, Raupach MR. **2008**. Managing Forests for Climate Change Mitigation. *Science* **320**: 1456–1457.

Cardoso AA, Batz TA, McAdam SAM. **2020**. Xylem Embolism Resistance Determines Leaf Mortality during Drought in *Persea americana*. *Plant Physiology* **182**: 547–554.

Charrier G, Torres-Ruiz JM, Badel E, Burlett R, Choat B, Cochard H, Delmas CEL, Domec J-C, Jansen S, King A, *et al.* 2016. Evidence for Hydraulic Vulnerability Segmentation and Lack of Xylem Refilling under Tension. *Plant Physiology* **172**: 1657–1668.

Choat B, Badel E, Burlett R, Delzon S, Cochard H, Jansen S. **2016**. Noninvasive Measurement of Vulnerability to Drought-Induced Embolism by X-Ray Microtomography. *Plant Physiology* **170**: 273–282.

Choat B, Brodersen CR, McElrone AJ. **2015**. Synchrotron X-ray microtomography of xylem embolism in *Sequoia sempervirens* saplings during cycles of drought and recovery. *New Phytologist* **205**: 1095–1105.

Choat B, Drayton WM, Brodersen C, Mattthews MA, Shackel KA, Wada H, Mcelrone AJ. **2010**. Measurement of vulnerability to water stress-induced cavitation in grapevine: a comparison of four techniques applied to a long-vesseled species: Comparison of vulnerability curve technique in grapevine. *Plant, Cell & Environment* **33**: 1502–1512.

Choat B, Jansen S, Brodribb TJ, Cochard H, Delzon S, Bhaskar R, Bucci SJ, Feild TS, Gleason SM, Hacke UG, *et al.* 2012. Global convergence in the vulnerability of forests to drought. *Nature* **491**: 752–755.

Choat B, Nolf M, Lopez R, Peters JMR, Carins-Murphy MR, Creek D, Brodribb TJ. **2019**. Non-invasive imaging shows no evidence of embolism repair after drought in tree species of two genera. *Tree Physiology* **39**: 113–121.

Christensen-Dalsgaard KK, Tyree MT. **2014**. Frost fatigue and spring recovery of xylem vessels in three diffuse-porous trees *in situ*: Frost fatigue in diffuse-porous trees. *Plant, Cell & Environment* **37**: 1074–1085.

Cobb AR, Choat B, Holbrook NM. **2007**. Dynamics of freeze–thaw embolism in Smilax

rotundifolia (Smilacaceae). *American Journal of Botany* **94**: 640–649.

Cochard H. **2002**. A technique for measuring xylem hydraulic conductance under high negative pressures. *Plant, Cell and Environment* **25**: 815–819.

Cochard H, Badel E, Herbette S, Delzon S, Choat B, Jansen S. **2013**. Methods for measuring plant vulnerability to cavitation: a critical review. *Journal of Experimental Botany* **64**: 4779–4791.

Cochard H, Coll L, Le Roux X, Améglio T. **2002**. Unraveling the Effects of Plant Hydraulics on Stomatal Closure during Water Stress in Walnut. *Plant Physiology* **128**: 282–290.

Cochard H, Damour G, Bodet C, Tharwat I, Poirier M, Améglio T. **2005**. Evaluation of a new centrifuge technique for rapid generation of xylem vulnerability curves. *Physiologia Plantarum* **124**: 410–418.

Cochard H, Delzon S, Badel E. **2015**. X-ray microtomography (micro-CT): a reference technology for high-resolution quantification of xylem embolism in trees: A reference method for xylem embolism. *Plant, Cell & Environment* **38**: 201–206.

Cochard H, Ewers FW, Tyree MT. **1994**. Water relations of a tropical vine-like bamboo (*Rhipidocladum racemiflorum*): root pressures, vulnerability to cavitation and seasonal changes in embolism. *Journal of Experimental Botany* **45**: 1085–1089.

Cochard H, Herbette S, Barigah T, Badel E, Ennajeh M, Vilagrosa A. **2010**. Does sample length influence the shape of xylem embolism vulnerability curves? A test with the Cavitron spinning technique: Shape of xylem embolism vulnerability curves. *Plant, Cell & Environment* **33**: 1543–1552.

Cook BI, Mankin JS, Anchukaitis KJ. **2018**. Climate Change and Drought: From Past to Future. *Current Climate Change Reports* **4**: 164–179.

Creek D, Lamarque L, Torres-Ruiz JM, Parise C, Burlett R, Tissue D, Delzon S. **2020**. Xylem embolism in leaves does not occur with open stomata: evidence from direct observations using the optical visualisation technique. *Journal of experimental botany* **71**: 1151–1159.

Curtis PG, Slay CM, Harris NL, Tyukavina A, Hansen MC. **2018**. Classifying drivers of global forest loss. *Science* **361**: 1108–1111.

Das AJ, Stephenson NL, Davis KP. **2016**. Why do trees die? Characterizing the drivers of background tree mortality. *Ecology* **97**: 2616–2627.

Denny M. **2012**. Tree hydraulics: how sap rises. *European Journal of Physics* **33**: 43–53.

Dixon HH, Joly J. **1894**. On the Ascent of Sap. [Abstract]. *Proceedings of the Royal Society of London* **57**: 3–5.

Domec J-C. **2011**. Let's not forget the critical role of surface tension in xylem water relations. *Tree Physiology* **31**: 359–360.

Drexler JZ, Ewel KC. **2001**. Effect of the 1997-1998 ENSO-Related Drought on Hydrology and Salinity in a Micronesian Wetland Complex. *Estuaries* **24**: 347.

Duke NC, Kovacs JM, Griffiths AD, Preece L, Hill DJE, van Oosterzee P, Mackenzie J, Morning HS, Burrows D. **2017**. Large-scale dieback of mangroves in Australia. *Marine and*

Freshwater Research **68**: 1816.

Ellison D, Morris CE, Locatelli B, Sheil D, Cohen J, Murdiyarso D, Gutierrez V, Noordwijk M van, Creed IF, Pokorny J, *et al.* 2017. Trees, forests and water: Cool insights for a hot world. *Global Environmental Change* **43**: 51–61.

Ennajeh M, Simões F, Khemira H, Cochard H. **2011**. How reliable is the double-ended pressure sleeve technique for assessing xylem vulnerability to cavitation in woody angiosperms? *Physiologia Plantarum* **142**: 205–210.

Ennajeh M, Tounekti T, Vadel AM, Khemira H, Cochard H. **2008**. Water relations and drought-induced embolism in olive (Olea europaea) varieties 'Meski' and 'Chemlali' during severe drought. *Tree Physiology* **28**: 971–976.

Ent RJ van der, Savenije HHG, Schaefli B, Steele-Dunne SC. **2010**. Origin and fate of atmospheric moisture over continents. *Water Resources Research* **46**.

Fettig CJ, Mortenson LA, Bulaon BM, Foulk PB. **2019**. Tree mortality following drought in the central and southern Sierra Nevada, California, U.S. *Forest Ecology and Management* **432**: 164–178.

Gleason SM, Wiggans DR, Bliss CA, Young JS, Cooper M, Willi KR, Comas LH. **2017**. Embolized Stems Recover Overnight in Zea mays: The Role of Soil Water, Root Pressure, and Nighttime Transpiration. *Frontiers in Plant Science* **8**.

Hacke U, Sauter JJ. **1995**. Vulnerability of xylem to embolism in relation to leaf water potential and stomatal conductance in *Fagus sylvatica* f. *purpurea* and *Populus balsamifera*. *Journal of Experimental Botany* **46**: 1177–1183.

Hao G-Y, Wheeler JK, Holbrook NM, Goldstein G. **2013**. Investigating xylem embolism formation, refilling and water storage in tree trunks using frequency domain reflectometry. *Journal of Experimental Botany* **64**: 2321–2332.

Hochberg U, Albuquerque C, Rachmilevitch S, Cochard H, David-Schwartz R, Brodersen CR, McElrone A, Windt CW. **2016**. Grapevine petioles are more sensitive to drought induced embolism than stems: evidence from *in vivo* MRI and microcomputed tomography observations of hydraulic vulnerability segmentation: Hydraulic vulnerability segmentation in grapevine. *Plant, Cell & Environment* **39**: 1886–1894.

Holbrook NM, Burns MJ, Field CB. **1995**. Negative Xylem Pressures in Plants: A Test of the Balancing Pressure Technique. *Science, New Series* **270**: 1193–1194.

Hubbard RM, Ryan MG, Stiller V, Sperry JS. **2001**. Stomatal conductance and photosynthesis vary linearly with plant hydraulic conductance in ponderosa pine. *Plant, Cell & Environment* **24**: 113–121.

Jacobsen AL, Rodriguez-Zaccaro FD, Lee TF, Valdovinos J, Toschi HS, Martinez JA, Pratt RB. **2015**. Grapevine Xylem Development, Architecture, and Function. In: Hacke U, ed. Functional and Ecological Xylem Anatomy. Cham: Springer International Publishing, 133–162.

Jarbeau JA, Ewers FW, Davis SD. **1995**. The mechanism of water-stress-induced embolism in two species of chaparral shrubs. *Plant, Cell & Environment* **18**: 189–196.

Johnson DM, Wortemann R, McCulloh KA, Jordan-Meille L, Ward E, Warren JM, Palmroth S, Domec J-C. **2016**. A test of the hydraulic vulnerability segmentation hypothesis in angiosperm and conifer tree species. *Tree Physiology* **36**: 983–993.

Kono Y, Ishida A, Saiki S-T, Yoshimura K, Dannoura M, Yazaki K, Kimura F, Yoshimura J, Aikawa S. **2019**. Initial hydraulic failure followed by late-stage carbon starvation leads to drought-induced death in the tree Trema orientalis. *Communications Biology* **2**: 1–9.

Kumagai T, Porporato A. **2012**. Strategies of a Bornean tropical rainforest water use as a function of rainfall regime: isohydric or anisohydric? *Plant, Cell & Environment* **35**: 61–71.

Lee S-J, Kim Y. **2008**. In vivo Visualization of the Water-refilling Process in Xylem Vessels Using X-ray Micro-imaging. *Annals of Botany* **101**: 595–602.

Lens F, Sperry JS, Christman MA, Choat B, Rabaey D, Jansen S. **2011**. Testing hypotheses that link wood anatomy to cavitation resistance and hydraulic conductivity in the genus Acer. *New Phytologist* **190**: 709–723.

Li X, Blackman CJ, Rymer PD, Quintans D, Duursma RA, Choat B, Medlyn BE, Tissue DT. **2018**. Xylem embolism measured retrospectively is linked to canopy dieback in natural populations of Eucalyptus piperita following drought. *Tree Physiology* **38**: 1193–1199.

Li X, Delzon S, Torres-Ruiz J, Badel E, Burlett R, Cochard H, Jansen S, King A, Lamarque LJ, Lenoir N, *et al.* 2020a. Lack of vulnerability segmentation in four angiosperm tree species: evidence from direct X-ray microtomography observation. *Annals of Forest Science* **77**.

Li Q, Zhao M, Wang N, Liu S, Wang J, Zhang W, Yang N, Fan P, Wang R, Wang H, *et al.* 2020b. Water use strategies and drought intensity define the relative contributions of hydraulic failure and carbohydrate depletion during seedling mortality. *Plant Physiology and Biochemistry* **153**: 106–118.

Liu D, Ogaya R, Barbeta A, Yang X, Peñuelas J. **2018**. Long-term experimental drought combined with natural extremes accelerate vegetation shift in a Mediterranean holm oak forest. *Environmental and Experimental Botany* **151**: 1–11.

López R, Nolf M, Duursma RA, Badel E, Flavel RJ, Cochard H, Choat B. **2019**. Mitigating the open vessel artefact in centrifuge-based measurement of embolism resistance. *Tree Physiology* **39**: 143–155.

Losso A, Bär A, Dämon B, Dullin C, Ganthaler A, Petruzzellis F, Savi T, Tromba G, Nardini A, Mayr S, *et al.* 2019. Insights from in vivo micro-CT analysis: testing the hydraulic vulnerability segmentation in *Acer pseudoplatanus* and *Fagus sylvatica* seedlings. *The New phytologist* **221**: 1831–1842.

Lovelock CE, Feller IC, Reef R, Hickey S, Ball MC. **2017**. Mangrove dieback during fluctuating sea levels. *Scientific Reports* **7**: 1680.

Madakumbura GD, Goulden ML, Hall A, Fu R, Moritz MA, Koven CD, Kueppers LM, Norlen CA, Randerson JT. **2020**. Recent California tree mortality portends future increase in drought-driven forest die-off. *Environ. Res. Lett.*: 10.

Martínez-Vilalta J, Lloret F. **2016**. Drought-induced vegetation shifts in terrestrial

ecosystems: The key role of regeneration dynamics. *Global and Planetary Change* **144**: 94–108.

Martin-StPaul N, Delzon S, Cochard H. **2017**. Plant resistance to drought depends on timely stomatal closure. *Ecology Letters* **20**: 1437–1447.

Maruta E, Kubota M, Ikeda T. **2020**. Effects of xylem embolism on the winter survival of Abies veitchii shoots in an upper subalpine region of central Japan. *Scientific Reports* **10**: 6594.

Mayr S, Schmid P, Laur J, Rosner S, Charra-Vaskou K, Dämon B, Hacke UG. **2014**. Uptake of Water via Branches Helps Timberline Conifers Refill Embolized Xylem in Late Winter. *Plant Physiology* **164**: 1731–1740.

McDowell N, Pockman WT, Allen CD, Breshears DD, Cobb N, Kolb T, Plaut J, Sperry J, West A, Williams DG, *et al.* 2008. Mechanisms of plant survival and mortality during drought: why do some plants survive while others succumb to drought? *New Phytologist* **178**: 719–739.

McElrone AJ, Choat B, Parkinson DY, MacDowell AA, Brodersen CR. **2013**. Using High Resolution Computed Tomography to Visualize the Three Dimensional Structure and Function of Plant Vasculature. *JoVE (Journal of Visualized Experiments)*: e50162.

Meinzer FC, Clearwater MJ, Goldstein G. **2001**. Water transport in trees: current perspectives, new insights and some controversies. *Environmental and Experimental Botany* **45**: 239–262.

Michaelian M, Hogg EH, Hall RJ, Arsenault E. **2011**. Massive mortality of aspen following severe drought along the southern edge of the Canadian boreal forest. *Global change biology.* **17**: 2084–2094.

Miller DM. **2020**. III. XYLEM SAP COMPOSITION AT.MAXIMUM ROOT PRESSURE PROVIDES EVIDENCE OF ACTIVE TRANSPORT INTO THE XYLEM AND A MEASUREMENT OF THE REFLECTION COEFFICIENT OF THE ROOT. **77**: 6.

Mrad A, Domec J-C, Huang C-W, Lens F, Katul G. **2018**. A network model links wood anatomy to xylem tissue hydraulic behaviour and vulnerability to cavitation. *Plant, Cell & Environment* **41**: 2718–2730.

Mueller RC, Scudder CM, Porter ME, Trotter RT, Gehring CA, Whitham TG. **2005**. Differential tree mortality in response to severe drought: evidence for long-term vegetation shifts. *Journal of Ecology* **93**: 1085–1093.

Mukherjee S, Mishra A, Trenberth KE. **2018**. Climate Change and Drought: a Perspective on Drought Indices. *Current Climate Change Reports* **4**: 145–163.

Nardini A, Luglio J. **2014**. Leaf hydraulic capacity and drought vulnerability: possible trade-offs and correlations with climate across three major biomes. *Functional Ecology* **28**: 810–818.

Nardini A, Ramani M, Gortan E, Salleo S. **2008**. Vein recovery from embolism occurs under negative pressure in leaves of sunflower (Helianthus annuus). *Physiologia Plantarum* **133**: 755–764.

Nardini A, Savi T, Losso A, Petit G, Pacilè S, Tromba G, Mayr S, Trifilò P, Lo Gullo MA, Salleo S. **2017**. X-ray microtomography observations of xylem embolism in stems of *Laurus nobilis* are consistent with hydraulic measurements of percentage loss of conductance. *New*

Phytologist **213**: 1068–1075.

Nardini A, Tyree MT, Salleo S. **2001**. Xylem Cavitation in the Leaf of *Prunus laurocerasus* and Its Impact on Leaf Hydraulics. *Plant Physiology* **125**: 1700–1709.

Nolan RH, Gauthey A, Losso A, Medlyn BE, Smith R, Chhajed SS, Fuller K, Song M, Li X, Beaumont LJ, *et al.* 2021. Hydraulic failure and tree size linked with canopy die-back in eucalypt forest during extreme drought. *New Phytologist*.

Nolf M, Creek D, Duursma R, Holtum J, Mayr S, Choat B. **2015**. Stem and leaf hydraulic properties are finely coordinated in three tropical rain forest tree species. *Plant, Cell & Environment* **38**: 2652–2661.

Nolf M, Lopez R, Peters JMR, Flavel RJ, Koloadin LS, Young IM, Choat B. **2017**. Visualization of xylem embolism by X-ray microtomography: a direct test against hydraulic measurements. *New Phytologist* **214**: 890–898.

Oyanoghafo OO, Brien CO, Choat B, Tissue D, Rymer, Paul D PD. **2020**. Drought tolerance of Hakea species (Proteaceae) from a range of biomes and life-histories predicted by climatic niche. *bioRxiv*.

Pajor R, Fleming A, Osborne CP, Rolfe SA, Sturrock CJ, Mooney SJ. **2013**. Seeing space: visualization and quantification of plant leaf structure using X-ray micro-computed tomography: View Point. *Journal of Experimental Botany* **64**: 385–390.

Pratt RB, Castro V, Fickle JC, Jacobsen AL. **2019**. Embolism resistance of different aged stems of a California oak species (Quercus douglasii): optical and microCT methods differ from the benchtop-dehydration standard (M Ball, Ed.). *Tree Physiology*.

Pugh TAM, Lindeskog M, Smith B, Poulter B, Arneth A, Haverd V, Calle L. **2019**. Role of forest regrowth in global carbon sink dynamics. *Proceedings of the National Academy of Sciences* **116**: 4382–4387.

Riascos JM, Cantera JR, Blanco-Libreros JF. **2018**. Growth and mortality of mangrove seedlings in the wettest neotropical mangrove forests during ENSO: Implications for vulnerability to climate change. *Aquatic Botany* **147**: 34–42.

Rodriguez-Dominguez CM, Buckley TN, Egea G, Cires A de, Hernandez-Santana V, Martorell S, Diaz-Espejo A. **2016**. Most stomatal closure in woody species under moderate drought can be explained by stomatal responses to leaf turgor. *Plant, Cell & Environment* **39**: 2014–2026.

Rodriguez-Dominguez CM, Carins Murphy MR, Lucani C, Brodribb TJ. **2018**. Mapping xylem failure in disparate organs of whole plants reveals extreme resistance in olive roots. *New Phytologist* **218**: 1025–1035.

Rolim SG, Jesus RM, Nascimento HEM, do Couto HTZ, Chambers JQ. **2005**. Biomass change in an Atlantic tropical moist forest: the ENSO effect in permanent sample plots over a 22-year period. *Oecologia* **142**: 238–246.

Rood SB, Patiño S, Coombs K, Tyree MT. **2000**. Branch sacrifice: cavitation-associated drought adaptation of riparian cottonwoods. *Trees* **14**: 0248–0257.

Rowland L, da Costa ACL, Galbraith DR, Oliveira RS, Binks OJ, Oliveira A a. R, Pullen

AM, Doughty CE, Metcalfe DB, Vasconcelos SS, *et al.* 2015. Death from drought in tropical forests is triggered by hydraulics not carbon starvation. *Nature* **528**: 119–122.

Santiago LS, Goldstein G, Meinzer FC, Fisher JB, Machado K, Woodruff D, Jones T. **2004**. Leaf photosynthetic traits scale with hydraulic conductivity and wood density in Panamanian forest canopy trees. *Oecologia* **140**: 543–550.

Savi T, Casolo V, Dal Borgo A, Rosner S, Torboli V, Stenni B, Bertoncin P, Martellos S, Pallavicini A, Nardini A. **2020**. Drought-induced dieback of Pinus nigra: a tale of hydraulic failure and carbon starvation. *Conservation Physiology* **7**.

Savi T, Miotto A, Petruzzellis F, Losso A, Pacilè S, Tromba G, Mayr S, Nardini A. **2017**. Drought-induced embolism in stems of sunflower: A comparison of in vivo micro-CT observations and destructive hydraulic measurements. *Plant Physiology and Biochemistry* **120**: 24–29.

Saxe H, Cannell MGR, Johnsen Ø, Ryan MG, Vourlitis G. **2001**. Tree and forest functioning in response to global warming. *New Phytologist* **149**: 369–399.

Schenk HJ, Jansen S, Hölttä T. **2020**. Positive pressure in xylem and its role in hydraulic function. *New Phytologist* **n/a**.

Schlesinger WH, Jasechko S. **2014**. Transpiration in the global water cycle. *Agricultural and Forest Meteorology* **189–190**: 115–117.

Secchi F, Gilbert ME, Zwieniecki MA. **2011**. Transcriptome Response to Embolism Formation in Stems of *Populus trichocarpa* Provides Insight into Signaling and the Biology of Refilling. *Plant Physiology* **157**: 1419–1429.

Secchi F, Zwieniecki MA. **2011**. Sensing embolism in xylem vessels: the role of sucrose as a trigger for refilling. *Plant, Cell & Environment* **34**: 514–524.

Senf C, Buras A, Zang CS, Rammig A, Seidl R. **2020**. Excess forest mortality is consistently linked to drought across Europe. *Nature Communications* **11**: 6200.

Sevanto S, Mcdowell NG, Dickman LT, Pangle R, Pockman WT. **2014**. How do trees die? A test of the hydraulic failure and carbon starvation hypotheses. *Plant, Cell & Environment* **37**: 153–161.

Sperry JS, Holbrook NM, Zimmermann MH, Tyree MT. **1987**. Spring Filling of Xylem Vessels in Wild Grapevine. *PLANT PHYSIOLOGY* **83**: 414–417.

Sperry JS, Ikeda T. **1997**. Xylem cavitation in roots and stems of Douglas-fir and white fir. *Tree Physiology* **17**: 275–280.

Sperry JS, Stiller V, Hacke UG. **2003**. Xylem Hydraulics and the Soil–Plant–Atmosphere Continuum: Opportunities and Unresolved Issues. *Agronomy Journal* **95**: 1362–1370.

Sperry JS, Tyree MT. **1988**. Mechanism of Water Stress-Induced Xylem Embolism. *Plant Physiology* **88**: 581–587.

Sperry JS, Tyree MT. **1990**. Water-stress-induced xylem embolism in three species of conifers. *Plant, Cell & Environment* **13**: 427–436.

Steppe K, Lemeur R. **2007**. Effects of ring-porous and diffuse-porous stem wood anatomy on

the hydraulic parameters used in a water flow and storage model. *Tree Physiology* **27**: 43–52.

Stiller V, Sperry JS, Lafitte R. **2005**. Embolized conduits of rice (Oryza sativa, Poaceae) refill despite negative xylem pressure. *American Journal of Botany* **92**: 1970–1974.

Taneda H, Sperry JS. **2008**. A case-study of water transport in co-occurring ring- versus diffuse-porous trees: contrasts in water-status, conducting capacity, cavitation and vessel refilling. *Tree Physiology* **28**: 1641–1651.

Tomasella M, Häberle K-H, Nardini A, Hesse B, Machlet A, Matyssek R. **2017**. Post-drought hydraulic recovery is accompanied by non-structural carbohydrate depletion in the stem wood of Norway spruce saplings. *Scientific Reports* **7**: 14308.

Torres-Ruiz JM, Cochard H, Choat B, Jansen S, López R, Tomášková I, Padilla-Díaz CM, Badel E, Burlett R, King A, *et al.* 2017. Xylem resistance to embolism: presenting a simple diagnostic test for the open vessel artefact. *New Phytologist* **215**: 489–499.

Trifilò P, Casolo V, Raimondo F, Petrussa E, Boscutti F, Lo Gullo MA, Nardini A. **2017**. Effects of prolonged drought on stem non-structural carbohydrates content and post-drought hydraulic recovery in Laurus nobilis L.: The possible link between carbon starvation and hydraulic failure. *Plant Physiology and Biochemistry* **120**: 232–241.

Trueba S, Pouteau R, Lens F, Feild TS, Isnard S, Olson ME, Delzon S. **2017**. Vulnerability to xylem embolism as a major correlate of the environmental distribution of rain forest species on a tropical island. *Plant, Cell & Environment* **40**: 277–289.

Tsuda M, Tyree MT. **1997**. Whole-plant hydraulic resistance and vulnerability segmentation in Acer saccharinum. *Tree Physiology* **17**: 351–357.

Tyree MT, Ewers FW. **1991**. The hydraulic architecture of trees and other woody plants. *New Phytologist* **119**: 345–360.

Tyree MT, Salleo S, Nardini A, Assunta Lo Gullo M, Mosca R. **1999**. Refilling of Embolized Vessels in Young Stems of Laurel. Do We Need a New Paradigm? *Plant Physiology* **120**: 11–22.

Tyree MT, Sperry JS. **1989**. Vulnerability of Xylem to Cavitation and Embolism. *Annual Review of Plant Physiology and Plant Molecular Biology* **40**: 19–36.

Tyree MT, Yang S. **1992**. Hydraulic Conductivity Recovery versus Water Pressure in Xylem of *Acer saccharum*. *Plant Physiology* **100**: 669–676.

Urli M, Porté AJ, Cochard H, Guengant Y, Burlett R, Delzon S. **2013**. Xylem embolism threshold for catastrophic hydraulic failure in angiosperm trees. *Tree Physiology* **33**: 672–683.

Utsumi Y, Sano Y, Fujikawa S, Funada R, Ohtani J. **1998**. Visualization of Cavitated Vessels in Winter and Refilled Vessels in Spring in Diffuse-Porous Trees by Cryo-Scanning Electron Microscopy. *Plant Physiology* **117**: 1463–1471.

Venturas MD, MacKinnon ED, Dario HL, Jacobsen AL, Pratt RB, Davis SD. **2016**. Chaparral Shrub Hydraulic Traits, Size, and Life History Types Relate to Species Mortality during California's Historic Drought of 2014. *PLOS ONE* **11**: e0159145.

Venturas MD, Pratt RB, Jacobsen AL, Castro V, Fickle JC, Hacke UG. **2019**. Direct

comparison of four methods to construct xylem vulnerability curves: Differences among techniques are linked to vessel network characteristics. *Plant, Cell & Environment* **42**: 2422–2436.

Wang B, Luo X, Yang Y-M, Sun W, Cane MA, Cai W, Yeh S-W, Liu J. **2019**. Historical change of El Niño properties sheds light on future changes of extreme El Niño. *Proceedings of the National Academy of Sciences* **116**: 22512–22517.

Wheeler JK, Huggett BA, Tofte AN, Rockwell FE, Holbrook NM. **2013**. Cutting xylem under tension or supersaturated with gas can generate PLC and the appearance of rapid recovery from embolism: Sampling induced embolism. *Plant, Cell & Environment* **36**: 1938–1949.

Yoshimura K, Saiki S-T, Yazaki K, Ogasa MY, Shirai M, Nakano T, Yoshimura J, Ishida A. **2016**. The dynamics of carbon stored in xylem sapwood to drought-induced hydraulic stress in mature trees. *Scientific Reports* **6**: 24513.

Zach A, Schuldt B, Brix S, Horna V, Culmsee H, Leuschner C. **2010**. Vessel diameter and xylem hydraulic conductivity increase with tree height in tropical rainforest trees in Sulawesi, Indonesia. *Flora - Morphology, Distribution, Functional Ecology of Plants* **205**: 506–512.

Zanne AE, Westoby M, Falster DS, Ackerly DD, Loarie SR, Arnold SEJ, Coomes DA. **2010**. Angiosperm wood structure: Global patterns in vessel anatomy and their relation to wood density and potential conductivity. *American Journal of Botany* **97**: 207–215.

Zhu S-D, Liu H, Xu Q-Y, Cao K-F, Ye Q. **2016**. Are leaves more vulnerable to cavitation than branches? *Functional Ecology* **30**: 1740–1744.

Zimmermann MH. **2013**. *Xylem Structure and the Ascent of Sap*. Springer Science & Business Media.

Zimmermann U, Schneider H, Wegner LH, Haase A. **2004**. Water ascent in tall trees: does evolution of land plants rely on a highly metastable state? *New Phytologist* **162**: 575–615.

Chapter 2: Visual and hydraulic techniques produce similar estimates of cavitation resistance in woody species

Published as: **Gauthey, A.**, Peters, J.M., Carins-Murphy, M.R., Rodriguez-Dominguez, C.M., Li, X., Delzon, S., King, A., López, R., Medlyn, B.E., Tissue, D.T. and Brodribb, T.J., 2020. Visual and hydraulic techniques produce similar estimates of cavitation resistance in woody species. *New Phytologist*, 228(3), pp.884-897. doi: 10.1111/nph.16746

2.1. Abstract

Hydraulic failure of the plant vascular system is a principal cause of forest die-off under drought. Accurate quantification of this process is essential to our understanding of the physiological mechanisms underpinning plant mortality. Imaging techniques are increasingly applied to estimate xylem cavitation resistance. These techniques allow for *in situ* measurement of embolism formation in real time, although the benefits and trade-offs associated with different techniques have not been evaluated in detail. Here we compare two imaging methods, micro-computed tomography (microCT) and optical vulnerability (OV), to standard hydraulic methods for measurement of cavitation resistance in seven woody species representing a diversity of major phylogenetic and xylem anatomical groups. Across the seven species, there was strong agreement between cavitation resistance values (P_{50}) estimated from visualisation techniques (microCT and OV) and between visual techniques and hydraulic techniques. The results indicate that visual techniques provide accurate estimates of cavitation resistance and the degree to which xylem hydraulic function is impacted by embolism. Results are discussed

in the context of trade-offs associated with each technique and possible causes of discrepancy between estimates of cavitation resistance provided by visual and hydraulic techniques.

2.2. Introduction

Drought has a defining influence on the structure and productivity of terrestrial ecosystems (Ledger *et al.*, 2011). Extreme drought events combined with heat waves have the potential to reduce primary productivity and trigger mass forest die-off (Ciais *et al.*, 2005; Michaelian *et al.*, 2011; Duke *et al.*, 2017). Increasing temperatures associated with climate change may lead to droughts of greater intensity and duration (Trenberth *et al.*, 2014). Such amplification of drought stress by high temperatures has already been detected in some recent extreme drought events (Adams *et al.*, 2009; Park Williams *et al.*, 2013). The impact of drought on plants is mediated by a complex interaction of traits that define drought tolerance, which include physiological, morphological and anatomical traits that govern water uptake and loss. Cavitation resistance has emerged as a mechanistic trait of primary importance in determining approximate thresholds of water stress that contribute to tree mortality (McDowell *et al.*, 2008; Choat *et al.*, 2018).

According to the cohesion-tension theory proposed by Dixon and Joly (1894), liquid water is transported through the xylem under tension. While the cohesion-tension mechanism allows large volumes of water to be transported from the roots to the leaves at little direct energetic cost to the plant, it relies on a system that is inherently unstable. Limited soil moisture and high evaporative demand cause increasing tension on the xylem water column. When tension reaches critical values, the water column ruptures (cavitation) leading to the formation of gas bubbles or "emboli" in xylem vessels and tracheids. Although the resultant air emboli are isolated within individual vessels or tracheids, embolism spreads rapidly through the network of xylem

conduits via air-seeding when critical xylem tensions are reached. Gas emboli block the transport of water and cause a progressive loss of xylem hydraulic conductivity until complete hydraulic failure occurs (Tyree & Sperry, 1989).

Xylem cavitation resistance, also referred to as vulnerability to embolism, is described by the relationship between the xylem water potential (Ψ_X in MPa) and the loss of hydraulic conductivity relative to a maximum reference state (PLC in %). This trait defines limits on the magnitude of water stress that a plant can withstand before complete loss of functionality occurs in the xylem. Cavitation resistance varies dramatically across species in accordance with site aridity (Brodribb & Hill, 1999; Pockman & Sperry, 2000; Choat *et al.*, 2012; Li *et al.*, 2018) and has been quantitatively linked to lethal (minimum recoverable) water potential (Brodribb & Cochard, 2009; Urli *et al.*, 2013; Hammond & Adams, 2019). Although drought tolerance and mortality processes are complex, hydraulic failure via cavitation is considered to be a principal cause of drought-induced tree mortality (Adams *et al.*, 2017; Choat *et al.*, 2018) and a key trait for understanding the evolution and ecology of plant species in relation to aridity (Pittermann, 2010; Larter *et al.*, 2017). It is therefore imperative that we have confidence in the accuracy of measurements and threshold values determined by standard measurement techniques.

Cavitation resistance is typically assessed by generating vulnerability curves for a given species or population of plants. Species hydraulic thresholds are often compared using the water potential at which 50% of conductivity is lost (P_{50}), with more negative P_{50} denoting greater cavitation resistance. Techniques used to quantify cavitation resistance have traditionally relied on measurements of water flow rates through detached plant organs (stems, roots, or leaves). While these techniques have provided the foundation for the field of plant hydraulics, a number of experimental artefacts associated with flow based methods have been identified in the last decade (Rockwell *et al.*, 2014). These artefacts are primarily related to cutting the xylem while

it is under tension (Wheeler *et al.*, 2013) or the generation of embolism by centrifugal force (Choat *et al.*, 2010; Cochard *et al.*, 2010) and air injection (Ennajeh *et al.*, 2011). It is important to note that while these artefacts may cause significant errors in the estimation of cavitation resistance, they can be largely eliminated by use of the appropriate precautions and selection of appropriate techniques for a given xylem anatomy (Torres-Ruiz *et al.*, 2017; López *et al.*, 2019). Additionally, in the last two decades, advances in imaging technologies have facilitated the development of new techniques to measure cavitation resistance (Cochard *et al.*, 2015; Choat *et al.*, 2015; Brodribb *et al.*, 2016). These methods are non-invasive or in-situ and allow us to visually detect embolism in intact plants while providing high spatial and temporal resolution of embolism spread through the conductive tissue.

X-ray computed micro-tomography (microCT) is an imaging technique that can provide non-invasive measurements of xylem functional status and cavitation resistance in intact plants (Choat *et al.*, 2016; Losso *et al.*, 2019). The very high spatial resolution (down to 1 μm/pixel) attainable by microCT (Cochard *et al.*, 2015) also allows the location and spread of embolism in the xylem to be observed at a level of detail that was not previously possible (Brodersen, 2013). Although microCT can potentially be applied to any species or plant organ, its use is constrained by access to synchrotron facilities or high cost laboratory instruments. Plants are also exposed to high doses of X-ray radiation, which may cause injury to living cells within the xylem (Kim & Lee, 2010; Choat *et al.*, 2016; Nardini *et al.*, 2017; Petruzzellis *et al.*, 2018). However, it is unlikely that X-ray exposure reduces the efficacy of microCT to measure cavitation resistance because the tracheary elements are dead at maturity and there is no evidence that X-rays generate cavitation events during scanning (Choat *et al.*, 2016; Venturas *et al.*, 2019).

The optical vulnerability (OV) technique (Brodribb *et al.*, 2016, 2017) is an in-situ imaging method initially developed to study cavitation in the leaf mid-rib and vein network. It allows

the dynamics of embolism formation to be followed during propagation in the venation system (Brodribb *et al.*, 2016). This method was subsequently adapted and used to visualise cavitation in flowers (Zhang & Brodribb, 2017), stems (Brodribb *et al.*, 2017) and roots (Rodriguez-Dominguez *et al.*, 2018). Stem P_{50} values estimated by the OV technique closely agree with values produced by a centrifuge based hydraulic method in 13 conifers species (Brodribb *et al.*, 2017), although disagreement between hydraulic and OV estimates of stem P_{50} have been reported for some angiosperm species (Venturas *et al.*, 2019; Pratt *et al.*, 2019). The OV technique is inexpensive and portable (i.e. can be used in the field or in the lab) with flexible configurations enabling increased automation and throughput. Potential limitations of the OV technique include the small region of the xylem surface observed, that only emboli in the outer layers of the xylem are captured, and that removal of the bark may potentially generate artifactual drying tissue or embolism (Venturas *et al.*, 2019). While the OV technique provides unparalleled temporal resolution when successful, incorrect implementation of this method, particularly by incomplete or interrupted image capture, can produce errors and vulnerability curves that are artificially vulnerable.

Imaging methods have been criticised on the grounds that they do not directly measure the impact of drought stress on xylem flow rates, instead relying on detection of embolism in xylem conduits at discrete locations (Jacobsen *et al.*, 2015). Errors may occur in the translation of conduit diameter measurements into theoretical flow rates (Venturas *et al.*, 2019), or if immature conduits that are fluid-filled but not yet functional are counted as functional conduits (Pratt & Jacobsen, 2018; Bouda *et al.*, 2019). Discrepancies between visual and hydraulic techniques could also occur if the area of embolised conduits observed is unrepresentative of decreases in xylem hydraulic conductivity caused to drought. Thus, a number of unresolved issues cloud our interpretation of cavitation resistance data and the application of various methods to the study of plant hydraulic function. In this study we compared estimates of

cavitation resistance generated by two in-situ imaging techniques (microCT and OV) with those obtained by standard hydraulic methods (bench dehydration or centrifuge). The principal objective of the study was to determine whether imaging and hydraulic techniques provided significantly different estimates of cavitation resistance.

Measurements were made on seven woody species encompassing a broad range of xylem anatomies, allowing us to evaluate trade-offs associated with each technique in relation to xylem anatomical grouping. Specifically, we tested the hypothesis that visual and hydraulic techniques would provide a similar estimate of cavitation resistance despite differences in the way the impact of embolism is quantified, i.e. vulnerability curves based of percent of embolised conduits, embolised area of xylem, and loss of hydraulic conductivity all produce similar estimates of P_{50}. The results are discussed in the context of advantages and disadvantages of techniques used.

2.3. Materials and methods

Vulnerability curves were constructed for each of the target species using three different methods: two in-situ imaging methods, Micro-computed tomography (CT) and the optical vulnerability method (OV), and one destructive method, either benchtop dehydration (BD) or the cavitron flow-centrifuge method (CA). The latter two are common hydraulic methods (HM) used to measure xylem cavitation resistance.

Plant material and experimental design

Plant material was selected in order to cover a range of xylem anatomies (tracheid bearing conifers, diffuse-porous and ring-porous angiosperms) and drought vulnerability. Plant material

from Australia included the following: 18 *Angophora costata* (OV=4, CT=4, BD=10) and 12 *Eucalyptus crebra* (OV=3, CT=4, BD=5) saplings from PlantsPlus Nursery (West Pennant Hills, NSW, Australia); 18 *Acacia aneura* (OV=3, CT=5, BD=10), 19 *Wisteria brachybotrys* (OV=3, CT=5, BD=11), 13 *Fraxinus oxycarpa* (OV=3, CT=4, BD=6), and 16 *Cedrus deodara* (OV=3, CT=5, BD=8) saplings from Plantmark nursery (Vineyard, NSW, Australia). All plants except *Acacia aneura* were grown in 20 cm deep, 4 litres plastic pots, using potting mix from the original nursery. At the point of measurement, plants were approximately 1 m to 1.50 m tall and between 1 and 3 years old. Saplings of *A. aneura* were raised from seed by Greening Australia (Richmond, NSW, Australia) and then replanted and grown in 25 L woven bags filled with native loamy sand soil, local to dry sclerophyll forest in Menangle (Menangle Sand & Soil, Menangle, NSW, Australia). At the time of the experiment, the *Acacias* were 18 months old. All plants were grown in a sunlit poly-tunnel under ambient environmental conditions on the Hawkesbury campus of Western Sydney University (Richmond, NSW, Australia). In France, measurements were made on 20 individuals of *Pinus pinaster* (CA=12, CT=5, OV=3) from Plantfor nursery (Uchacq, France) and grown on the INRA campus (Bordeaux, France). Individuals from the same species were purchased together and therefore age and height differed between but not within species. Note that some techniques produce curves that are composites of individuals points (BD and CT) while others produce full curves for each replicate individual (OV and CA).

All plants were maintained in well-watered conditions until experiments commenced in order to minimise native embolism formation in our samples. All experiments were carried out within 2 months of purchasing the plants. OV, BD and CA measurements were made either directly before or after CT measurements were undertaken at synchrotron facilities. Due to low sample size for the CA technique applied to *Pinus pinaster*, data for an additional 10 individuals were

added. These measurements were made on the same plants material and did not differ from P_{50} values obtained from the initial measurements.

Water potential

Stem water potential was assessed with a pressure chamber or stem psychrometer depending on experimental requirements. Stem water potential (Ψ_x) was measured by sealing a leaf in plastic film covered in aluminium foil for a minimum of 30 min before excision and measurement (McCutchan & Shackel, 1992). Three leaves per plant were selected and measured at each time point. Leaves were slowly pressurized in a Scholander pressure chamber (PMS Instrument Company, Albany, OR, USA) until water was visible on the cut end of the petiole (Scholander *et al.*, 1965). Stem water potential was also recorded using a PSY1 Stem Psychrometer sensor coupled with a microvolt data logger used to store data (ICT International, Armidale, NSW, Australia) every ten minutes. The psychrometer was installed mid-plant, approximately 30 to 50cm from the point where PLC was measured. The bark was removed gently, and the xylem washed with Milli-Q (deionised and filtered water). Then the sensor was installed on the bare xylem and parafilm was wrapped around it to effectively seal the chamber. As the Ψ_x decreased, the waiting and cooling times were increased, to ensure a sufficient volume of water condensed onto the thermocouples during measurement cycles. For the benchtop dehydration measurements, water potential was measured on non-transpiring leaves using the Scholander pressure chamber. For OV and microCT measurements, a psychrometer was installed on the stem of the sample, recording water potential every ten minutes. Stem psychrometer and pressure chamber measurements were compared regularly and showed close agreement (Fig. S2-1).

Benchtop dehydration

The benchtop dehydration method was applied following Sperry and Tyree (1988) and Choat et al. (2010). This method was selected for six of the seven target species because it is generally considered to be a reliable method (Cochard *et al.*, 2013). In this case plants were dehydrated intact, rather than as cut branches. Plants were transported to the lab where their roots were washed gently with tap water to remove soil and facilitate dehydration. Plants were allowed to dehydrate freely for varying lengths of time and then sealed in a plastic bag for 30 mins, so the water potential of the leaves would equilibrate with the stem and thus stem water potential measured. When the desired water potential was reached, plants were cut at the base of the stem under water. The cut end of the sample was then submerged in water for approximately 30 minutes. This allowed the xylem tension in the branch segment to relax, significantly minimising potential artefacts associated with cutting xylem under tension (Wheeler *et al.*, 2013). The first cut was made at ~30 cm upstream (i.e. at the base) from the intended final cut. The sample was slowly cut back from either end until only a final segment of approximately ~10 cm in length with a diameter between 0.4 cm and 1.2 cm remains. If the sapling had more than 3 developed branches, then 2 to 3 sample per plant may have been used. The segment was then connected to silicone rubber tubing filled with filtered perfusing solution (deionised water and KCl, 2mmol/L) and attached to the flow meter (LiquiFlow L13-AAD-11-K-10S; Bronkhorst High-Tech B.V., Ruurlo, the Netherlands). This first measurement yielded the initial hydraulic conductivity (K_{ini}, kg s^{-1} m^{-1} MPa^{-1}) of the sample which was calculated as:

$$K_{ini} = \frac{Q.l}{A.\Delta P}$$

with Q the sap flow rate (kg s^{-1}), l the segment length (m), A the xylem cross-sectional area (m^2) and ΔP the pressure drops across a segment of conducting tissue (MPa).

The segment was then connected to a pressurized tank filled containing a degassed and filtered perfusing solution under 100-150 kPa for 30 minutes. This step flushed the sample, dissolving emboli inside the conduits and replacing it with the solution to regain maximum conductivity. Thus, when the segment was subsequently connected to the flowmeter (Liqui-Flow L10, Bronkhorst High-Tech BV, Ruurlo, Gelderland, The Netherlands), the hydraulic conductivity was assumed to be at its maximum. The percentage loss of conductivity was determined by:

$$PLC = \frac{K_{max} - K_{ini}}{K_{max}} \times 100$$

where PLC is the percentage loss of conductivity and K_{max} is the maximum hydraulic conductivity attained after flushing.

Cavitron

The cavitron technique (Cochard, 2002) was used to measure cavitation resistance in *Pinus pinaster*. This technique uses centrifugal force to create tension (negative pressure) in the xylem by spinning stem samples at their centre. The loss of hydraulic conductance is measured while the sample is spinning (under tension) in the centrifuge by generating a positive hydrostatic pressure difference between the two ends of the sample. Although centrifuge based techniques are prone to an "open vessel" artefact when applied to some angiosperm species (López *et al.*, 2019), previous validation experiments have shown that the cavitron technique is reliable for tracheid bearing species such as conifers (Cochard *et al.*, 2005, 2010) .

Measurements were performed at the University of Bordeaux (Talence, France) using a custom-built honeycomb rotor (SamPrecis 2000, Bordeaux, France) mounted on a Sorvall RC5 superspeed centrifuge (Thermo Fisher Scientific, Munich, Germany). Samples were cut under water with all of the bark carefully removed. The stem was then recut under water to obtain a 22 cm sample in order to fit the stem into the cavitron. Both ends of the sample were sealed in plastic cuvettes filled with water. A solution of ultrapure and degassed water including 10mM KCl and 1 mM $CaCl_2$ was used as the reference solution for hydraulic measurements. Flow rates through samples were measured by following the progress of a meniscus with a CCD camera. Cavi_soft software (University of Bordeaux, v 5.0) was used to control centrifuge speed and each sample was stepped a set of increasing tensions. Meniscus position was logged for 1 minute at each step after the desired rotor speed was reached. Sample hydraulic conductivity and percentage of loss of conductivity was calculated by Cavi_soft software at each step. At least two measures of PLC were taken for each pressure step until the sample reached 100% of PLC.

MicroCT

X-ray microCT enables non-invasive generation of xylem vulnerability curves from intact plants by means of visualisation (McElrone *et al.*, 2013; Choat *et al.*, 2016). Data were acquired at two synchrotron facilities, the Australian Synchrotron (Clayton, VIC, Australia) and Synchrotron SOLEIL (Gif-sur-Yvette, France). All species except *Pinus pinaster* were scanned at the Australian Synchrotron, using the Imaging and Medical Beamline (IMBL). Samples were positioned in the beam using a robotic arm (Kuka, KR1000 Titan) and scanned on the main stem axis with a field of view of 28 mm x 20 mm. Scans were conducted at an X-ray energy of 30 keV while the sample was rotated through 180 degrees using continuous rotation with

images recorded at 0.1° angle increments. This yielded 1800 projections with additional flat field and dark field images recorded before and after each scan. Exposure time at each angle was 0.45–0.60 s giving a total scan time of 18–23 min. Scan volumes were reconstructed using XLICT Workflow 2015 (CSIRO) using either the Gridrec or FBP (Paganin *et al.*, 2002) reconstruction algorithm, which resulted in better image contrast based on X-ray phase retrieval The final resolution of images was 9.7 μm per voxel. Imaging of *Pinus pinaster* was undertaken at SOLEIL using the PSICHÉ beamline. Scans were carried out using a 25 keV monochromatic X-ray beam, while samples were rotated from 0° to 180° using a continuous rotation mode. The scan time was 75 s for each sample and yielded a stack of 1500 TIFF image slices and a field of view of 6 mm x 1.5 mm. Tomographic reconstructions were conducted using in PyHST2 software (Mirone *et al.*, 2014) and resulted in images with a resolution of 2.9 μm per voxel. Cross-sections were compiled to generate 3D rendering using the free software Drishti (http://anusf.anu.edu.au/Vizlab/drishti/) (Fig. S2-2).

Dehydration of plant material followed a similar protocol to that described for bench dehydration hydraulic measurements. Potted plants were transported to the facility where their roots were gently washed to facilitate dehydration. During dehydration, Ψ_x was primarily monitored by stems psychrometers with occasional measurements using pressure chamber as described above. After installation of psychrometers, plants were initially scanned while they were still fully hydrated and then placed outside to dry. When plants reached the desired Ψ_x (to generate a vulnerability curve for each species), they were rescanned at the same site. The stem scan location was marked on each plant with correction fluid, which provided a marker that was easily identified in X-ray images. This procedure continued until more than 80% of the vessels were embolized (approximately 4 scans per plant). A final scan was made of each plant after the stem was cut just above the scan location to ensure all vessels were filled with air,

providing us with the number of total vessels embolised which was assumed to be equivalent to a PLC of 100%. Dehydration of plants occurred over a period of five days.

MicroCT images provided good contrast between water-filled (grey) and air-filled (black) vessels. Image analysis was performed on a median scan (10 middle scans were compressed to make a single scan) by counting embolised vessels (darker than water-filled ones) using the 'Threshold' and 'Analyse Particles' functions in ImageJ, or by counting vessels manually using the "multi-point" action (Nolf *et al.*, 2017). For all angiosperm species and *Pinus pinaster*, vulnerability curves were based on the percentage of conduits embolised at a given Ψ_x. Percentage embolism was calculated for each scan image following:

$$\%\ embolism = \frac{Number\ of\ vessels\ embolised}{Total\ number\ of\ vessels} \times 100$$

Vulnerability curves for *Cedrus deodara* were based on measurement of embolised xylem cross sectional area, since the spatial resolution of images attained at IMBL was not sufficient to count individual tracheids in this species. The embolised area of tracheids was transformed to an estimate of percentage embolised tracheids with the aid of light microscope images, which allowed tracheid number per area to be accurately assessed (Fig. S2-3). In selected species, we examined the relationship between the percentage of embolised conduits and the percentage of loss of theoretical conductivity (PLC). The theoretical hydraulic conductivity (K_h) for a given stems was calculated from conduit diameters measured in microCT images following the Poiseuille-Hagen law (Tyree & Ewers, 1991; Nolf *et al.*, 2017):

$$K_h \frac{\pi\rho}{128\eta} \sum_{i-1}^{n} (d_i^4)$$

Where η = coefficient of viscosity of water (=10^{-9} MPa s at 20 °C), D = conduit diameter (m) and ρ = the density of water (=998.2 kg m^{-3}).

Optical vulnerability technique

The optical vulnerability (OV) method was initially described in Brodribb et al. (2017). Briefly, a Raspberry Pi single board computer (Raspberry Pi Foundation, http://www.raspberrypi.org) was used to control and store images produced by a 8-megapixel camera, which was contained within a 3D-printed clamp used to fix the sample in place. The sample field of view was magnified by a 20× lens and illuminated by six bright light-emitting diodes (LEDs) that provided reflected light from the sample surface. Details of the clamp construction and data analysis are provided at https://github.com/OpenSourceOV.

Intact plants were installed on the benchtop and a small section (rectangle of 2.5 x 1cm) of the bark was removed from the stem 40 to 90cm from the root collar to expose the xylem. This distance varied between plants with differing stem diameters and lengths such that the target segment was of similar diameter between measurements. Stems ranged from ranged from 0.5 to 1.2cm in diameter. Exposed xylem was covered with a conductive adhesive gel (Tensive®) in order to reduce heterogeneity in the speed of desiccation across different xylem layers. The camera clamp assembly was positioned to best view the prepared xylem and fixed in place. Stem water potential was measured concurrently using a stem psychrometer installed at the base of the stem between 30-50 cm form the camera. Images were recorded every 5 minutes until the sample was completely dry or until no more cavitation events were observed for at least 10 hours. Image sequences were downloaded from the Raspberry Pi and processed using ImageJ (Schneider *et al.*, 2012) to calculate the area of embolism, which was coupled with a

concomitant measurement of water potential. Cavitation events were identified with the aid of image subtraction, which clearly reveals areas of embolism in the field of view (Brodribb *et al.*, 2016). These data were used to determine the percentage of embolism as:

$$\%\ embolism = \frac{A_{cav}}{A_{max}} \times 100$$

where A_{cav} is the cumulative area of cavitated xylem at time t and A_{max} is the maximum area of cavitated xylem at the end of each sample dehydration (Fig. S2-4).

Data analysis

All statistical analyses were conducted with R 3.1.2 (R Core Team, 2017) using RStudio (RStudio Team, 2015). We compared P_{50} for techniques measuring loss of hydraulic conductivity (BD and CA) with techniques that allow for visual measurement of the percentage embolism (CT and OV). Vulnerability curves were fitted to a Weibull function with the *fitplc* package following methods developed by Duursma & Choat (2017). For two of the methods (CA and OV), a full vulnerability curve was generated for each replicate individual. For these methods, sample was incorporated as a random effect to account for repeated measures on a single individual. A 95% confidence interval (CI) for P_{50} was obtained using a standard profiling method. The CT and BD methods produce ensemble curves, in which measurements from multiple individuals are used to produce a curve. For these methods, a 95% CI for the estimate of P_{50} was generated using a bootstrapping approach with 2000 resamples.

Previously, estimates of P_{50} from different techniques have been compared by testing whether 95% CI's overlap; P_{50} values generated from different methods have been considered to be statistically different if there is no overlap in the confidence intervals (Nolf *et al.*, 2017; Bourne *et al.*, 2017). However, it is possible for estimates to be statistically different even where CI's

overlap (Cumming *et al.*, 2007). Here, we compared estimates from different techniques by generating bootstrapped 95% CI's for the difference in estimates between each pair of methods. Bootstrap distributions generated as part of curve fitting in *fitplc* were extracted for CT and BD methods. For OV and CA methods, bootstrap distributions were generated to represent the confidence intervals obtained. We then resampled 2000 values from each of these distributions and used them to generate a bootstrap CI's for the difference between each pair of techniques. Where these CI's do not overlap zero, there is no significant difference between these two methods.

The relationship between theoretical PLC values and percent embolised vessels extracted from microCT images was examined using regression analysis. A Standardised Major Axis (SMA) approach was used to test the if the slope or elevation of the line differed from the 1:1 relationship using the 'smatr' package (Warton *et al.*, 2012).

2.4. Results

Imaging techniques (CT and OV) for measuring cavitation resistance were compared with standard hydraulic methods using a range of species with diverse xylem anatomy: two conifers (*Cedrus deodara* and *Pinus pinaster*), three diffuse porous angiosperms (*Angophora costata*, *Acacia aneura* and *Eucalyptus crebra*), a ring porous angiosperm (*Fraxinus oxycarpa*) and a liana (*Wisteria brachybotrys*). The degree of embolism and its impact on xylem hydraulic function was evaluated differently in each technique. MicroCT produces visualisation of embolism within a stem that can be viewed as two dimensional slices or three-dimensional volume renderings (Fig. 2-1a, b). In this case, images clearly showed the size and location of embolised conduits, allowing for counts and morphometric analysis. It was also possible to track how embolism spreads through the xylem with increasing water stress and to separate

different regions of the stem for independent analysis. The OV technique detects the area of embolised conduits from one surface of the stem (Fig. 2-1c). While the full cross section of the xylem is not sampled, imaging occurs every 5 minutes allowing the temporal dynamics of embolism development to be explored in greater detail.

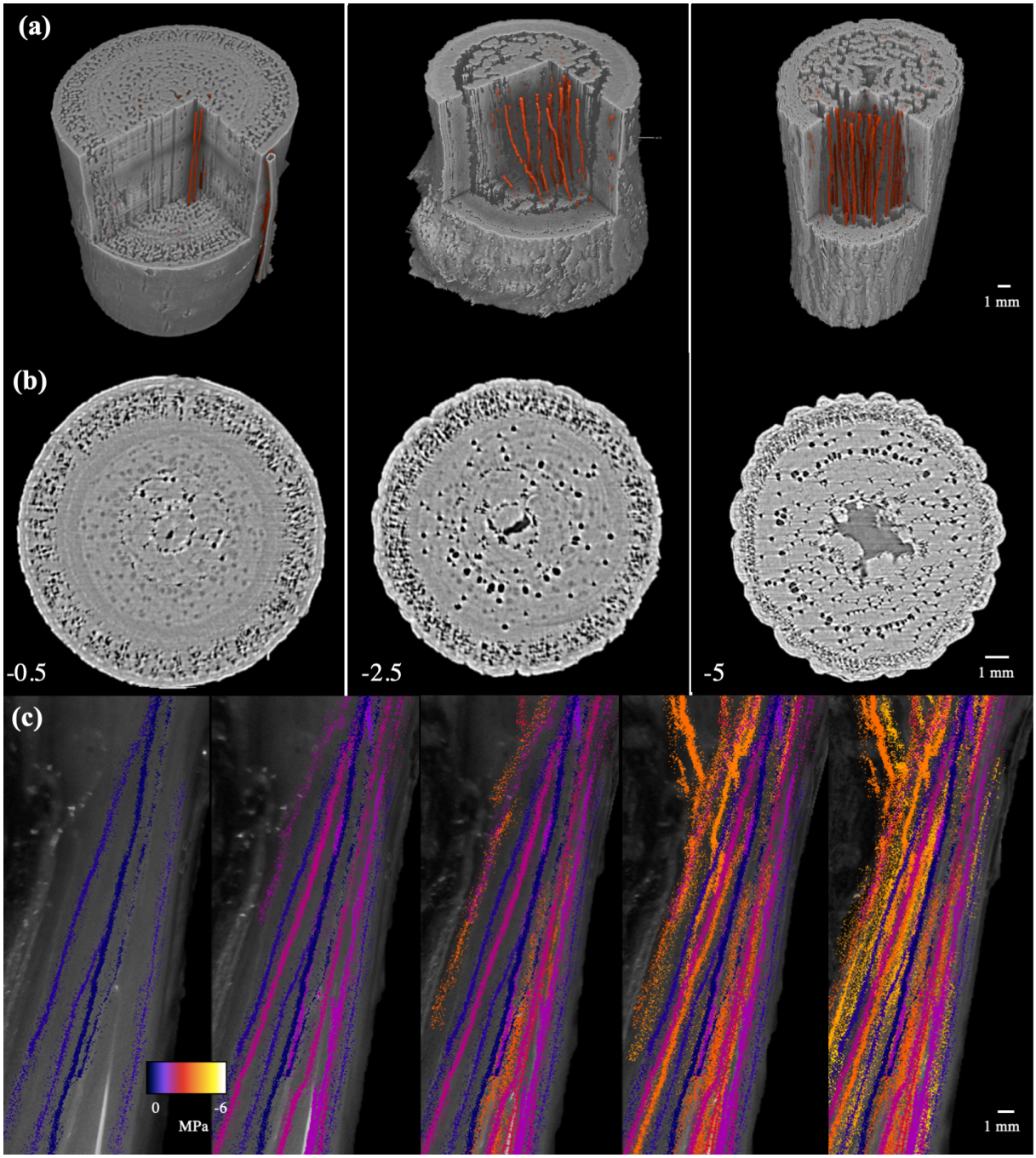

Figure 2- 1 Visualization of embolism in stems of Wisteria brachybotrys during dehydration by microcomputed tomography (microCT) and the optical vulnerability (OV) technique. (a) Three-dimensional reconstruction of the stem volumes acquired by microCT. The accumulation

of gas-filled vessels during dehydration is shown in orange. (b) Single transverse slice from within the microCT volume showing the location of embolized vessels (black) within the stem. The xylem water potential (Ψ; MPa) corresponding to each microCT image is indicated in grey. (c) Cavitation events recorded during dehydration by the OV technique. A colour map shows the spatial progression of cavitation with declining Ψ_x over the course of dehydration.

Previous studies utilizing microCT to measure cavitation resistance have based vulnerability curves on calculations of theoretical hydraulic conductance from measured vessel diameters. In this study, we compared metrics derived from analysis of microCT images to estimate the impact of embolism on xylem hydraulic function. For species in which vessel diameters could be measured, we observed strong agreement (r^2 = 0.94, P < 3.4844e-16) between theoretical PLC and PLV, with the slope and elevation of the regression line not significantly different from the 1:1 relationship (Fig. 2-2). This indicates that percent embolised vessels provides an accurate estimate of loss in hydraulic capacity for the target species. This is consistent with previous studies showing good agreement between PLC and PLV data (Li *et al.*, 2020). However, we note that values of PLC and PLV may diverge when working with species that have bimodal distributions of vessel diameters and caution should be used in these cases.

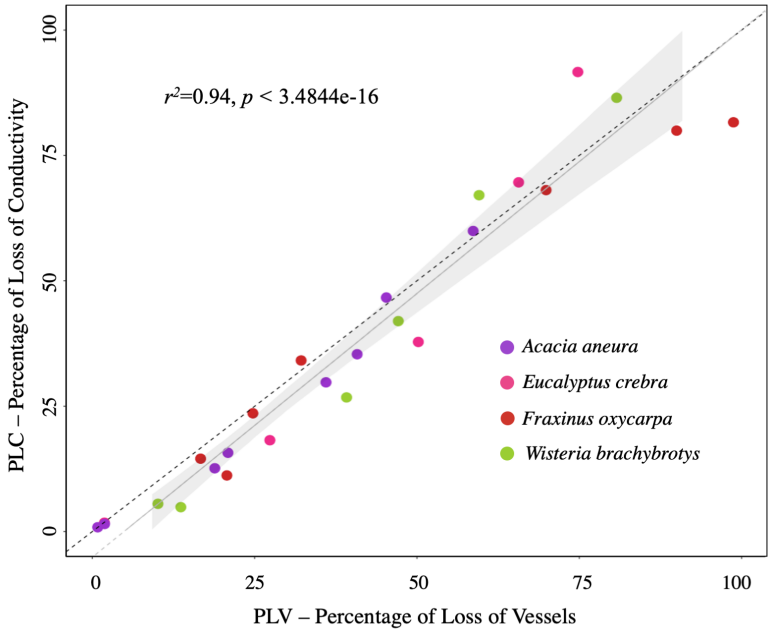

Figure 2- 2 Vulnerability curves for three diffuse porous angiosperm species produced using visual and hydraulic techniques (blue line, hydraulic method (a, d, g); pink line, microcomputed tomography (microCT) (b, e, h); and orange line, optical technique (c, f, i)). Coloured lines show the relationships between stem water potential (Ψ_x) and percentage of loss of conductivity (PLC, for hydraulic method), percentage of embolized conduits (for microCT) and percentage of embolized area (for optical technique). Each filled black dot is a measured datum. Vertical lines represent the P_{50} (thick line) and the 95% confidence interval (CI, dotted lines). Grey area represents the CI of the curve.

Differences among methods were assessed by comparing P_{50} values produced for each species by the different methods (Figs. 2-3, 2-4, 2-5; Table S2-1). For some highly resistant species, it was not possible to obtain the final part of the HM and CT curves because of limitations in the measurement range of the pressure chamber (see Fig. 2-3a, b, *Acacia aneura*).

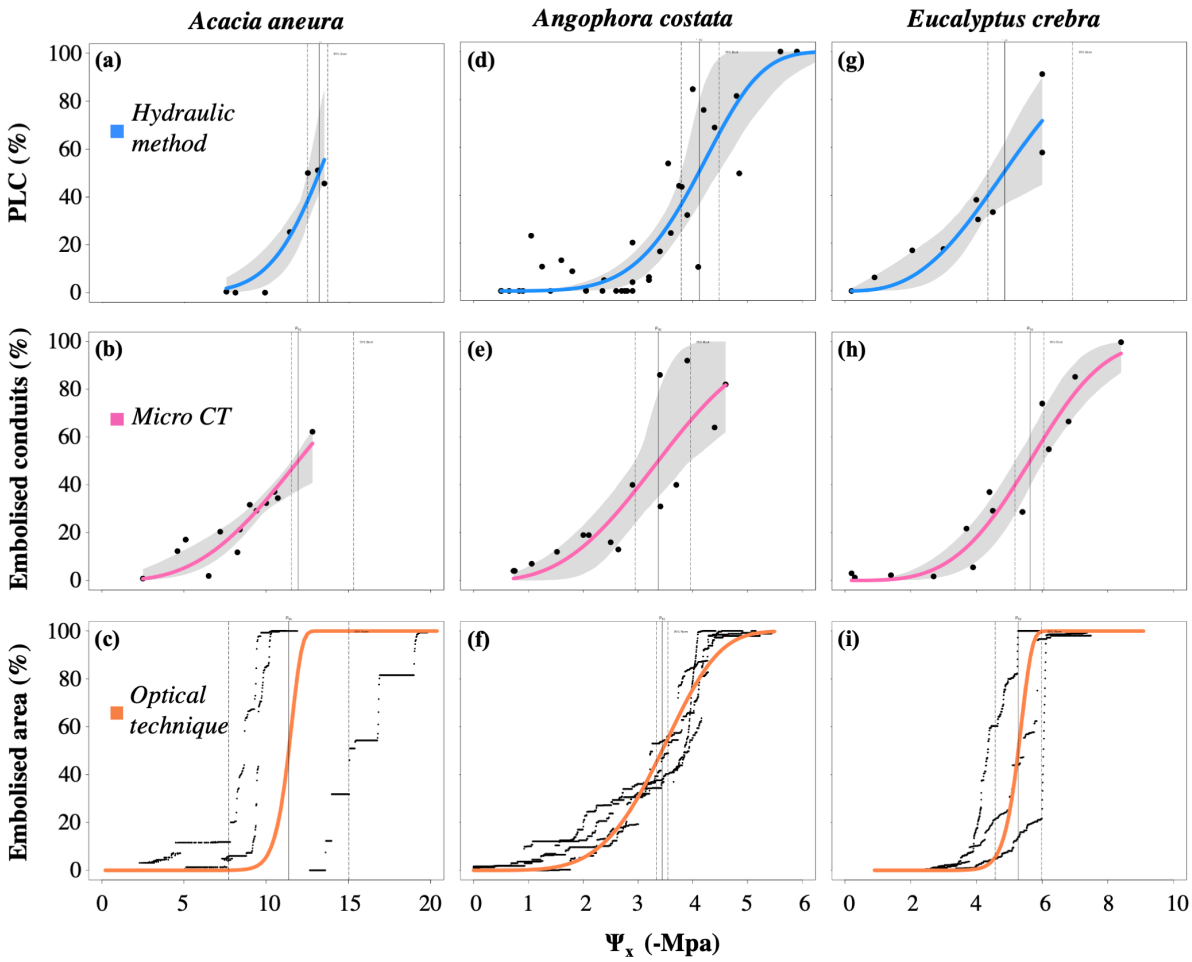

Figure 2- 3 Vulnerability curves for three diffuse porous angiosperm species produced using visual and hydraulic techniques (blue line, hydraulic method (a, d, g); pink line, microcomputed tomography (microCT) (b, e, h); and orange line, optical technique (c, f, i)). Coloured lines show the relationships between stem water potential (Ψ_x) and percentage of loss of conductivity (PLC, for hydraulic method), percentage of embolized conduits (for microCT) and percentage of embolized area (for optical technique). Each filled black dot is a measured datum. Vertical lines represent the P50 (thick line) and the 95% confidence interval (CI, dotted lines). Grey area represents the CI of the curve.

The OV technique generates a full vulnerability curve for each replicate stem, providing more detailed data on the timing of cavitation events over the range of water potentials measured. For some species, cavitation resistance curves were very similar between replicate stems (e.g. Fig. 2-3f, *Angophora costata*; Fig. 2-5f, *Pinus pinaster*), while in others there were large differences between replicate stem curves (e.g. Fig. 2-4c, *Fraxinus oxycarpa*).

Results from the centrifuge-based measurements on *Pinus pinaster* yielded the least variation between replicate stems and the smallest confidence intervals around P_{50}.

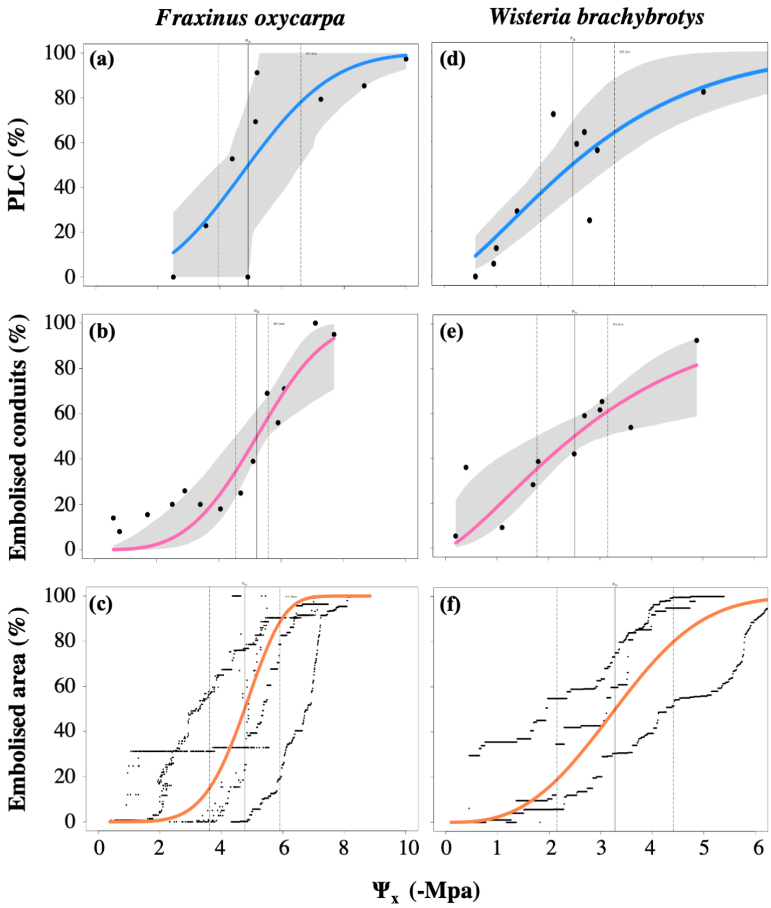

Figure 2- 4 Vulnerability curves for one ring porous and one liana angiosperm species produced using visual and hydraulic techniques (blue line, hydraulic method (a, d); pink line, microcomputed tomography (microCT) (b, e); and orange line, optical technique (c, f)). Coloured lines show the relationships between stem water potential (Ψ_x) and percentage of loss of conductivity (PLC, for hydraulic method), percentage of embolized conduits (for microCT) and percentage of embolized area (for optical technique). Each filled black dot is a measured datum. Vertical lines represent the P50 (thick line) and the 95% confidence interval (CI, dotted lines). Grey area represents the CI of the curve.

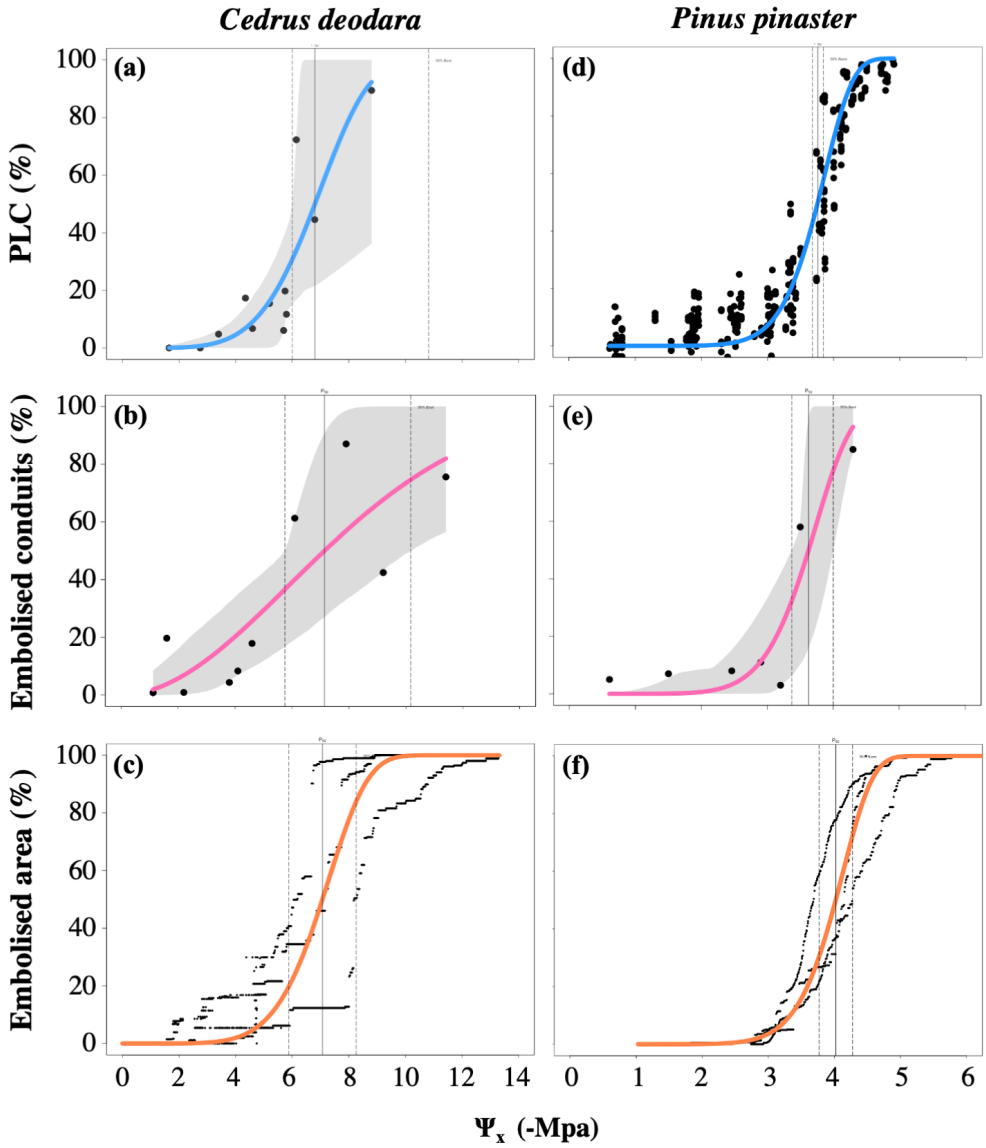

Figure 2- 5 Vulnerability curves for two conifer species produced using visual and hydraulic techniques (blue line, hydraulic method (a, d); pink line, microcomputed tomography (microCT) (b, e); and orange line, optical technique (c, f)). Coloured lines show the relationships between stem water potential (Ψ_x) and percentage of loss of conductivity (PLC, for hydraulic method), percentage of embolized conduits (for microCT) and percentage of embolized area (for optical technique). Each filled black dot is a measured datum. Vertical lines represent the P50 (thick line) and the 95% confidence interval (CI, dotted lines). Grey area represents the CI of the curve.

The target species covered a wide range of cavitation resistance values, with P_{50} ranging from -2.41 MPa in the liana species *Wisteria brachybotrys* to -13.18 MPa (Fig. 2-4d, e, f) in the arid land shrub species *Acacia aneura* (Fig. 2-3a, b, c). After creating a bootstrap CI for the difference between each pair of techniques, we found no significant differences for P_{50} between

techniques (i.e. CI overlap 0) for the majority of species and techniques (Fig. 2-6d, e, f). The only statistically significant differences were found between BD and CT and BD and OV for *Angophora costata*. However, the bootstrap CI did not fall far from zero and the magnitude of this difference was very small (0.04 between BD and CT and 0.33 between BD and OV). Overall, the results demonstrate strong agreement between techniques, despite differences in the way that hydraulic impairment from water stress is assessed.

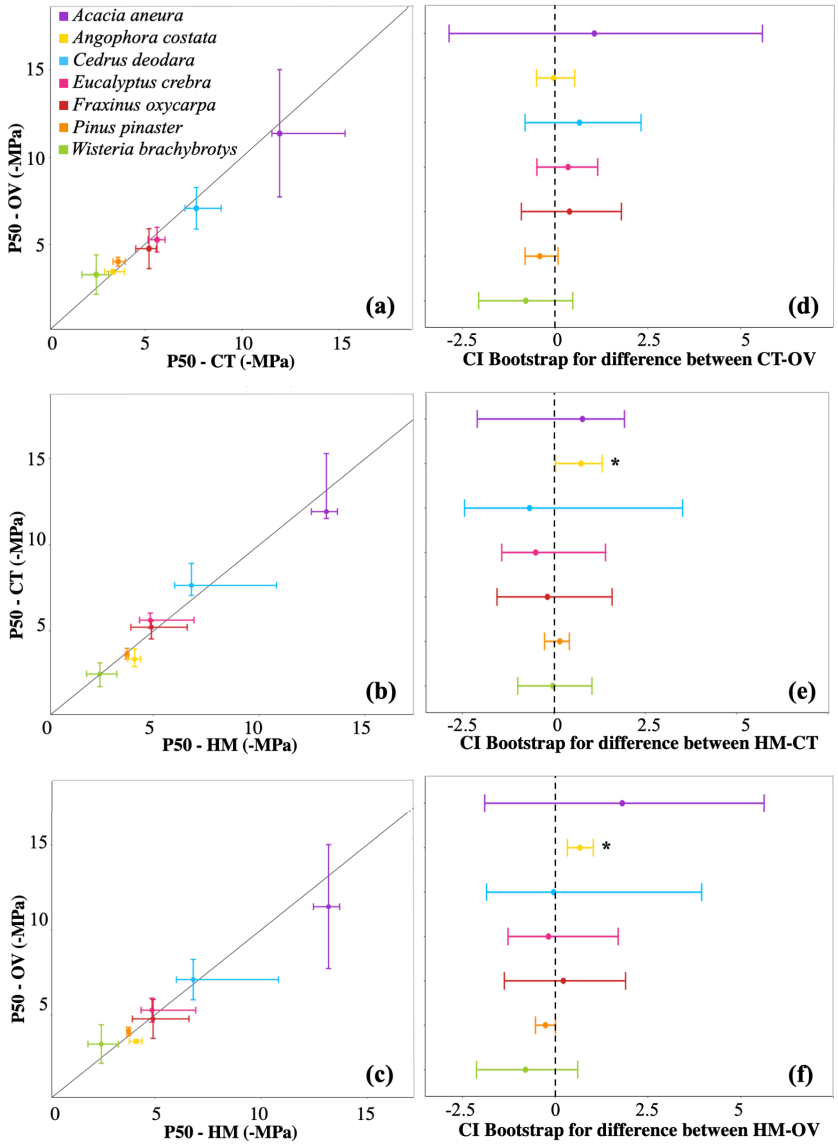

Figure 2- 6 Correlations between P50 values (means (95% confidence interval (CI)) obtained with microcomputed tomography (CT), optical vulnerability (OV) and hydraulic methods (HM) across seven species (a, b and c). The black line represents the 1:1 relationship. Confidence intervals (CI) for difference between the extracted bootstrap of two techniques (d, e and f). If this CI overlaps zero, then the two methods are not significantly different. Asterisks highlight the significant differences between methods.

In this study, P_{50} represented the best characterised point in vulnerability curves across species and methods and therefore the best metric for comparison of techniques. While other vulnerability curves parameters such as P_{12} and P_{88} have functional significance, they were not ideal metrics for comparison in this dataset. We note that P_{88} was usually the least well characterised part of the curve because of difficultly reaching the required water potential values in very resistant species and limitation set by plant material and beamtime at synchrotron facilities. Estimates of P_{12} can be strongly influenced by the presence of native embolism, which introduces error into comparisons that is not associated with differences in methodology. For completeness, analyses differences between P_{12} and P_{88} values for each method and species are shown in Fig. S2-5. Despite variation unrelated to methodology, we observed good agreement between P_{12} and P_{88} values for the majority (75%) of comparisons.

2.5. Discussion

We found that visual and hydraulic techniques produced similar estimates of xylem cavitation resistance (P_{50}) across a range of woody plant species. Our results demonstrate that visual estimation of embolised conduits can accurately capture the impact of cavitation and embolism on xylem hydraulic function. While some previous studies have compared visual and hydraulic techniques, this is the first study to compare microCT and OV techniques directly with hydraulic methods across a diverse range of species representing major xylem anatomical groupings (tracheid bearing, diffuse porous, ring porous). We note that our results contrast with some recent studies reporting differences in estimates of P_{50} obtained from visual and hydraulic methods for two angiosperm species (Venturas *et al.*, 2019; Pratt *et al.*, 2019). Below, we

discuss the advantages and disadvantages offered by each technique as well as causes of potential discrepancies between methods when estimating cavitation resistance.

Measurement of cavitation resistance with microCT

Trade-offs in sampling regime, image resolution, accessibility and expense were apparent between the techniques utilised in this study. MicroCT provides several advantages, including non-invasive assessment of plant hydraulic parameters and precise visualisation of embolism spread through the xylem network. However, it also requires access to specialised facilities and instrumentation. This precludes the application of microCT in remote field-based studies, while lab-based studies are usually limited by relatively short periods of beamtime or the expense of using commercial instruments. Additionally, recent work has identified potential sources of error and artefacts associated with microCT that bear further discussion.

Potential errors and artefacts may be derived from damage to xylem tissue caused by high doses of X-ray radiation during scanning (Savi *et al.*, 2017). With regards to measurements of cavitation resistance, there is no evidence that X-ray absorption during scanning causes cavitation; previous work has demonstrated that repeated scans do not alter the number of embolized vessels (Brodersen *et al.*, 2010; Choat *et al.*, 2016; Bouche *et al.*, 2016; Venturas *et al.*, 2019). In the current study, we observed no burning or damage to stems resulting from multiple scans. The strong agreement between hydraulic and microCT based estimates of P_{50} shown here and in previous studies provides further evidence that any damage caused by X-ray radiation has little impact on measurement of cavitation resistance.

Discrepancies between estimates of cavitation resistance may also arise from translation of microCT into theoretical hydraulic conductance, PLC, or PLV (Venturas *et al.*, 2019). These effects could be derived from the presence of immature vessels, which appear water-filled but

are not yet active (Pratt & Jacobsen, 2018; Bouda *et al.*, 2019), or the influence of network level properties that are not taken into account when estimates of K_h, PLC, or PLV are based are based on measurements of conduit dimensions in cross section (Bouda *et al.*, 2019). Our results show agreement between vulnerability curves constructed with microCT imaging and hydraulic methods, indicating that any discrepancies associated with translating visual data into loss of hydraulic function were small. This is consistent with previous studies that have shown good agreement between vulnerability curves constructed with hydraulic methods and microCT (Torres-Ruiz *et al.*, 2014; Choat *et al.*, 2016; Losso *et al.*, 2019). However, it is possible that small discrepancies observed between microCT and hydraulic measurements in our dataset are related to errors discussed above and these effects are important to consider when utilizing microCT for estimation of cavitation resistance. In some cases these effects can be easily accounted for; Nolf et al. (2017) demonstrated that P_{50} derived from hydraulic measurements matched most closely to the P_{50} of current year xylem estimated from microCT rather than the entire xylem cross section (Nolf *et al.*, 2017). This provides an example of how our understanding of hydraulic dysfunction caused by water stress is enhanced by the application of non-invasive imaging techniques, which provide detailed information on the functional significance of embolism in different regions of the xylem.

The optical vulnerability technique

The OV technique provides a low cost and portable alternative to microCT that may be utilized in laboratory or field settings. When used in conjunction with psychrometers, the technique allows measurements of cavitation resistance to be fully automated, with water potential and cavitation monitored at short time intervals (Brodribb *et al.*, 2017). This high temporal resolution reduces errors that may arise from less frequent sampling along the curve of one

individual or construction of curves from multiple individuals. The technique also requires less plant material as a full curve is acquired for each individual and can be applied to multiples organs or sites on a given individual, e.g. simultaneous measurement of leaf, stem and root vulnerability (Rodriguez-Dominguez *et al.*, 2018; Skelton *et al.*, 2018).

In our dataset, P_{50} values obtained with the OV technique were in close agreement with values obtained from hydraulic techniques and microCT (Fig. 2-6). Likewise, Brodribb et al. (2017) reported that estimates of P_{50} provided by OV and hydraulic measurements matched closely for 13 conifer species and one angiosperm (Brodribb *et al.*, 2017). However, two recent studies have reported differences between vulnerability parameters derived from the OV method and hydraulic methods (Venturas *et al.*, 2019; Pratt *et al.*, 2019) and there are potential sources of experimental error that must be considered. Images are taken from a small region of the xylem on one side of a young stem and light only penetrates a short distance into the stem. This may create bias if the area of xylem visualised is not representative of the whole xylem cross section, e.g. if recently formed outer conduits are more vulnerable to cavitation than conduits located deeper in the xylem. Additionally, if cavitation events within the xylem are patchy, as observed in some individuals with microCT imaging, then estimates of P_{50} will depend upon the timing of cavitation in the particular area of xylem being visualised. Such effects may explain the high level of variation in P_{50} observed in some cases (e.g. Fig. 2-4c. *Fraxinus oxycarpa*), although it is also possible that this variation represents plasticity between samples measured. However, the ability of the OV technique to capture entire replicate curves at high temporal resolution may be especially helpful in the quantifying plasticity. Overall, the strong agreement between estimates of mean P_{50} for OV vs. hydraulic and microCT techniques provides confidence that experimental error associated with the OV techniques can be overcome by sufficient sample size and care in preparation of plant material.

Considerations for hydraulic measurements

With reference to hydraulic techniques, we used the bench dehydration method for the majority of species in order to avoid issues associated with centrifuge and air injection techniques. Centrifuge based techniques offer advantages in terms of time and plant material required to construct vulnerability curves, but can significantly underestimate cavitation resistance in angiosperm species with long vessels (Choat *et al.*, 2010; Torres-Ruiz *et al.*, 2014) . However, centrifuge based techniques are reliable for conifer species regardless of the variant of technique applied (Alder *et al.*, 1997; Cochard *et al.*, 2005, 2010; Li *et al.*, 2007). Therefore, although the flow centrifuge (cavitron) method was used for measurement of *Pinus pinaster* in our study, the estimate of P_{50} is directly comparable to those obtained from bench dehydration. While the bench dehydration technique is labour intensive, it is regarded as the most reliable hydraulic technique for measurement of cavitation resistance and provides a direct measure of impacts on hydraulic conductance. Even so, we note that a number of sources of experimental error have been identified with the bench dehydration method, including those associated with excision of plant material (Wheeler *et al.*, 2013) and measurement of xylem flow rates on the bench (Espino & Schenk, 2011; De Baerdemaeker *et al.*, 2019). In this context, the close agreement between hydraulic methodology and in-situ visual techniques suggests that all techniques tested here produce reliable estimates of cavitation resistance if the appropriate precautions are taken.

2.6. Conclusions

MicroCT and OV techniques produced similar estimates of P_{50} to hydraulic techniques when applied to the same plant material. This result held across seven species with contrasting xylem anatomy, demonstrating the general applicability of the techniques examined here. This is

consistent with previous validation studies showing agreement between visual and hydraulic techniques for a further five angiosperm and 14 conifer species (Torres-Ruiz *et al*., 2014; Choat *et al*., 2016; Brodribb *et al*., 2017; Losso *et al*., 2019). We found that visualisation of embolism produced similar vulnerability curves to those based on measurements of xylem hydraulic conductivity despite differences in the way embolism was quantified, i.e. area of embolised xylem, counts of embolised vessels, theoretical hydraulic conductivity calculated from conduit diameter. Overall, these results provide confidence that a range of techniques can be employed to measure cavitation resistance, with the choice of technique dependent upon the particular questions posed, the location of experiments, and access to specialised facilities. The development of visual techniques presents numerous opportunities for improvements, including non-invasive observation of hydraulic function and full automation of measurements. Further work is required to resolve discrepancies between techniques observed by some authors (Venturas *et al.*, 2019; Pratt *et al.*, 2019), and to reduce potential sources of error that may arise from translation of visual data into loss of hydraulic capacity.

2.7. Supplementary figures

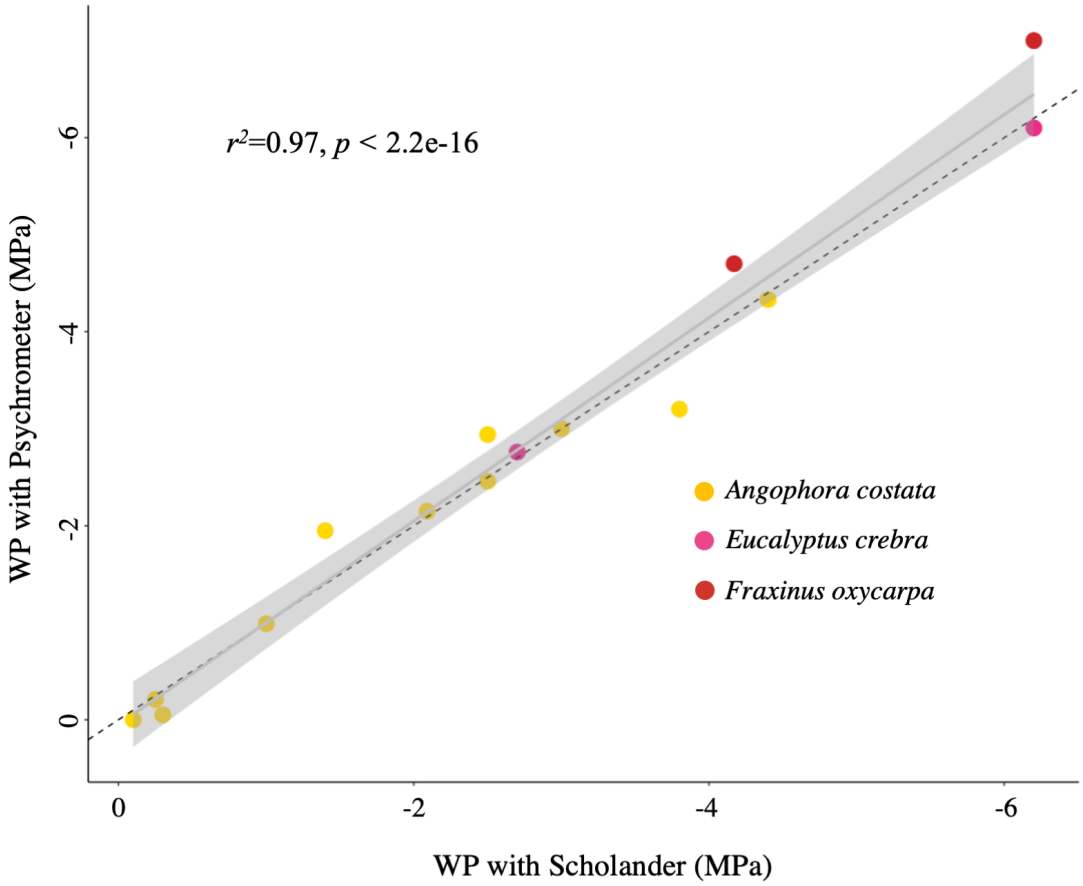

Figure S2-1 Example of stem reconstruction for four species with different xylem anatomy using the software DRISHTI

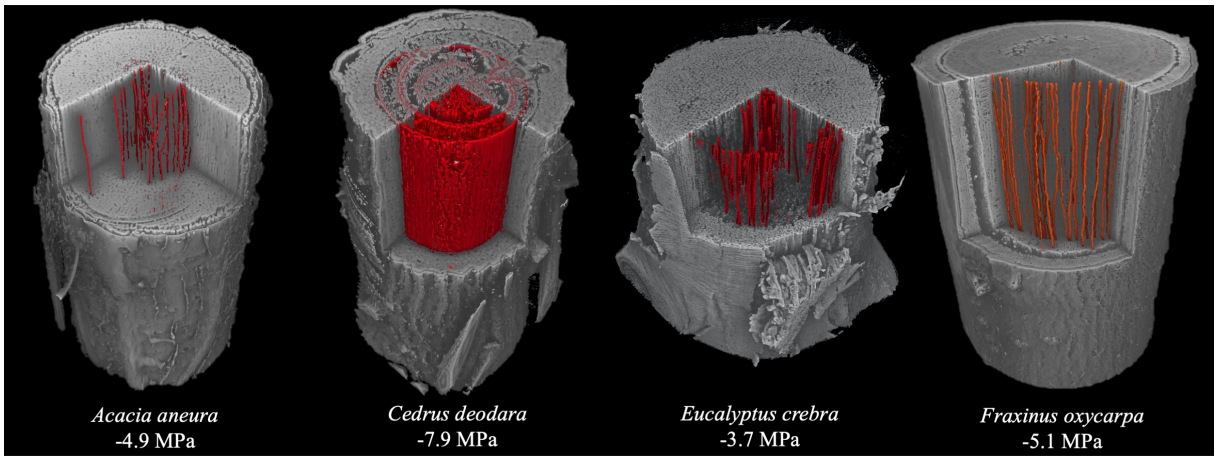

Figure S2-2 Relationship between the bagged leaf water potential measured using a Scholander chamber and the stem water potential measured using a psychrometer across three species with different xylem anatomy.

.

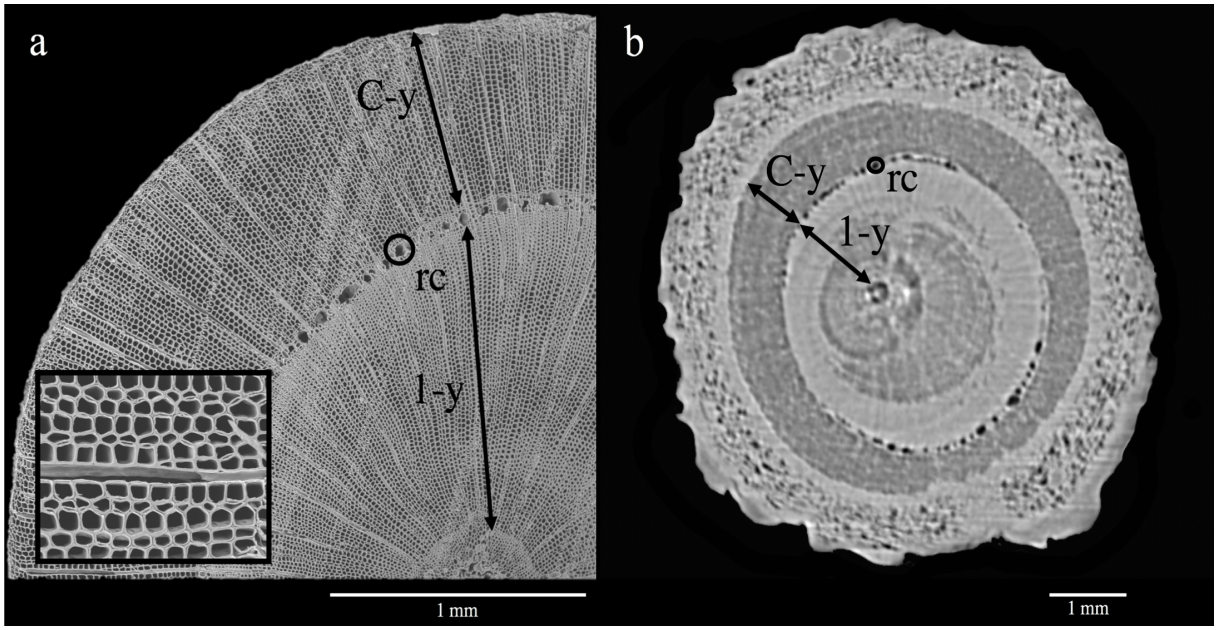

Figure S2- 3 Transverse surfaces of Cedrus deodara visualized by SEM and X-ray microCT.

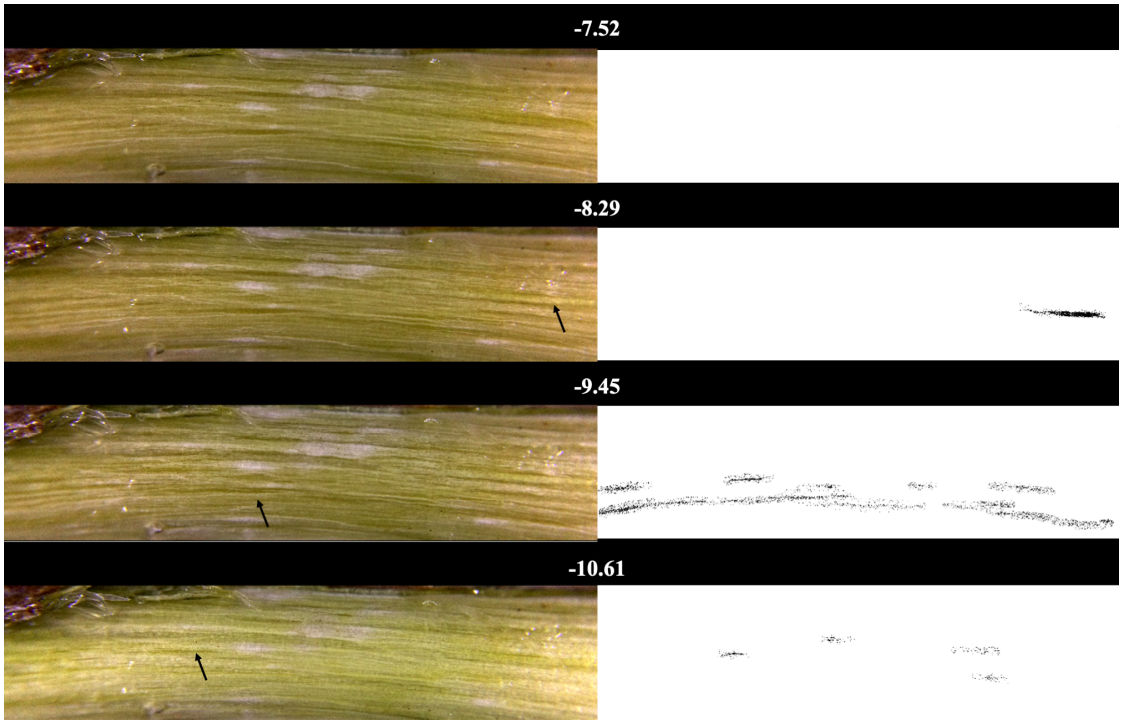

Figure S2- 4 Transverse slices produced with the OV technique for Acacia aneura.

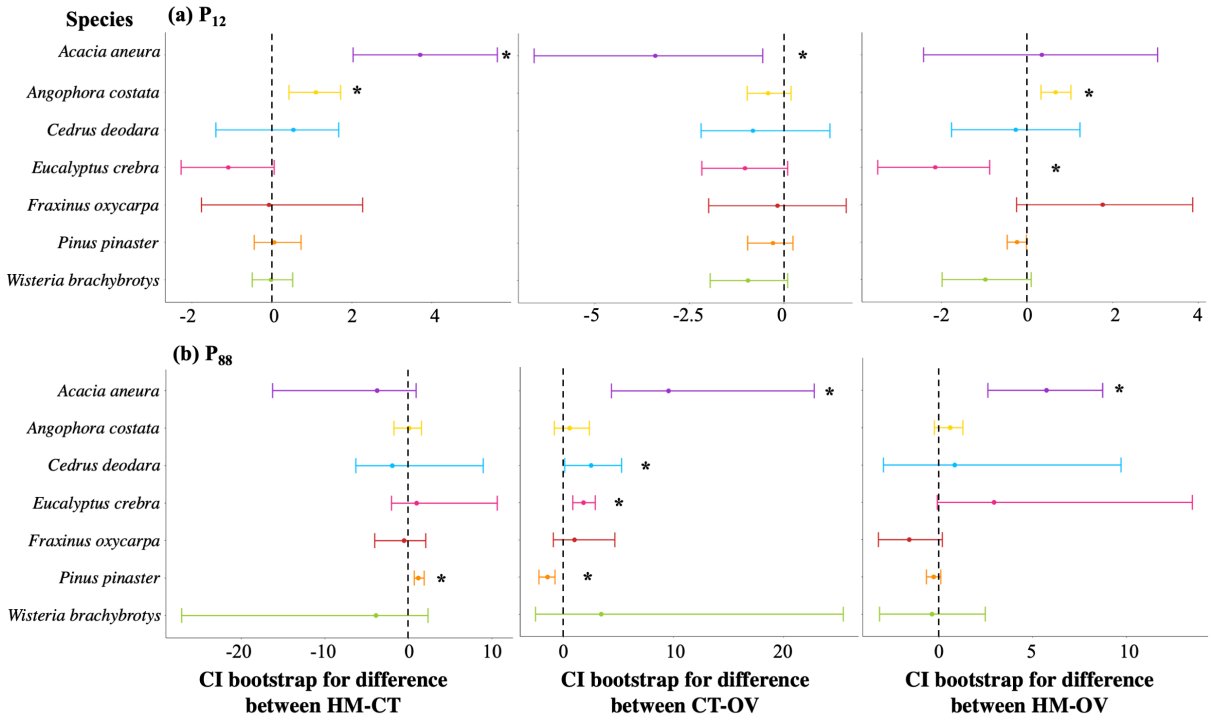

Figure S2- 5 P50 with CIs for the three different techniques and across seven species.

Species	Hydraulic methods	Micro CT	Optical vulnerability (OV)
Acacia aneura	**-13.18** +0.52/−0.71	**-11.94** +3.37/−0.4	**-11.36** ± 3.65
Angophora costata	**-4.12** +0.28/−0.33	**-3.37** +0.59/−0.43	**-3.44** ± 0.11
Cedrus deodara	**-6.8** +4.02/−0.79	**-7.65** +1.28/−0.58	**-7.07** ± 1.19
Eucalyptus crebra	**-4.86** +2.06/−0.51	**-5.63** +0.41/−0.46	**-5.27** ± 0.7
Fraxinus oxycarpa	**-4.91** +1.69/−0.97	**-5.22** +0.37/−0.68	**-4.76** ± 1.14
Pinus pinaster	**-3.76** ± 0.08	**-3.63** +0.37/−0.26	**-4.02** ± 0.26
Wisteria brachybotrys	**-2.48** +0.8/−0.63	**-2.51** +0.64/−0.74	**-3.28** ± 1.13

Table S2- 1 P_{50} (in bold characters) with confidence intervals for the three different techniques and across seven species.

2.8. References

Adams HD, Guardiola-Claramonte M, Barron-Gafford GA, Villegas JC, Breshears DD, Zou CB, Troch PA, Huxman TE. **2009**. Temperature sensitivity of drought-induced tree mortality portends increased regional die-off under global-change-type drought. *Proceedings of the National Academy of Sciences* **106**: 7063–7066.

Adams HD, Zeppel MJB, Anderegg WRL, Hartmann H, Landhäusser SM, Tissue DT, Huxman TE, Hudson PJ, Franz TE, Allen CD, *et al.* 2017. A multi-species synthesis of physiological mechanisms in drought-induced tree mortality. *Nature Ecology & Evolution* **1**: 1285–1291.

Alder NN, Pockman WT, Sperry JS, Nuismer S. **1997**. Use of centrifugal force in the study of xylem cavitation. *Journal of Experimental Botany* **48**: 665–674.

Bouche PS, Delzon S, Choat B, Badel E, Brodribb TJ, Burlett R, Cochard H, Charra-Vaskou K, Lavigne B, Li S, *et al.* 2016. Are needles of *Pinus pinaster* more vulnerable to xylem embolism than branches? New insights from X-ray computed tomography: Embolism resistance of pine needles. *Plant, Cell & Environment* **39**: 860–870.

Bouda M, Windt CW, McElrone AJ, Brodersen CR. **2019**. In vivo pressure gradient heterogeneity increases flow contribution of small diameter vessels in grapevine. *Nature Communications* **10**: 1–10.

Bourne AE, Creek D, Peters JMR, Ellsworth DS, Choat B. **2017**. Species climate range influences hydraulic and stomatal traits in Eucalyptus species. *Annals of Botany* **120**: 123–133.

Brodersen CR. **2013**. Visualizing wood anatomy in three dimensions with high-resolution X-ray micro-tomography (μCT) – a review –. *IAWA Journal* **34**: 408–424.

Brodersen CR, McElrone AJ, Choat B, Matthews MA, Shackel KA. **2010**. The Dynamics of Embolism Repair in Xylem: In Vivo Visualizations Using High-Resolution Computed Tomography. *PLANT PHYSIOLOGY* **154**: 1088–1095.

Brodribb TJ, Carriqui M, Delzon S, Lucani C. **2017**. Optical Measurement of Stem Xylem Vulnerability. *Plant Physiology* **174**: 2054–2061.

Brodribb TJ, Cochard H. **2009**. Hydraulic Failure Defines the Recovery and Point of Death in Water-Stressed Conifers. *Plant Physiology* **149**: 575–584.

Brodribb T, Hill RS. **1999**. The importance of xylem constraints in the distribution of conifer species. *New Phytologist* **143**: 365–372.

Brodribb TJ, Skelton RP, McAdam SAM, Bienaimé D, Lucani CJ, Marmottant P. **2016**. Visual quantification of embolism reveals leaf vulnerability to hydraulic failure. *New Phytologist* **209**: 1403–1409.

Choat B, Badel E, Burlett R, Delzon S, Cochard H, Jansen S. **2016**. Noninvasive Measurement of Vulnerability to Drought-Induced Embolism by X-Ray Microtomography. *Plant Physiology* **170**: 273–282.

Choat B, Brodersen CR, McElrone AJ. **2015**. Synchrotron X-ray microtomography of xylem embolism in *Sequoia sempervirens* saplings during cycles of drought and recovery. *New*

Phytologist **205**: 1095–1105.

Choat B, Brodribb TJ, Brodersen CR, Duursma RA, López R, Medlyn BE. **2018**. Triggers of tree mortality under drought. *Nature* **558**: 531–539.

Choat B, Drayton WM, Brodersen C, Mattthews MA, Shackel KA, Wada H, Mcelrone AJ. **2010**. Measurement of vulnerability to water stress-induced cavitation in grapevine: a comparison of four techniques applied to a long-vesseled species: Comparison of vulnerability curve technique in grapevine. *Plant, Cell & Environment* **33**: 1502–1512.

Choat B, Jansen S, Brodribb TJ, Cochard H, Delzon S, Bhaskar R, Bucci SJ, Feild TS, Gleason SM, Hacke UG, *et al.* 2012. Global convergence in the vulnerability of forests to drought. *Nature* **491**: 752–755.

Ciais Ph, Reichstein M, Viovy N, Granier A, Ogée J, Allard V, Aubinet M, Buchmann N, Bernhofer Chr, Carrara A, *et al.* 2005. Europe-wide reduction in primary productivity caused by the heat and drought in 2003. *Nature* **437**: 529–533.

Cochard H. **2002**. A technique for measuring xylem hydraulic conductance under high negative pressures. *Plant, Cell and Environment* **25**: 815–819.

Cochard H, Badel E, Herbette S, Delzon S, Choat B, Jansen S. **2013**. Methods for measuring plant vulnerability to cavitation: a critical review. *Journal of Experimental Botany* **64**: 4779–4791.

Cochard H, Damour G, Bodet C, Tharwat I, Poirier M, Améglio T. **2005**. Evaluation of a new centrifuge technique for rapid generation of xylem vulnerability curves. *Physiologia Plantarum* **124**: 410–418.

Cochard H, Delzon S, Badel E. **2015**. X-ray microtomography (micro-CT): a reference technology for high-resolution quantification of xylem embolism in trees: A reference method for xylem embolism. *Plant, Cell & Environment* **38**: 201–206.

Cochard H, Herbette S, Barigah T, Badel E, Ennajeh M, Vilagrosa A. **2010**. Does sample length influence the shape of xylem embolism vulnerability curves? A test with the Cavitron spinning technique: Shape of xylem embolism vulnerability curves. *Plant, Cell & Environment* **33**: 1543–1552.

Cumming G, Fidler F, Vaux DL. **2007**. Error bars in experimental biology. *Journal of Cell Biology* **177**: 7–11.

De Baerdemaeker NJF, Arachchige KNR, Zinkernagel J, Van den Bulcke J, Van Acker J, Schenk HJ, Steppe K. **2019**. The stability enigma of hydraulic vulnerability curves: addressing the link between hydraulic conductivity and drought-induced embolism. *Tree Physiology* **39**: 1646–1664.

Duke NC, Kovacs JM, Griffiths AD, Preece L, Hill DJE, van Oosterzee P, Mackenzie J, Morning HS, Burrows D. **2017**. Large-scale dieback of mangroves in Australia. *Marine and Freshwater Research* **68**: 1816.

Duursma R, Choat B. **2017**. fitplc - an R package to fit hydraulic vulnerability curves. *Journal of Plant Hydraulics* **4**: 002.

Duursma et Choat - 2017 - fitplc - an R package to fit hydraulic vulnerabili.pdf.

Ennajeh M, Nouiri M, Khemira H, Cochard H. **2011**. Improvement to the air-injection technique to estimate xylem vulnerability to cavitation. *Trees* **25**: 705–710.

Espino S, Schenk HJ. **2011**. Mind the bubbles: achieving stable measurements of maximum hydraulic conductivity through woody plant samples. *Journal of Experimental Botany* **62**: 1119–1132.

Hammond WM, Adams HD. **2019**. Dying on time: traits influencing the dynamics of tree mortality risk from drought. *Tree Physiology* **39**: 906–909.

Jacobsen AL, Rodriguez-Zaccaro FD, Lee TF, Valdovinos J, Toschi HS, Martinez JA, Pratt RB. **2015**. Grapevine Xylem Development, Architecture, and Function. In: Hacke U, ed. Functional and Ecological Xylem Anatomy. Cham: Springer International Publishing, 133–162.

Kim HK, Lee SJ. **2010**. Synchrotron X-ray imaging for nondestructive monitoring of sap flow dynamics through xylem vessel elements in rice leaves. *New Phytologist* **188**: 1085–1098.

Larter M, Pfautsch S, Domec J-C, Trueba S, Nagalingum N, Delzon S. **2017**. Aridity drove the evolution of extreme embolism resistance and the radiation of conifer genus *Callitris*. *New Phytologist* **215**: 97–112.

Ledger ME, Edwards FK, Brown LE, Milner AM, Woodward G. **2011**. Impact of simulated drought on ecosystem biomass production: an experimental test in stream mesocosms. *Global Change Biology* **17**: 2288–2297.

Li X, Blackman CJ, Choat B, Duursma RA, Rymer PD, Medlyn BE, Tissue DT. **2018**. Tree hydraulic traits are coordinated and strongly linked to climate-of-origin across a rainfall gradient: Hydraulic traits coordination and link to climate. *Plant, Cell & Environment* **41**: 646–660.

Li X, Delzon S, Torres-Ruiz J, Badel E, Burlett R, Cochard H, Jansen S, King A, Lamarque LJ, Lenoir N, *et al.* 2020. Lack of vulnerability segmentation in four angiosperm tree species: evidence from direct X-ray microtomography observation. *Annals of Forest Science* **77**.

Li Y, Sperry JS, Taneda H, Bush SE, Hacke UG. **2007**. Evaluation of centrifugal methods for measuring xylem cavitation in conifers, diffuse- and ring-porous angiosperms. *New Phytologist* **177**: 558–568.

López R, Nolf M, Duursma RA, Badel E, Flavel RJ, Cochard H, Choat B. **2019**. Mitigating the open vessel artefact in centrifuge-based measurement of embolism resistance. *Tree Physiology* **39**: 143–155.

Losso A, Bär A, Dämon B, Dullin C, Ganthaler A, Petruzzellis F, Savi T, Tromba G, Nardini A, Mayr S, *et al.* 2019. Insights from in vivo micro-CT analysis: testing the hydraulic vulnerability segmentation in *Acer pseudoplatanus* and *Fagus sylvatica* seedlings. *The New phytologist* **221**: 1831–1842.

McCutchan H, Shackel KA. **1992**. Stem-water Potential as a Sensitive Indicator of Water Stress in Prune Trees (*Prunus domestica* L. cv. French). *Journal of the American Society for Horticultural Science* **117**: 607–611.

McDowell N, Pockman WT, Allen CD, Breshears DD, Cobb N, Kolb T, Plaut J, Sperry J,

West A, Williams DG, *et al.* 2008. Mechanisms of plant survival and mortality during drought: why do some plants survive while others succumb to drought? *New Phytologist* **178**: 719–739.

McElrone AJ, Choat B, Parkinson DY, MacDowell AA, Brodersen CR. **2013**. Using High Resolution Computed Tomography to Visualize the Three Dimensional Structure and Function of Plant Vasculature. *JoVE (Journal of Visualized Experiments)*: e50162.

Michaelian M, Hogg EH, Hall RJ, Arsenault E. **2011**. Massive mortality of aspen following severe drought along the southern edge of the Canadian boreal forest. *Global change biology.* **17**: 2084–2094.

Mirone A, Brun E, Gouillart E, Tafforeau P, Kieffer J. **2014**. The PyHST2 hybrid distributed code for high speed tomographic reconstruction with iterative reconstruction and a priori knowledge capabilities. *Nuclear Instruments and Methods in Physics Research Section B: Beam Interactions with Materials and Atoms* **324**: 41–48.

Nardini A, Savi T, Trifilò P, Lo Gullo MA. **2017**. Drought Stress and the Recovery from Xylem Embolism in Woody Plants. In: Cánovas FM, Lüttge U, Matyssek R, eds. Progress in Botany Vol. 79. Cham: Springer International Publishing, 197–231.

Nolf M, Lopez R, Peters JMR, Flavel RJ, Koloadin LS, Young IM, Choat B. **2017**. Visualization of xylem embolism by X-ray microtomography: a direct test against hydraulic measurements. *New Phytologist* **214**: 890–898.

Paganin D, Mayo SC, Gureyev TE, Miller PR, Wilkins SW. **2002**. Simultaneous phase and amplitude extraction from a single defocused image of a homogeneous object. *Journal of Microscopy* **206**: 33–40.

Park Williams A, Allen CD, Macalady AK, Griffin D, Woodhouse CA, Meko DM, Swetnam TW, Rauscher SA, Seager R, Grissino-Mayer HD, *et al.* 2013. Temperature as a potent driver of regional forest drought stress and tree mortality. *Nature Climate Change* **3**: 292–297.

Petruzzellis F, Pagliarani C, Savi T, Losso A, Cavalletto S, Tromba G, Dullin C, Bär A, Ganthaler A, Miotto A, *et al.* 2018. The pitfalls of in vivo imaging techniques: evidence for cellular damage caused by synchrotron X-ray computed micro-tomography. *New Phytologist* **220**: 104–110.

Pittermann J. **2010**. The evolution of water transport in plants: an integrated approach. *Geobiology* **8**: 112–139.

Pockman WT, Sperry JS. **2000**. Vulnerability to xylem cavitation and the distribution of Sonoran Desert vegetation. *American Journal of Botany* **87**: 1287–1299.

Pratt RB, Castro V, Fickle JC, Jacobsen AL. **2019**. Embolism resistance of different aged stems of a California oak species (Quercus douglasii): optical and microCT methods differ from the benchtop-dehydration standard (M Ball, Ed.). *Tree Physiology*.

Pratt RB, Jacobsen AL. **2018**. Identifying which conduits are moving water in woody plants: a new HRCT-based method. *Tree Physiology* **38**: 1200–1212.

R Core Team. **2017**. R: A language and environment for statistical computing. *R Foundation for Statistical Computing, Vienna, Austria. URL https://www.R-project.org/.*

Rockwell FE, Wheeler JK, Holbrook NM. **2014**. Cavitation and Its Discontents: Opportunities for Resolving Current Controversies. *Plant Physiology* **164**: 1649–1660.

Rodriguez-Dominguez CM, Carins Murphy MR, Lucani C, Brodribb TJ. **2018**. Mapping xylem failure in disparate organs of whole plants reveals extreme resistance in olive roots. *New Phytologist* **218**: 1025–1035.

RStudio Team. **2015**. RStudio: Integrated Development for R. *RStudio, Inc., Boston, MA URL http://www.rstudio.com/*.

Savi T, Miotto A, Petruzzellis F, Losso A, Pacilè S, Tromba G, Mayr S, Nardini A. **2017**. Drought-induced embolism in stems of sunflower: A comparison of in vivo micro-CT observations and destructive hydraulic measurements. *Plant Physiology and Biochemistry* **120**: 24–29.

Schneider CA, Rasband WS, Eliceiri KW. **2012**. NIH Image to ImageJ: 25 years of Image Analysis. *Nature methods* **9**: 671–675.

Scholander PF, Hammel HT, Bradstreet ED, Hemmingsen EA. **1965**. Sap Pressure in Vascular Plants. *Science* **148**: 339–346.

Skelton RP, Dawson TE, Thompson SE, Shen Y, Weitz AP, Ackerly D. **2018**. Low Vulnerability to Xylem Embolism in Leaves and Stems of North American Oaks. *Plant Physiology* **177**: 1066–1077.

Sperry and Tyree - 1988 - Mechanism of Water Stress-Induced Xylem Embolism.pdf.

Sperry JS, Tyree MT. **1988**. Mechanism of Water Stress-Induced Xylem Embolism. *Plant Physiology* **88**: 581–587.

Torres-Ruiz JM, Cochard H, Choat B, Jansen S, López R, Tomášková I, Padilla-Díaz CM, Badel E, Burlett R, King A, *et al.* 2017. Xylem resistance to embolism: presenting a simple diagnostic test for the open vessel artefact. *New Phytologist* **215**: 489–499.

Torres-Ruiz JM, Cochard H, Mayr S, Beikircher B, Diaz-Espejo A, Rodriguez-Dominguez CM, Badel E, Fernández JE. **2014**. Vulnerability to cavitation in *Olea europaea* current-year shoots: further evidence of an open-vessel artifact associated with centrifuge and air-injection techniques. *Physiologia Plantarum* **152**: 465–474.

Torres-Ruiz JM, Jansen S, Choat B, McElrone AJ, Cochard H, Brodribb TJ, Badel E, Burlett R, Bouche PS, Brodersen CR, *et al.* 2015. Direct X-Ray Microtomography Observation Confirms the Induction of Embolism upon Xylem Cutting under Tension. *Plant Physiology* **167**: 40–43.

Trenberth KE, Dai A, van der Schrier G, Jones PD, Barichivich J, Briffa KR, Sheffield J. **2014**. Global warming and changes in drought. *Nature Climate Change* **4**: 17–22.

Tyree MT, Ewers FW. **1991**. The hydraulic architecture of trees and other woody plants. *New Phytologist* **119**: 345–360.

Tyree MT, Sperry JS. **1989**. Vulnerability of Xylem to Cavitation and Embolism. *Annual Review of Plant Physiology and Plant Molecular Biology* **40**: 19–36.

Urli M, Porté AJ, Cochard H, Guengant Y, Burlett R, Delzon S. **2013**. Xylem embolism

threshold for catastrophic hydraulic failure in angiosperm trees. *Tree Physiology* **33**: 672–683.

Venturas MD, Pratt RB, Jacobsen AL, Castro V, Fickle JC, Hacke UG. **2019**. Direct comparison of four methods to construct xylem vulnerability curves: Differences among techniques are linked to vessel network characteristics. *Plant, Cell & Environment* **42**: 2422–2436.

Warton DI, Duursma RA, Falster DS, Taskinen S. **2012**. smatr 3– an R package for estimation and inference about allometric lines. *Methods in Ecology and Evolution* **3**: 257–259.

Wheeler JK, Huggett BA, Tofte AN, Rockwell FE, Holbrook NM. **2013**. Cutting xylem under tension or supersaturated with gas can generate PLC and the appearance of rapid recovery from embolism: Sampling induced embolism. *Plant, Cell & Environment* **36**: 1938–1949.

Zhang F-P, Brodribb TJ. **2017**. Are flowers vulnerable to xylem cavitation during drought? *Proceedings of the Royal Society B: Biological Sciences* **284**: 20162642.

Chapter 3: Absence of embolism repair after long-term drought recovery observed with micro-computed tomography in *Eucalyptus saligna*

Submitted as: Gauthey, A., Peters, J.M., Lòpez, R., Carins-Murphy, M.R., Rodriguez-Dominguez, C.M., Tissue, D.T., Medlyn, B.E., Brodribb, T.J., Choat, B.

3.1. Abstract

The mechanisms by which woody plants recover xylem hydraulic capacity after drought stress are not well understood, particularly with regards to the role of embolism refilling. In this study, we evaluated the recovery of xylem hydraulic capacity in young *Eucalyptus saligna* plants exposed to cycles of drought stress and rewatering. Plants were exposed to moderate and severe drought stress treatments, with recovery monitored at time intervals from 24 hrs to 6 months after rewatering. The percentage loss of xylem vessels due to embolism (PLV) was quantified at each time point using non-invasive imaging (micro-computed tomography) with water potential (Ψ_x) and whole plant transpiration (E_{plant}) measured concurrently. Plants exposed to a moderate intensity drought treatment did not exhibit any increase in PLV and recovered Ψ_x and E_{plant} rapidly after rewatering. Plants exposed to severe drought stress suffered high levels of embolism (47.38 ± 10.97 % PLV) and almost complete canopy loss. No evidence of embolism refilling was observed at 24 hrs, one week, and three weeks after rewatering despite rapid recovery in Ψ_x. In fact, mean PLV increased after rewatering in both moderate and severe drought treatments. Recovery of hydraulic capacity was achieved over a 6 months period by growth of new xylem tissue, with canopy leaf area and E_{plant} recovering over the same period.

3.2. Introduction

Water is transported through the xylem as a liquid under tension (Tyree & Ewers, 1991; Tyree, 1997; Steudle, 2001). In this physical state, water may undergo cavitation, resulting in the formation of gas emboli and blockage of xylem conduits. Water stress causes tension in the xylem to increase, which leads to a higher probability of cavitation. Although the structure of the xylem has evolved to limit the impact of embolism, at a critical tension, embolism will begin to spread rapidly through the network of conduits leading to a sharp decrease in xylem hydraulic conductivity (Brodersen, 2013; Lens *et al.*, 2013; Knipfer *et al.*, 2015b). As a consequence, the capacity of plants to move water from the roots to the leaves is reduced, affecting leaf gas exchange and tissue hydration (Nardini *et al.*, 2003; Martorell *et al.*, 2014; Knipfer *et al.*, 2015b). During periods of severe water stress, embolism can lead to complete hydraulic failure in roots, stems and leaves, which has been linked to canopy dieback and whole plant mortality during drought.

Plants have developed a range of strategies to survive and recover from water stress, which include avoidance of water stress by stomatal regulation, leaf shedding, and access to ground water (Čermák *et al.*, 1980; Molyneux & Davies, 1983; Robichaux *et al.*, 1987; Cochard *et al.*, 1996; David *et al.*, 2013), or tolerance of water stress due to high resistance to cavitation, low turgor loss points and wider hydraulic safety margins (Choat *et al.*, 2012). However, regardless of strategy, when the xylem tension reaches critical thresholds set by cavitation resistance, blockage of xylem conduits by embolism will progressively reduce xylem hydraulic conductivity. Physiological mechanisms that restore xylem hydraulic capacity are a key component of recovery from drought stress.

A large body of research has focused on mechanisms that allow plants to refill embolized xylem conduits on short time scales (ca. 6-12 hrs), thus providing rapid recovery of hydraulic capacity after drought. The process of embolism repair (i.e. refilling) requires a mechanism by which gas is reabsorbed into the water and removed from xylem conduits. The exact physiological mechanisms responsible for refilling, and the prevalence of embolism repair across plant taxa, are issues that have been widely debated over the last 40 years (Sperry *et al.*, 1988; Borghetti *et al.*, 1991; Salleo *et al.*, 1996, 2009; Tyree *et al.*, 1999; Holbrook *et al.*, 2001; Zwieniecki & Holbrook, 2009; Brodersen *et al.*, 2010; Brodersen & McElrone, 2013). Pickard (1989) hypothesised that root pressure could dissolve gas bubbles during the night-time when transpiration was minimal and soil water availability was high. Springtime refilling is commonly observed in some plant species exposed to freezing conditions during winter, including vines and tree species that are known to generate strong positive root and stem pressures (Sperry *et al.*, 1987; Pockman & Sperry, 1997; Utsumi *et al.*, 1998; Ewers *et al.*, 2001; Cobb *et al.*, 2007; Mayr *et al.*, 2014; Christensen-Dalsgaard & Tyree, 2014). It is important to note that such springtime refilling is an adaptation to embolism caused by successive freeze-thaw cycles during winter and occurs in concert with major remobilisation of water and carbohydrates reserves after winter dormancy (Charrier *et al.*, 2013; Mayr *et al.*, 2014; Plavcová & Jansen, 2015). It is therefore distinct in a number of important ways from the proposed diurnal refilling process or refilling after drought stress during the growing season (Klein *et al.*, 2018).

Without conditions creating positive pressures throughout the xylem, refilling is difficult to explain in terms consistent with the laws of thermodynamics (Holbrook & Zwieniecki, 1999; Zwieniecki & Holbrook, 2009). However, several studies suggest that refilling under tension is not only possible, but could be used on a daily basis in certain species to repair embolised vessels (*Vitis vinifera*, Jacobsen & Pratt, 2012; *Quercus gambelii,* Taneda and Sperry, 2008).

A number of theories have been advanced to explain refilling under tension, with most centring on osmotic activity of xylem parenchyma cells adjacent to embolised conduits and the isolation of refilling conduits from the transpiration stream (Clearwater & Goldstein, 2005; Salleo *et al.*, 2009; Zwieniecki & Holbrook, 2009; Nardini *et al.*, 2011; Brodersen & McElrone, 2013). Observations suggest that refilling takes places over a period of hours, allowing restoration of xylem function within relatively short time periods (Nardini *et al.*, 2011). An alternative mechanism of recovery is the growth of new xylem tissue. In this case, recovery of hydraulic capacity would occur over much longer time frame (weeks, months) and require significantly more investment of carbon. In conifer species, two studies have demonstrated that recovery of hydraulic capacity after severe drought stress is facilitated by growth of new xylem tissue rather than refilling of embolised tracheids 25/11/21 10:26:00 am.

The application of non-invasive imaging techniques allowed researchers to visualise refilling in intact plants, including observations based on Magnetic Resonance Imaging (MRI) (Holbrook *et al.*, 2001; Zwieniecki *et al.*, 2013) and micro computed tomography (microCT) (Brodersen *et al.*, 2010; Ryu *et al.*, 2016; Gleason *et al.*, 2017; Secchi *et al.*, 2020). These studies have provided evidence of embolism repair in a limited number of species (grapevine, maize, poplar) capable of producing strong root pressure (Charrier *et al.*, 2016). However, other studies using MRI and microCT have provided evidence that refilling does not occur after drought, despite water potentials recovering to pre-drought levels on short time scales (Clearwater & Clark, 2003; Brodribb *et al.*, 2010; Choat *et al.*, 2015; Knipfer *et al.*, 2015b; Johnson *et al.*, 2018; Choat *et al.*, 2018). Additionally, there is evidence that observations of refilling based on hydraulic (flow-based) measurements may be flawed because of experimental artefacts relating to excision of samples under tension (Wheeler *et al.*, 2013; Torres-Ruiz *et al.*, 2015; Lamarque *et al.*, 2018). This work has raised questions regarding the generality of

embolism repair mechanisms across plant taxa and the processes that plants use to recover hydraulic capacity in the absence of refilling.

In this study, we used microCT visualisation to investigate whether refilling is a routine mechanism of recovery from drought stress in the evergreen tree species, *Eucalyptus saligna*. In a recent study utilising microCT, we observed partial refilling in a small fraction of embolised vessels in *Eucalyptus saligna* plants recovering from drought stress, although this did not result in a significant decrease in the number of embolised vessels over all (Choat *et al.*, 2019). However, two studies have also suggested that X-ray damage caused by microCT scans may impact xylem physiological function, including mechanisms of embolism refilling that rely on the metabolic activity of living cells in the xylem (Savi *et al.*, 2017; Petruzzellis *et al.*, 2018). In order to address this issue and avoid artefacts associated with X-ray damage, data in the current study were acquired from single scans of multiple replicate plants, rather than repeated scans on individual plants. Recovery of hydraulic capacity, plant water status, and canopy transpiration rates were evaluated in plants exposed to moderate drought (MD) and severe drought (SD) stress over time scales ranging from 24 hrs to 6 months. Monitoring recovery over longer time periods allowed us to examine embolism refilling and growth of new xylem tissue as alternative mechanisms of recovery.

3.3. Materials and methods

Plant material

Eucalyptus saligna (Sydney Blue Gum) is fast growing tree species used extensively in timber plantations. It is native to mesic areas along the eastern coast of Australia in New South Wales and Queensland and is vulnerable to drought relative to other *Eucalyptus* species (Bourne *et al.*, 2017). Thirty-three plants were purchased from PlantPlus Cumberland forest nursery

(Pennant Hills, NSW, Australia). Plants were grown in 4 litres plastic pots, using potting mix from the original nursery and were kept in a sunlit poly-tunnel on the Hawkesbury Campus of Western Sydney University (Richmond, NSW, Australia) for a few weeks. Plants were approximately 1-year-old and 1 meter in height at the beginning of the experiment. The experiment commenced in September 2017 and finished in March 2018.

Drought treatment

A first subset of plants were allocated to 2 different treatments: (1) medium drought (MD) (n=5) in which plants were dried to a water potential target of ~ -2 MPa and were then rewatered, (2) severe drought (SD) (n=9) in which plants were dried to a water potential target of ~ -3.5 MPa and were then rewatered. These water potential targets were based on previous studies (Bourne *et al.*, 2017; Choat *et al.*, 2019) and were expected to induce complete stomatal closure and ~10% PLC in MD and ~50% PLC in SD. Whole canopy transpiration rate (E_{plant}) and bagged leaf water potential (Ψ_x) were tracked during the drydown and the recovery for these two treatments (Fig. S3-1).

The two drought treatments allowed us to assess recovery of leaf gas exchange as a function of the severity of the water stress (minimum water potential reached) and the impact on theoretical hydraulic conductivity. All plants were kept in a sunlit polytunnel for three weeks prior to the start of drought treatments. In order to impose uniform conditions during the application of drought treatments, individuals assigned to MD and SD treatments were moved to a controlled environment chamber (Thermoline, Australia) maintained at 21°C constant temperature with a 11h/13h light/dark cycle with a photon flux density of 700 µmols m^{-2} s^{-1} and 60% relative humidity. Water was withheld from plants until the desired Ψ_x for each treatment was reached. At this point, plants were moved to a second growth chamber and E_{plant} was measured (see

details below). Plants were returned to the poly-tunnel during the recovery phase and watered daily to maintain high plant and soil water status.

In order to address issues regarding the impacts of X-ray radiation on xylem physiological processes raised in recent studies (Savi *et al.*, 2017; Petruzzellis *et al.*, 2018), the majority of plants included in this experiment were scanned only once. In this experimental design, changes in the number of embolised vessels at different time points were measured on separate cohorts of individuals, rather than by repeated measurements on individual plants. While this approach does not allow changes in the status of individual vessels to be tracked, it avoids any potential impacts of X-ray radiation on the activity of living parenchyma cells within the xylem, which theoretically drive embolism refilling. As such, a second subset of plants (n=19) was assigned to allow for micro-CT visualisation of xylem tissue at different points during drought and recovery treatments. Groups of plants scanned in this manner were assigned to well-watered (n=4), dried to MD (n=5), dried to SD (n=5), and dried to MD and rewatered 24 hours (R24h) before scanning (n=5). After initial scans, the well-watered group of plant was scanned three further times to allow for construction of a dehydration vulnerability curve (see below). Previous work has demonstrated that multiple scans on individual plants do not alter vulnerability curves (Choat *et al.*, 2016; Gauthey *et al.*, 2020). Canopy transpiration rates and water potential were recorded for each replicate plant immediately before microCT scans took place. In order to track long-term recovery from drought, SD individuals from the first plant subset were scanned after 3 weeks (R3wk) (n=5) and 6 months (R6mo) of recovery (n=4) after rewatering (Fig. S3.1).

Physiological and morphological measurements

Bagged leaf water potential (Ψ_x) was measured by sealing a leaf in plastic film, covered in aluminium foil, for a minimum of 30 min before excision and measurement (Choat *et al.*, 2010, 2016). Leaves were slowly pressurized with a Scholander pressure chamber (PMS Instrument Company, Albany, OR, USA) until water was visible on the cut end of the leaf (Scholander *et al.*, 1965). Two to three leaves (or small branch tips when leaves became too dry) per individual were measured for each water potential measurement. When Ψ_x could not be measured using the pressure chamber method because of canopy leaf loss, Ψ_x was assessed using PSY1 Stem Psychrometer sensor coupled with a microvolt data logger used to store data **(**ICT International, Armidale, NSW, Australia).

A separate growth-chamber was used to measure canopy transpiration rate (E_{plant}) throughout the experiment. The chamber environmental conditions were maintained at 25°C, constant light intensity of 700 μmols m^{-2} s^{-1} and 60% relative humidity during measurement periods. Plants were placed on a precision balance with a resolution of 0.1g (MS8001TS, Mettler-Toledo, Columbus, OH, USA) connected to a data logger (CR1000, Campbell Scientific, UT, USA). Changes in weight were recorded with LoggerNet software (Campbell Scientific, UT, USA). Prior to measurements, a plastic bag was sealed around the pots to cover the soil and minimise soil evaporation. Weight was logged from the balance every minute for a 1 to 2 hr period per plant with differences in weight attributed to plant water loss. Whole canopy transpiration rate (g hr^{-1}) was calculated as the slope of a linear regression between plant water loss and time. Throughout the experiment, the canopy leaf area was recorded by counting the number of mature leaves on each plant. A relationship between leaf number, weight and area was established to allow calculation of total canopy leaf area at each time point.

Micro-CT scans

MicroCT visualisations were undertaken at the Australian Synchrotron (Clayton, VIC, Australia) Imaging and Medical Beamline (IMBL) during two periods: late October of 2017 and early March of 2018. Samples were positioned in the beam using a robotic arm (Kuka, KR1000 Titan) and scanned at the main stem axis with a field of view of 28 mm x 20 mm. Scans were conducted at an X-ray energy of 30 keV, while the sample was rotated through 180 degrees using continuous rotation; images were recorded at 0.1° angle increments. This yielded 1800 projections with additional flat-field and dark-field images recorded before and after each scan. Exposure time at each angle was 0.45–0.60 s giving a total scan time of 18–23 min. Scan volumes were reconstructed using XLICT Workflow 2015 (CSIRO) using either the Gridrec or FBP (Paganin *et al.*, 2002) reconstruction algorithm. The final resolution of images was 9.7 μm per voxel. MicroCT images provided good contrast between water-filled (grey) and air-filled (black) vessels. Image analysis was performed on a median scan (10 middle scans were compressed to make a single scan) by counting embolised vessels (darker than water-filled ones) using the 'Threshold' and 'Analyse Particles' functions in ImageJ, or by counting vessels manually using the "multi-point" action (Nolf *et al.*, 2017). Percentage of loss of vessels (PLV) was calculated for each scan image following:

$$PLV = \frac{Number\ of\ vessels\ embolised}{Total\ number\ of\ vessels} \times 100$$

The strong correlation between PLV and PLC is supported by numerous studies (Gauthey *et al.*, 2020; Li *et al.*, 2020; Peters *et al.*, 2020) which suggests that loss of conductivity in this species can be approximated by counting gas filled vessels.

In order to estimate what percentage of new xylem was regrown after rewatering, we used cross-sections of the 6 months recovery plants to analyse the area of xylem occupied by newly

grown xylem or older xylem. Images were processed with ImageJ where pit and bark were removed and old and new xylem area where calculated.

Vulnerability curve

Three vulnerability curves (VCs) were generated using PLV and Ψ_x measurements from plants in drought and recovery treatments. The first VC was fitted to data from plants that were scanned during the dehydration phase (dehydration curve). Plants that were scanned during recovery (i.e. after being rewatered for a set amount of time) were plotted at the Ψ_x values measured after rehydration (rehydration points). These rehydration points were also transposed to the minimum Ψ_x that the plant reached before rewatering, and a second VC was fitted to these data (transposition curve). A third VC was fit to the combined dehydration and transposition datasets.

Statistical analysis

All statistical analyses were conducted with R 3.1.2 (R Core Team, 2017) using RStudio (RStudio Team, 2015). Comparison of the physiological and morphological traits between the two treatments were tested for significant differences with a one-way ANOVA. Analyses were conducted on untransformed data which were normally distributed. Vulnerability curves were fit to PLA using the *fitplc* package following methods developed by Duursma & Choat (2017). Curves were fit with a Weibull function and the mean P_{50} and confidence intervals were extracted using a standard profiling method. For these methods, a 95% CI for the estimate of P_{50} was generated using a bootstrapping approach with 2000 resamples. To test for significant differences between vulnerability curves (dehydration and transposition), we generated a

bootstrap confidence intervals (CIs) for the difference in estimates of P_{50} for each dataset (Gauthey *et al.*, 2020).

3.4. Results

Dynamics of transpiration and plant water status

At the commencement of the experiment, plants in the SD treatment had high mean stem water potential (Ψ_x = -0.44 ± 0.02 MPa) and a mean E_{plant} of 48.34 ± 2.65 g hr^{-1} (Fig. 3-1). As SD plants were dehydrated to a mean Ψ_x of -2.11 ± 0.21 MPa, stomata closed and E_{plant} was sharply reduced to 15.73 ± 3.03 g hr^{-1}. When plants reached the severe drought target water potential (Ψ_x = -3.17 ± 0.17 MPa), E_{plant} was further reduced to 1.89 ± 0.25 g hr^{-1}. At this time point, leaves on all plants in the SD treatment had become severely wilted. Upon release from drought, stem water status slowly recovered to Ψ_x = -2.1 ± 0.33 MPa at 24 hr after rewatering and to Ψ_x = -1.34 ± 0.42 MPa at 1 week after rewatering. During this time, the majority of plants in the SD treatment experienced complete canopy loss (100% leaf death) and E_{plant} remained unchanged at 1.3 ± 0.28 g hr^{-1}. By 3 weeks after rewatering, Ψ_x had recovered to -0.37 ± 0.07 MPa, excluding one individual that did not recover after rewatering (Ψ_x = -5.00 MPa). At 3 weeks post drought, two plants had recovered a small proportion (~30%) of their initial canopy area, while most other individuals were in the initial phases of resprouting from epicormic buds; mean E_{plant} remained low at 2.98 ± 1.7 g hr^{-1}. Over the longer term, plants from the SD treatment fully recovered water status, canopy leaf area, and transpiration rate. At 18 weeks post drought, with mean Ψ_x = -0.58 ± 0.08 MPa and mean E_{plant} of 44.85 ± 7.46 g hr^{-1}. In all long-term recovery plants, some proportion of main stem axis had died, and recovery of leaf area occurred from growth of new branches and from epicormic buds. After 6 months under well-watered conditions, plants had 1.3 to 2.4 fold higher canopy leaf area and significantly higher canopy

transpiration rates (E_{plant} = 78.95 ± 5.29 g hr^{-1}) than at the time of initial measurements, while plant water status remained high (Ψ_x = -0.56 ± 0.04 MPa) (Fig. 3-1B and 3-1D). When transpiration rate was expressed on a leaf area basis (E_c), it was slightly, although not significantly, lower than at the initial measurement point (Fig. S3-2).

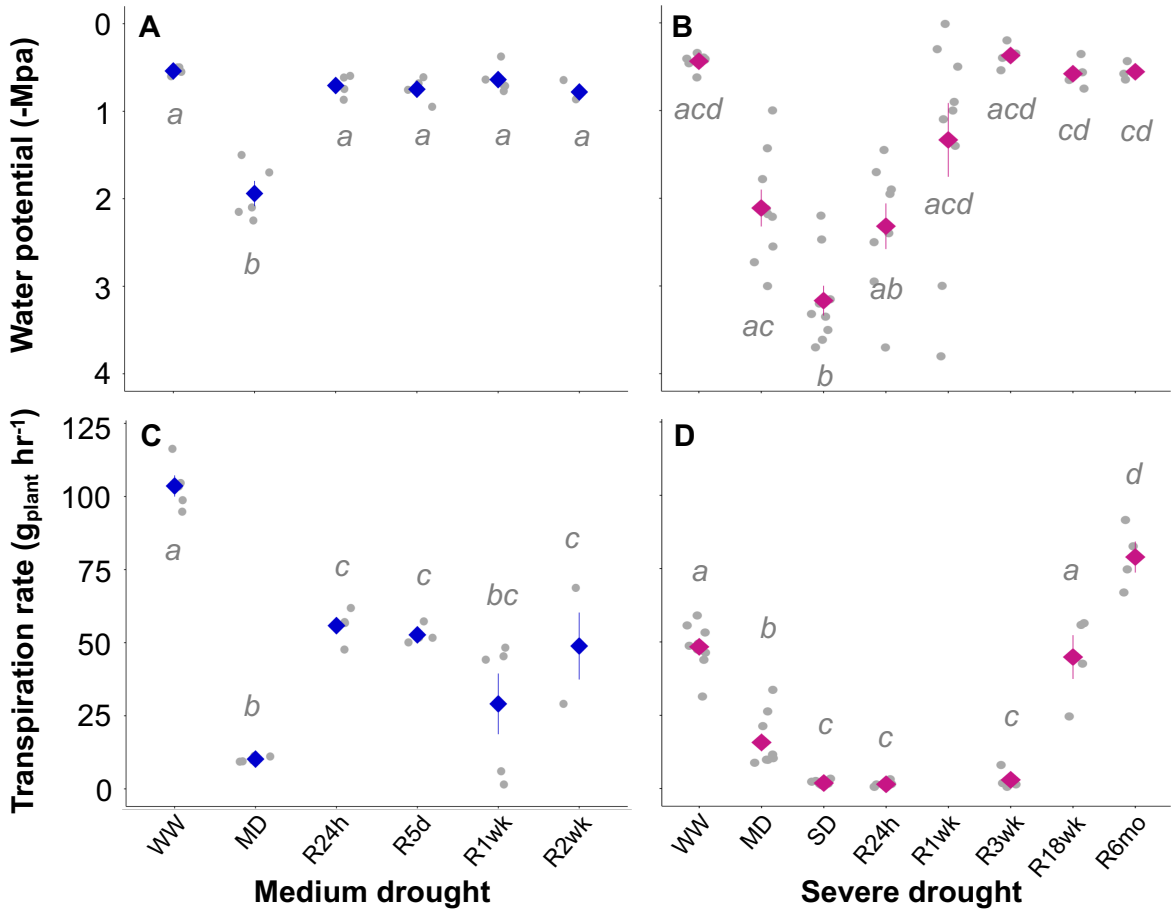

Figure 3- 1 Mean (± SE) water potential (-MPa) and transpiration rate per plant (g h-1) according to the treatment (medium drought in blue n=5; severe drought in magenta n=9) and the time of measurement. Different letters highlight the significant differences within drought treatments from the Tukey test. Grey points represent individual sapling.

In the MD treatment, stomatal closure reduced E_{plant} from an initial rate of 103.59 ± 3.62 g hr^{-1} to 10.19 ± 0.42 g hr^{-1} at the peak of the drought treatment (Ψ_x = -1.94 ± 0.14 MPa) (Fig. 3-1A and C). No canopy loss and only mild wilting was observed at the peak of this moderate drought stress treatment. At 24 hrs after rewatering, MD plants had recovered close to their initial pre-treatment water status (Ψ_x = -0.90 ± 0.20 MPa), while E_{plant} had recovered to approximately

half of initial values (55.82 ± 2.96 g hr^{-1}) in all but one individual, for which E_{plant} was 3.93 g hr^{-1}. Mean E_{plant} remained unchanged 5 days after rewatering, at 52.68 ± 1.57 g hr^{-1} for four individuals and 5.02 g hr^{-1} for one outlier. At 10 days after rewatering, two individuals experienced approximately 90% loss of canopy leaf area, leading to sharply lower E_{plant} (3.75 ± 2.23 g hr^{-1}) for these two individuals compared to a mean E_{plant} of 45.96 ± 1.20 g hr^{-1} for the three individuals that retained their full canopies. At 2 weeks after rewatering, the three plants with canopy remaining had a mean E_{plant} of 48.86 ± 11.45 g hr^{-1} and mean Ψ_x of -0.78 ± 0.07 MPa (Fig. 3-1A and C).

Refilling observation

Well-watered plant exhibited negligible levels of native embolism for both the SD and MD treatments (Figs. 3-2 and 3-3).

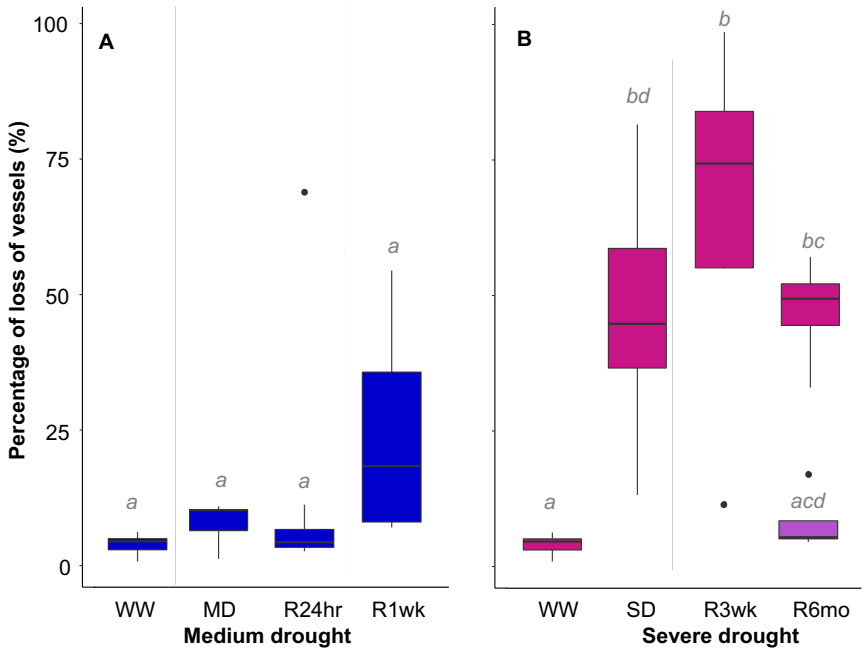

Figure 3- 2 Mean (± SE) percentage loss of vessels (PLV) at different time points (WW: well-water; MD: medium drought; R24hr:recovery 24 hours; R1wk: recovery 1 week; R3wk: recovery 3 weeks; R6mo: recovery 6 months) during two treatments (A. medium drought, blue; B. severe drought, magenta). Grey points are individual saplings. PLV after 6 months recovery is shown as the PLV of the total stem cross-section in magenta, and the PLV of only the new ring of xylem in purple.

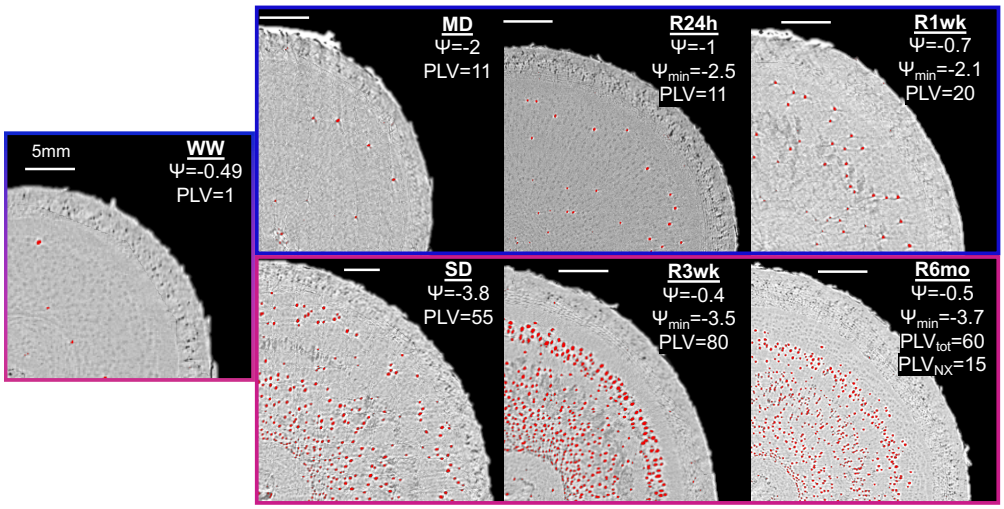

Figure 3- 3 Micro-CT scans of Eucalyptus saligna at different times during dry down and recovery. At left, well-watered (WW) treatment. In blue (top panel), medium drought treatment (medium drought MD, recovery at 24 hours R24h and recovery at 1-week R1w). In magenta (bottom panel), severe drought treatment (severe drought SD, recovery at 3 weeks R3wk, recovery at 6 months R6mo). Red dots highlight the embolised vessels. The corresponding water potential and PLC are indicated on each image. For the recovery treatment, Ψmin corresponds to the most negative water potential reached by the plant before rewatering. For the 6 months recovery, PLVtot is the PLC inside the whole cross section and PLVNX is the PLC measured in the new xylem ring.

In the SD treatment, PLV increased to 47.38 ± 10.97 % at the peak of the drought (Ψ_x = -3.26 ± 0.15 MPa). After rewatering in the SD treatment, the lack of transpiration due to leaf shedding and a well-watered soil were expected to offer favourable conditions for refilling. However, at 3 weeks after rewatering, mean PLV was 64.72 ± 18.71 %, higher than PLV recorded for SD plants at the peak of drought stress. After six months under well water conditions, plants exposed to severe drought treatment retained very high levels of embolism in xylem that had been exposed to the severe drought treatment (Fig. 3-2B). New xylem growth with relatively few embolised vessels surrounded the core of embolised vessels in the old xylem (Fig. 3-4).

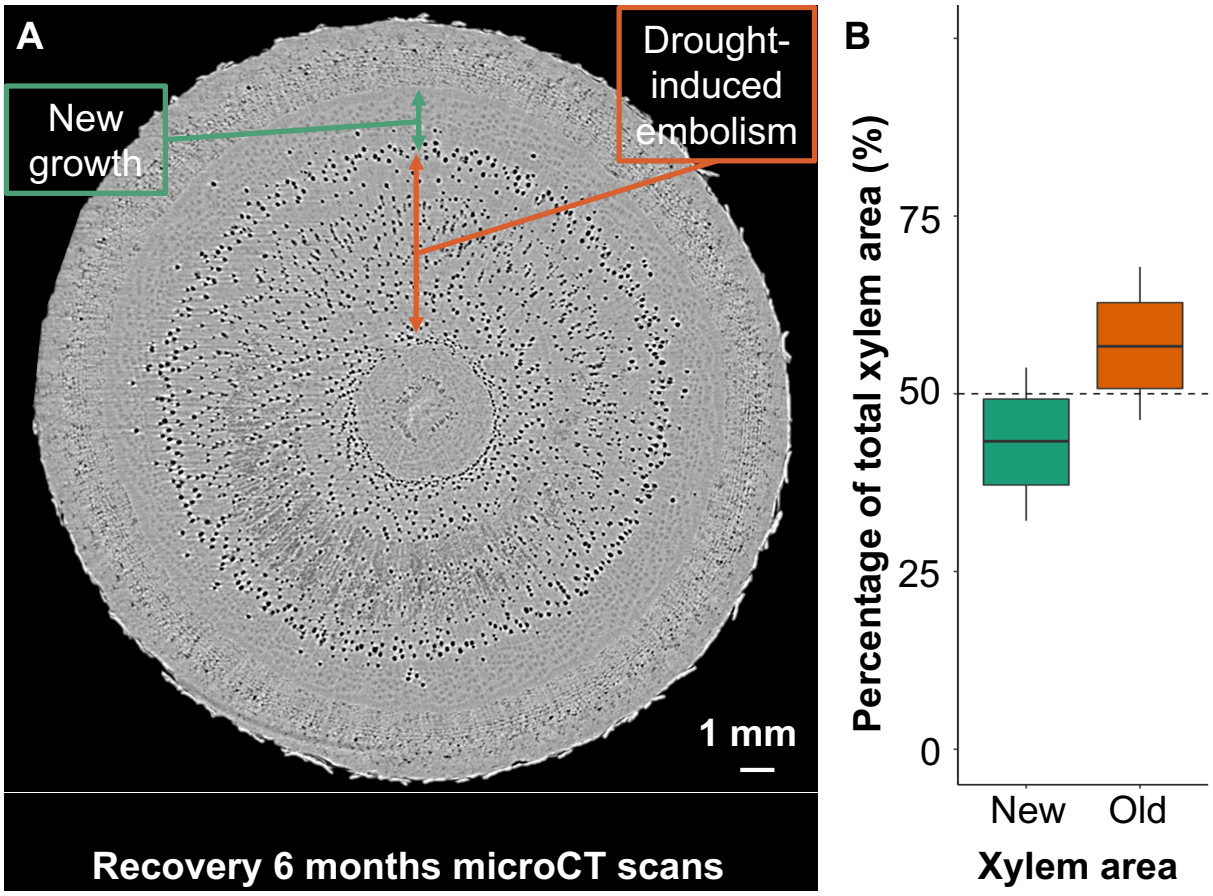

Figure 3- 4 Micro-CT scan of Eucalyptus saligna after 6 months recovery from severe drought stress (B). The xylem previously embolised by drought stress is highlighted in orange and the new ring of xylem responsible for the restoration of conductivity is highlighted in green. Percentage of xylem area occupied by the new growth is nearly 50% of the total xylem area (n=4) (A).

MicroCT visualisation allowed us to quantify the level of embolism in the old xylem and the new xylem grown during the 6 months recovery period. This analysis yielded a mean PLV of xylem 8.01 ± 2.99 % for the new ring and mean PLV of 47.22 ± 5.10 % for the whole stem cross section (Fig. 3-2).

MicroCT visualisations indicated that the MD treatment (Ψ_x = -1.98 ± 0.17 MPa) resulted in a small increase in the number of embolised vessels (PLV of 7.8 ± 1.83 %), although this was not significantly different from native embolism in well-watered plants. In samples exposed to a MD treatment (Ψ_x = -2.02 ± 0.21 MPa) and then allowed to recover for 24 hours, the PLV

was 4.98 ± 0.11 %, which was not significantly different from PLV observed for the MD treatment. However, in plants allowed to recover for one week after MD, the number of embolised vessels was significantly higher (PLV = 24.64 ± 9.02 %) than that observed for MD or 24 hours recovery treatments (Fig. 3-4A). It is notable that this increase was primarily due to higher PLV in two individuals, which were also the only plants to suffer significant canopy leaf loss as a result of the MD treatment (see above). The occurrence of higher PLV in plants that had been recovering from MD or SD treatments for 1 week and 3 weeks, respectively, was an unexpected result that could not be explained by differences in the minimum water potential reached in different treatments.

No evidence of embolism repair was observed in microCT scans during the recovery period, regardless of drought stress intensity (MD or SD) or the time length of recovery (Fig. 3-2). Where recovery in hydraulic capacity did occur, it was over longer time frames (6 months) and was due to growth of new xylem tissue rather than embolism repair (Figs. 3-4 and 3-5).

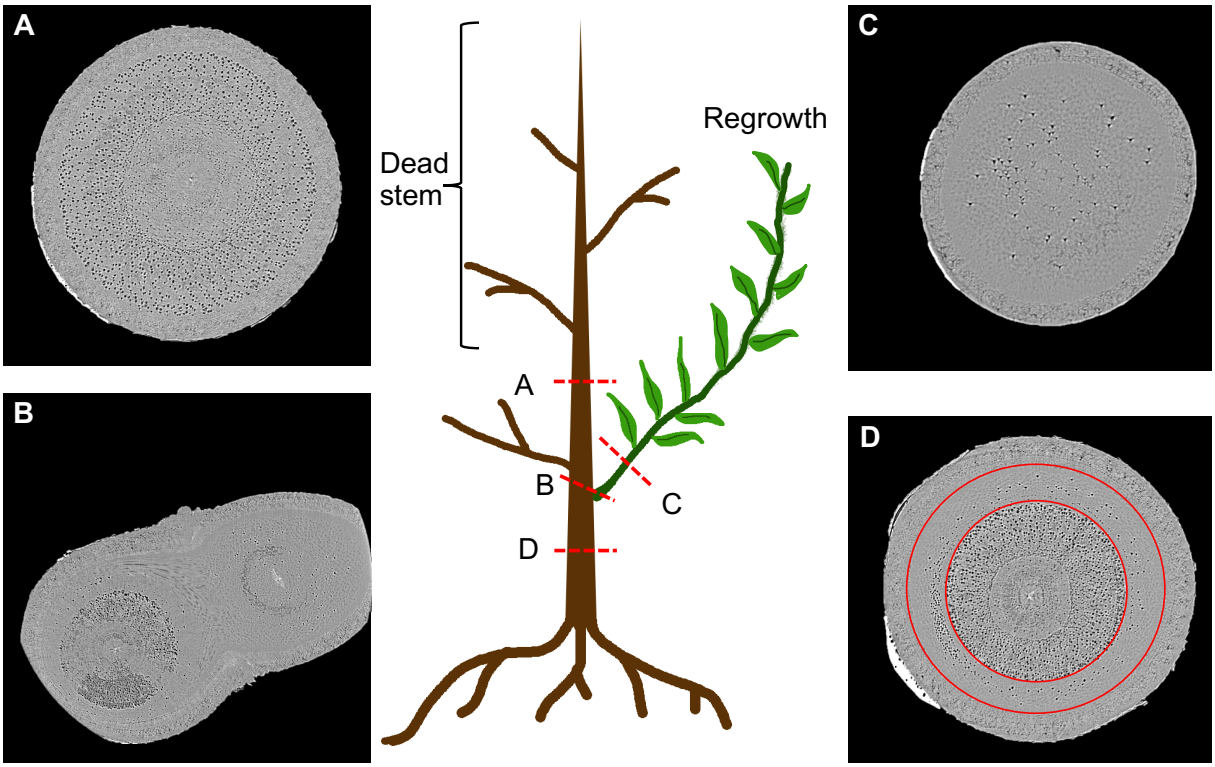

Figure 3- 5 MicroCT scans along the plant axis of an individual after 6 months of recovery. In this individual, the upper stem died after severe drought and a new shoot was regrown after rewatering. A. Dead upper stem remains embolised. B. Pathway to upper stem remains embolised; functional xylem leads to shoot regrowth shown in C. D. Conductivity at stem base has been re-established by growing a new ring of xylem (shown in red) rather than by refilling the vessels.

Vulnerability curves

The hydraulic vulnerability curves during drought (VC_D) indicated that saplings were mildly resistant with a P_{50} = -3.3 MPa. To further examine evidence of refilling, we developed vulnerability curves following recovery (VC_R) by plotting the PLC of recovered plants versus the minimum water potential that they experienced during drought. We predicted that if the VC_R and VC_D were similar, then xylem refilling was unlikely to have occurred. The VC_R exhibited a P_{50} of -3.1 MPa, which was not significantly different from the P_{50} estimated from the VC_D. This provides evidence that embolism which occurred as a result of drought stress treatments was preserved in the xylem even after rewatering for a number of weeks (Fig. 3-6).

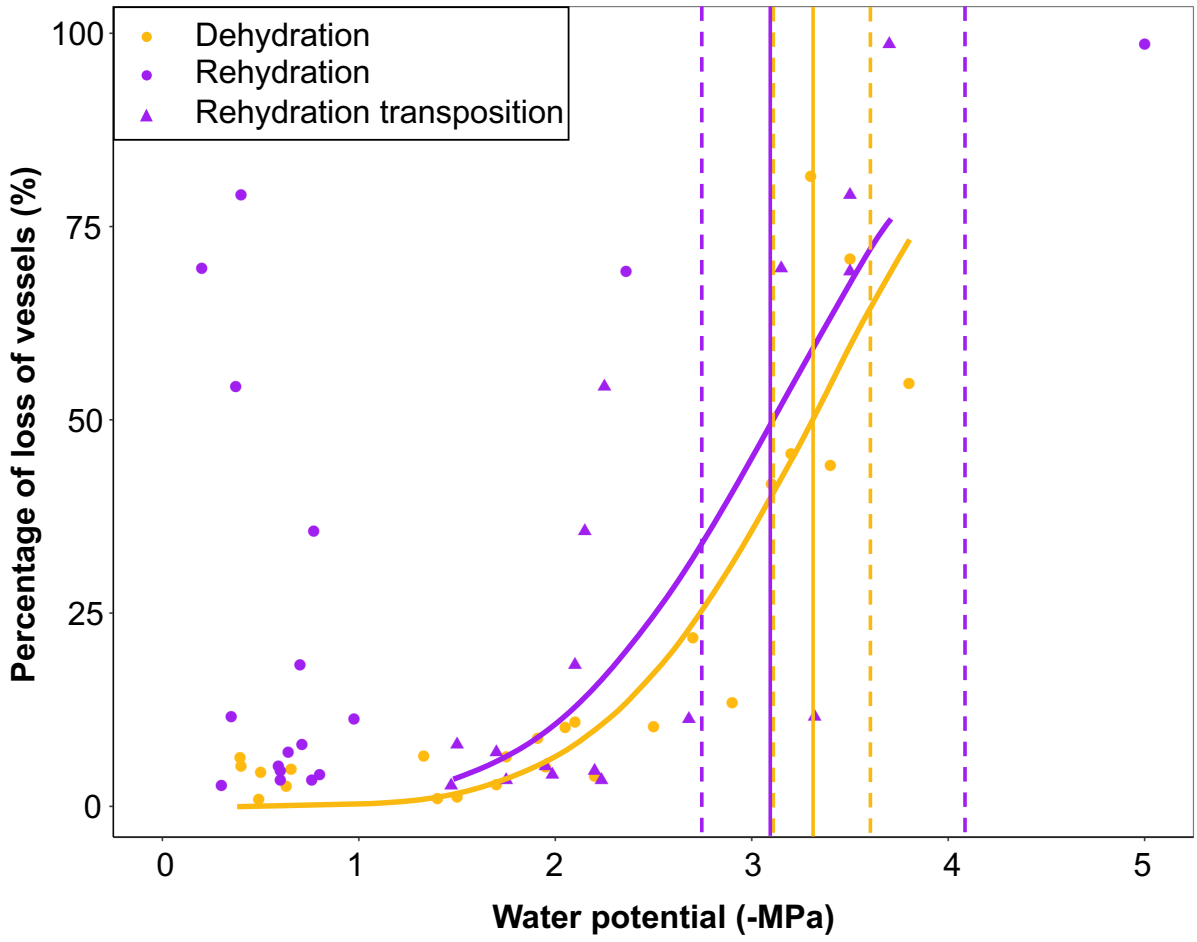

Figure 3- 6 Percentage loss of vessels as a function of (stem water potential) at different time points. VCD is constructed from dehydration points (yellow) and VCR transposed rehydration triangles (purple). Purple points represent samples that were dried and rewatered after 24h, 1 week or 3 weeks. Purple triangles show the same PEV as the purple points but are transposed to the most negative water potential reached by the individual before rewatering. The purple curve (VCR) was constructed from these last triangles. The vertical solid lines indicate the P50 values corresponding to the vulnerability curves and the two dashed lines represent the 95% confidence interval.

3.5. Discussion

We observed that recovery of xylem hydraulic capacity from severe water stress and high levels of xylem embolism was facilitated by growth of new xylem rather than embolism refilling in a diffuse porous angiosperm species, *Eucalyptus saligna*. Despite recovery in plant water potential after irrigation, microCT observations of embolism in the stem xylem revealed no evidence of embolism repair between 24 hrs and 3 weeks after water stress was relieved. Over

longer time periods (6 months), plants recovered xylem hydraulic capacity by growth of new xylem, while the older xylem remained embolised and non-functional. Whole plant transpiration rates recovered over this time period in proportion to re-expansion of canopy leaf area following rewatering. In plants that were subjected to moderate water stress, reductions in whole plant transpiration were observed, indicating stomatal closure, but there was no significant increase in mean PLV relative to pre-drought values. Plant water status and whole plant transpiration recovered rapidly after irrigation in the majority of MD plants, with individuals that suffered higher levels of embolism exhibiting more limited recovery. Despite numerous studies suggesting that refilling can occur under low tensions in the xylem, we did not observe embolism repair in MD or SD treatments, even when xylem water potentials recovered to high values (> -0.5 MPa). These results provide further evidence that embolism refilling may not be a widespread mechanism of hydraulic recovery in woody plants following drought stress events.

Previous experimental work provides contrasting evidence regarding the extent of embolism repair during recovery from drought. While some studies suggest that refilling is a routine process that occurs on diurnal timescales (Canny, 1997), other studies indicate that refilling does not play a major role in the recovery of xylem hydraulic capacity after drought (Clearwater & Clark, 2003; Brodribb *et al.*, 2010; Choat *et al.*, 2015; Knipfer *et al.*, 2015b; Hammond *et al.*, 2019; Choat *et al.*, 2019). Similarly, our micro-CT observations demonstrated that embolism repair did not occur in *E. saligna*, regardless of water stress intensity or time period after rewatering (Figs. 3-4 and 3-5). The introduction of non-invasive imaging techniques has provided opportunities to examine the refilling process in unprecedented spatial and temporal detail, while avoiding artefacts associated with destructive sampling (Holbrook *et al.*, 2001; Brodersen *et al.*, 2010). However, a number of studies that utilize non-invasive imaging techniques have shown limited evidence of refilling after drought in angiosperm and

gymnosperm species (Choat *et al.*, 2015; Knipfer *et al.*, 2015b; Choat *et al.*, 2018; Lamarque *et al.*, 2018; Rehschuh *et al.*, 2020).

While non-invasive methods have many advantages in the study of xylem function, recent work has highlighted potential artefacts associated with microCT studies of embolism repair (Savi *et al.*, 2017; Petruzzellis *et al.*, 2018). Expose to high doses of X-ray radiation during image acquisition have been observed to cause rapid cell death in some plant species. If mechanisms of embolism repair involve living cells in the xylem, which seems most likely, there is clear potential that X-rays may damage these living cells and inhibit refilling. Here, we eliminated the potential for tissue damage from microCT scans by using cohorts of plants, with each individual scanned once, rather than rescanning the same individuals many times during the experiment. While we could not track the status of individual vessels using this approach, it did allow us to assess the refilling mechanism by determining (a) differences in mean PLV values between treatments, and (b) the presence or absence of partially refilled vessels in the scans of recovering plants. Based on these observations, we concluded that no repair mechanism was operating in *E. saligna* during recovery from drought stress.

Recovery of hydraulic capacity in the 6-month recovery treatment was achieved by growth of new xylem tissue, rather than refilling of existing xylem. This finding is consistent with studies that have tracked recovery in conifer species over long time periods (~11 weeks) using dye staining techniques (Brodribb et al., 2010; Hammond et al., 2019). In the SD treatment, we found that 50-98% of vessels were embolised due to water stress, while plants in the MD treatment exhibited minimal embolism in the majority of replicates. Over the 6-month recovery period, microCT visualisation revealed that a new ring of xylem had formed outside the older xylem, in which the vast majority of vessels remained embolised. The newly formed xylem contained low levels of embolism and was of equivalent cross-sectional area to the older xylem (Fig. 3-6). These results demonstrate that recovery of xylem capacity occurred via growth of

new xylem over a period of months, rather than by a refilling mechanism that repaired embolisms on a shorter time scale. The mechanism and rate of recovery observed in *E. saligna* has implications for our understanding of the overall 'cost' of xylem embolism to woody plants and for process-based models that simulate recovery of woody vegetation after drought.

Interestingly, in the MD and SD treatments, the proportion of embolised vessels increased after rewatering; despite recovery of Ψ_x, the proportion of embolised vessels was higher after 1-3 weeks of recovery. This surprising and counter-intuitive result suggests embolism may continue to spread through the xylem network even after drought stress has been relieved. In the MD 1-week recovery treatment, two individuals suffered almost complete canopy loss after appearing to have initially recovered at 24hrs post drought. Notably, these two individuals also suffered significantly higher PLV compared with the three other plants in the treatment block that maintained canopy. In the 3-week recovery time point, the higher mean PLV was driven primarily by one individual that never recovered Ψ_x, suggesting that it died as a result of the severe drought treatment. The high PLV observed for some individuals at 1 and 3 weeks after rewatering has important implications for our understanding of mortality and canopy dieback processes in the field. In some instances, trees exposed to severe drought die well after being released from drought stress by significant rainfall events (Mueller *et al.*, 2005; Breshears *et al.*, 2009; Gu *et al.*, 2015; Matusick *et al.*, 2016). This has been interpreted by some as evidence that water stress and hydraulic failure and not playing a significant role in mortality (Gu *et al.*, 2015), however, the high level of embolism retained in stems post drought, and the possibility that this can spread further within the xylem while canopy transpiration is recovering, suggest that hydraulic injury continues to play a major role in mortality processes even after plant water status has improved.

In terms of vulnerability to embolism, leaf turgor loss, and stomatal regulation during drought, *E. saligna* is sensitive to water stress relative to other *Eucalyptus* species (Bourne et al. 2017).

Consistent with this, E_{plant} declined rapidly as a result of stomatal closure with the onset of drought stress in both SD and MD treatments. This decrease in E_{plant} occurred prior to embolism formation and is consistent with previous studies showing that stomatal closure is coordinated to protect the plant from catastrophic spread of embolism within the xylem (Cochard *et al.*, 1996; Irvine *et al.*, 1998; Bartlett *et al.*, 2016; Martin-StPaul *et al.*, 2017). In the MD treatment, E_{plant} recovered to approximately half of pre-treatment values 24 hrs after rewatering and remained at this level for 2 weeks after rewatering, despite full recovery of plant water status within 24 hrs (Fig. 3-3). The post drought reduction in E_{plant} relative to pre-drought values observed for the MD treatment was not associated with xylem hydraulic limitations in three of the individuals, since PLV remained low in these plants. However, it is notable that one individual never recovered E_{plant}; this plant had higher PLV and shed its canopy 1 week after rewatering commenced. The dynamics of recovery in the MD plants provides evidence that elevated levels of xylem embolism lead to slower recovery of leaf gas exchange, consistent with other studies on this topic (Resco *et al.*, 2009; Brodribb *et al.*, 2010; Skelton *et al.*, 2017). In the absence of increased embolism, reduced transpiration rates after drought likely reflects enhanced water use efficiency, which is commonly observed after moderate drought treatments (Pou *et al.*, 2008; Martorell *et al.*, 2014).

The SD treatment induced high levels of stem embolism and complete canopy loss in the majority of individuals exposed to this level of drought stress (ca. -3.7 MPa), despite *E. saligna* having evergreen leaf phenology. Leaf shedding has been proposed as a "hydraulic fuse" allowing plants to reduce canopy transpiration and the probability of runaway embolism in stem xylem (Tyree *et al.*, 1993; Pineda-García *et al.*, 2013; Hochberg *et al.*, 2017). It could also be that leaf water potential declined to more negative values than measured for stem water potential, leading to catastrophic embolism within the leaf and subsequent leaf mortality (Cardoso *et al.*, 2020). In SD plants, E_{plant} recovered as plants were re-expanding leaf area, and

it was therefore difficult to assess the role that hydraulic limitation in the stem xylem played in recovery of leaf gas exchange. However, transpiration rates normalised to leaf area (E_c) were lower than pre-treatment levels at 3-weeks post rewatering, suggesting limitations to recovery caused by hydraulic dysfunction (Fig. S3-2). By 18 weeks after the SD treatment, E_c had recovered close to pre-treatment levels and this value remained unchanged at the 6 months recovery time point. This long-term recovery in transpiration rates was associated with growth of new xylem, as seen in microCT visualisation (Figs. 3-3, 3-4 and 3-5).

3.6. Conclusions

Our data demonstrate that recovery of xylem hydraulic capacity after a severe drought treatment was effected by growth of new xylem tissue rather than refilling of embolised vessels. There was no evidence of embolism repair, regardless of drought treatment (moderate or severe) or time point after rewatering. Over a time period of 6 months, plants exposed to severe drought stress recovered from complete canopy loss and very high levels of stem embolism. This is consistent with the ecology of *Eucalyptus* species, which are well adapted to recover from extreme drought stress by re-sprout from epicormic buds following canopy dieback. As such, our results suggest that slow recovery from catastrophic levels of embolism by growth of new xylem tissue is the most likely mechanism for Eucalypt species following a severe drought. These data suggest are consistent with recent studies suggesting that embolism repair is not a common mechanism of recovery in woody plants after drought recovery (Clearwater & Clark, 2003; Brodribb *et al.*, 2010; Knipfer *et al.*, 2015a). However, other studies have provided evidence of embolism repair mechanisms, with some data suggesting that these mechanisms can operate while the xylem is under mild tension (Holbrook *et al.*, 2001; Hacke & Sperry, 2003; Brodersen *et al.*, 2010; Yang *et al.*, 2012). Clearly, we require further studies that address the impact of variable intensity and duration droughts, and the following recovery periods, to

determine whether xylem refilling is an important or common physiological process across woody species.

3.7. Supplementary figures

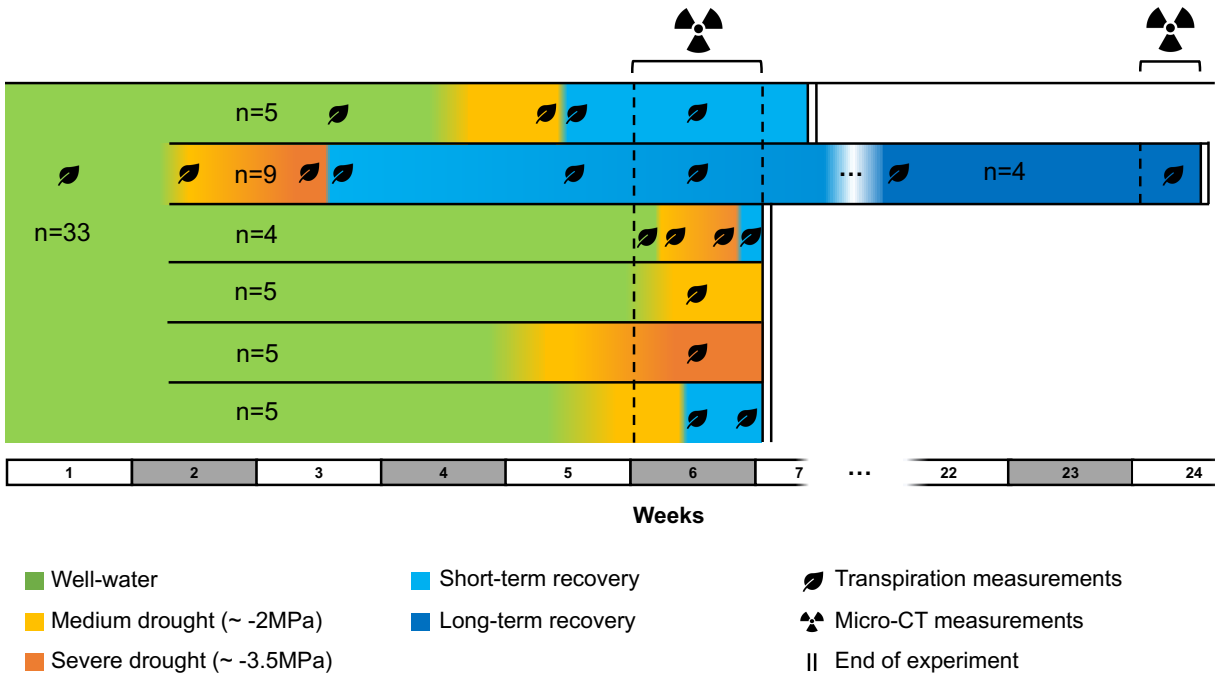

Figure S3- 9 Description of the experimental timeline of the watering treatments throughout the different stages of the experiment. At the beginning, all plants were kept well- watered. We formed five cohorts of plants. The first cohort was submitted to a cycle of mild drought and long-term recovery. The second cohort was submitted to a cycle of severe drought and long-term recovery. The third one was submitted to a severe drought and short-term recovery. The fourth cohort was submitted to a severe drought. The fifth one was submitted to a mild drought and short-term recovery. Transpiration rate and embolism (via microCT) measurements were carried on all cohorts of plants in order to cover the whole period of drought and recovery.

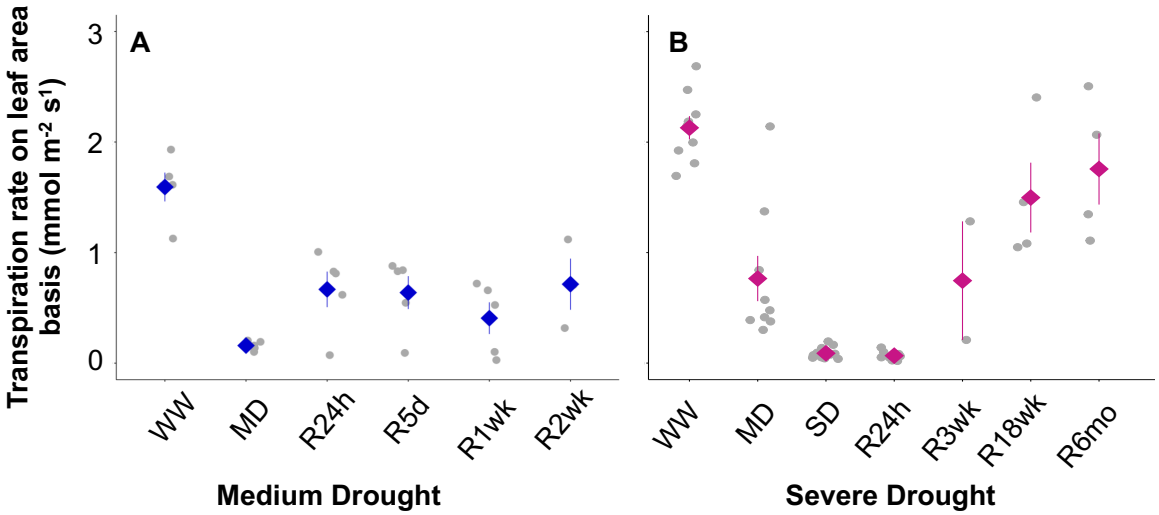

Figure S3- 2 Transpiration rate on leaf area basis (mmol m-2 s1) at different timepoints during medium drought (blue) and severe drought (magenta).

3.8. References

Bartlett MK, Klein T, Jansen S, Choat B, Sack L. **2016**. The correlations and sequence of plant stomatal, hydraulic, and wilting responses to drought. *Proceedings of the National Academy of Sciences* **113**: 13098–13103.

Borghetti M, Edwards WRN, Grace J, Jarvis PG, Raschi A. **1991**. The refilling of embolized xylem in Pinus sylvestris L. *Plant, Cell & Environment* **14**: 357–369.

Bourne AE, Creek D, Peters JMR, Ellsworth DS, Choat B. **2017**. Species climate range influences hydraulic and stomatal traits in Eucalyptus species. *Annals of Botany* **120**: 123–133.

Breshears DD, Myers OB, Meyer CW, Barnes FJ, Zou CB, Allen CD, McDowell NG, Pockman WT. **2009**. Tree die-off in response to global change-type drought: mortality insights from a decade of plant water potential measurements. *Frontiers in Ecology and the Environment* **7**: 185–189.

Brodersen CR. **2013**. Visualizing wood anatomy in three dimensions with high-resolution X-ray micro-tomography (μCT) – a review –. *IAWA Journal* **34**: 408–424.

Brodersen CR, McElrone AJ. **2013**. Maintenance of xylem Network Transport Capacity: A Review of Embolism Repair in Vascular Plants. *Frontiers in Plant Science* **4**.

Brodersen CR, McElrone AJ, Choat B, Matthews MA, Shackel KA. **2010**. The Dynamics of Embolism Repair in Xylem: In Vivo Visualizations Using High-Resolution Computed Tomography. *PLANT PHYSIOLOGY* **154**: 1088–1095.

Brodribb TJ, Bowman DJMS, Nichols S, Delzon S, Burlett R. **2010**. Xylem function and growth rate interact to determine recovery rates after exposure to extreme water deficit. *New Phytologist* **188**: 533–542.

Canny MJ. **1997**. Vessel contents during transpiration—embolisms and refilling. *American Journal of Botany* **84**: 1223–1230.

Cardoso AA, Batz TA, McAdam SAM. **2020**. Xylem Embolism Resistance Determines Leaf Mortality during Drought in *Persea americana*. *Plant Physiology* **182**: 547–554.

Čermák J, Huzulák J, Penka M. **1980**. Water potential and sap flow rate in adult trees with moist and dry soil as used for the assessment of root system depth. *Biologia Plantarum* **22**: 34–41.

Charrier G, Cochard H, Améglio T. **2013**. Evaluation of the impact of frost resistances on potential altitudinal limit of trees. *Tree Physiology* **33**: 891–902.

Charrier G, Torres-Ruiz JM, Badel E, Burlett R, Choat B, Cochard H, Delmas CEL, Domec J-C, Jansen S, King A, *et al.* 2016. Evidence for Hydraulic Vulnerability Segmentation and Lack of Xylem Refilling under Tension. *Plant Physiology* **172**: 1657–1668.

Choat B, Badel E, Burlett R, Delzon S, Cochard H, Jansen S. **2016**. Noninvasive Measurement of Vulnerability to Drought-Induced Embolism by X-Ray Microtomography. *Plant Physiology* **170**: 273–282.

Choat B, Brodersen CR, McElrone AJ. **2015**. Synchrotron X-ray microtomography of xylem

embolism in *Sequoia sempervirens* saplings during cycles of drought and recovery. *New Phytologist* **205**: 1095–1105.

Choat B, Brodribb TJ, Brodersen CR, Duursma RA, López R, Medlyn BE. **2018**. Triggers of tree mortality under drought. *Nature* **558**: 531–539.

Choat B, Drayton WM, Brodersen C, Mattthews MA, Shackel KA, Wada H, Mcelrone AJ. **2010**. Measurement of vulnerability to water stress-induced cavitation in grapevine: a comparison of four techniques applied to a long-vesseled species: Comparison of vulnerability curve technique in grapevine. *Plant, Cell & Environment* **33**: 1502–1512.

Choat B, Jansen S, Brodribb TJ, Cochard H, Delzon S, Bhaskar R, Bucci SJ, Feild TS, Gleason SM, Hacke UG, *et al.* 2012. Global convergence in the vulnerability of forests to drought. *Nature* **491**: 752–755.

Choat B, Nolf M, Lopez R, Peters JMR, Carins-Murphy MR, Creek D, Brodribb TJ. **2019**. Non-invasive imaging shows no evidence of embolism repair after drought in tree species of two genera. *Tree Physiology* **39**: 113–121.

Christensen-Dalsgaard KK, Tyree MT. **2014**. Frost fatigue and spring recovery of xylem vessels in three diffuse-porous trees *in situ*: Frost fatigue in diffuse-porous trees. *Plant, Cell & Environment* **37**: 1074–1085.

Clearwater MJ, Clark CJ. **2003**. In vivo magnetic resonance imaging of xylem vessel contents in woody lianas. *Plant, Cell & Environment* **26**: 1205–1214.

Clearwater MJ, Goldstein G. **2005**. 18 - Embolism Repair and Long Distance Water Transport. In: Holbrook NM, Zwieniecki MA, eds. Physiological Ecology. Vascular Transport in Plants. Burlington: Academic Press, 375–399.

Cobb AR, Choat B, Holbrook NM. **2007**. Dynamics of freeze–thaw embolism in Smilax rotundifolia (Smilacaceae). *American Journal of Botany* **94**: 640–649.

Cochard H, Bréda N, Granier A. **1996**. Whole tree hydraulic conductance and water loss regulation in Quercus during drought: evidence for stomatal control of embolism? *Annales des Sciences Forestières* **53**: 197–206.

David TS, Pinto CA, Nadezhdina N, Kurz-Besson C, Henriques MO, Quilhó T, Cermak J, Chaves MM, Pereira JS, David JS. **2013**. Root functioning, tree water use and hydraulic redistribution in Quercus suber trees: A modeling approach based on root sap flow. *Forest Ecology and Management* **307**: 136–146.

Ewers FW, Ameglio T, Cochard H, Beaujard F, Martignac M, Vandame M, Bodet C, Cruiziat P. **2001**. Seasonal variation in xylem pressure of walnut trees: root and stem pressures. *Tree Physiology* **21**: 1123–1132.

Gauthey A, Peters JMR, Carins-Murphy MR, Rodriguez-Dominguez CM, Li X, Delzon S, King A, López R, Medlyn BE, Tissue DT, *et al.* 2020. Visual and hydraulic techniques produce similar estimates of cavitation resistance in woody species. *New Phytologist* **228**: 884–897.

Gleason SM, Wiggans DR, Bliss CA, Young JS, Cooper M, Willi KR, Comas LH. **2017**. Embolized Stems Recover Overnight in Zea mays: The Role of Soil Water, Root Pressure, and Nighttime Transpiration. *Frontiers in Plant Science* **8**.

Gu L, Pallardy SG, Hosman KP, Sun Y. **2015**. Drought-influenced mortality of tree species with different predawn leaf water dynamics in a decade-long study of a central US forest. *Biogeosciences* **12**: 2831–2845.

Hacke UG, Sperry JS. **2003**. Limits to xylem refilling under negative pressure in Laurus nobilis and Acer negundo. *Plant, Cell and Environment* **26**: 303–311.

Hammond WM, Yu K, Wilson LA, Will RE, Anderegg WRL, Adams HD. **2019**. Dead or dying? Quantifying the point of no return from hydraulic failure in drought-induced tree mortality. *New Phytologist* **223**: 1834–1843.

Hochberg U, Windt CW, Ponomarenko A, Zhang Y-J, Gersony J, Rockwell FE, Holbrook NM. **2017**. Stomatal Closure, Basal Leaf Embolism, and Shedding Protect the Hydraulic Integrity of Grape Stems. *Plant Physiology* **174**: 764–775.

Holbrook NM, Ahrens ET, Burns MJ, Zwieniecki MA. **2001**. In Vivo Observation of Cavitation and Embolism Repair Using Magnetic Resonance Imaging. *Plant Physiology* **126**: 27–31.

Holbrook NM, Zwieniecki MA. **1999**. Embolism Repair and Xylem Tension: Do We Need a Miracle? **120**: 4.

Irvine J, Perks MP, Magnani F, Grace J. **1998**. The response of Pinus sylvestris to drought: stomatal control of transpiration and hydraulic conductance. *Tree Physiology* **18**: 393–402.

Jacobsen AL, Pratt RB. **2012**. No evidence for an open vessel effect in centrifuge-based vulnerability curves of a long-vesselled liana (Vitis vinifera). *New Phytologist* **194**: 982–990.

Johnson KM, Jordan GJ, Brodribb TJ. **2018**. Wheat leaves embolized by water stress do not recover function upon rewatering. *Plant, Cell & Environment* **41**: 2704–2714.

Klein T, Zeppel MJB, Anderegg WRL, Bloemen J, De Kauwe MG, Hudson P, Ruehr NK, Powell TL, von Arx G, Nardini A. **2018**. Xylem embolism refilling and resilience against drought-induced mortality in woody plants: processes and trade-offs. *Ecological Research*.

Knipfer T, Brodersen CR, Zedan A, Kluepfel DA, McElrone AJ. **2015a**. Patterns of drought-induced embolism formation and spread in living walnut saplings visualized using X-ray microtomography. *Tree Physiology* **35**: 744–755.

Knipfer T, Eustis A, Brodersen C, Walker AM, Mcelrone AJ. **2015b**. Grapevine species from varied native habitats exhibit differences in embolism formation/repair associated with leaf gas exchange and root pressure: Contrasting response of wild grapevines to drought stress. *Plant, Cell & Environment* **38**: 1503–1513.

Lamarque LJ, Corso D, Torres-Ruiz JM, Badel E, Brodribb TJ, Burlett R, Charrier G, Choat B, Cochard H, Gambetta GA, *et al.* 2018. An inconvenient truth about xylem resistance to embolism in the model species for refilling Laurus nobilis L. *Annals of Forest Science* **75**: 88.

Lens F, Tixier A, Cochard H, Sperry JS, Jansen S, Herbette S. **2013**. Embolism resistance as a key mechanism to understand adaptive plant strategies. *Current Opinion in Plant Biology* **16**: 287–292.

Li X, Delzon S, Torres-Ruiz J, Badel E, Burlett R, Cochard H, Jansen S, King A,

Lamarque LJ, Lenoir N, *et al.* 2020. Lack of vulnerability segmentation in four angiosperm tree species: evidence from direct X-ray microtomography observation. *Annals of Forest Science* **77**.

Martin-StPaul N, Delzon S, Cochard H. **2017**. Plant resistance to drought depends on timely stomatal closure. *Ecology Letters* **20**: 1437–1447.

Martorell S, Diaz-Espejo A, Medrano H, Ball MC, Choat B. **2014**. Rapid hydraulic recovery in Eucalyptus pauciflora after drought: linkages between stem hydraulics and leaf gas exchange. *Plant, Cell & Environment* **37**: 617–626.

Matusick G, Ruthrof KX, Fontaine JB, Hardy GESJ. **2016**. Eucalyptus forest shows low structural resistance and resilience to climate change-type drought. *Journal of Vegetation Science* **27**: 493–503.

Mayr S, Schmid P, Laur J, Rosner S, Charra-Vaskou K, Dämon B, Hacke UG. **2014**. Uptake of Water via Branches Helps Timberline Conifers Refill Embolized Xylem in Late Winter. *Plant Physiology* **164**: 1731–1740.

Molyneux DE, Davies WJ. **1983**. Rooting pattern and water relations of three pasture grasses growing in drying soil. *Oecologia* **58**: 220–224.

Mueller RC, Scudder CM, Porter ME, Trotter RT, Gehring CA, Whitham TG. **2005**. Differential tree mortality in response to severe drought: evidence for long-term vegetation shifts. *Journal of Ecology* **93**: 1085–1093.

Nardini A, Lo Gullo MA, Salleo S. **2011**. Refilling embolized xylem conduits: Is it a matter of phloem unloading? *Plant Science* **180**: 604–611.

Nardini A, Salleo S, Raimondo F. **2003**. Changes in leaf hydraulic conductance correlate with leaf vein embolism in Cercis siliquastrum L. *Trees - Structure and Function* **17**: 529–534.

Nolf M, Lopez R, Peters JMR, Flavel RJ, Koloadin LS, Young IM, Choat B. **2017**. Visualization of xylem embolism by X-ray microtomography: a direct test against hydraulic measurements. *New Phytologist* **214**: 890–898.

Paganin D, Mayo SC, Gureyev TE, Miller PR, Wilkins SW. **2002**. Simultaneous phase and amplitude extraction from a single defocused image of a homogeneous object. *Journal of Microscopy* **206**: 33–40.

Peters JMR, Gauthey A, Lopez R, Carins-Murphy MR, Brodribb TJ, Choat B. **2020**. Non-invasive imaging reveals convergence in root and stem vulnerability to cavitation across five tree species (H Griffiths, Ed.). *Journal of Experimental Botany*.

Petruzzellis F, Pagliarani C, Savi T, Losso A, Cavalletto S, Tromba G, Dullin C, Bär A, Ganthaler A, Miotto A, *et al.* 2018. The pitfalls of in vivo imaging techniques: evidence for cellular damage caused by synchrotron X-ray computed micro-tomography. *New Phytologist* **220**: 104–110.

Pineda-García F, Paz H, Meinzer FC. **2013**. Drought resistance in early and late secondary successional species from a tropical dry forest: the interplay between xylem resistance to embolism, sapwood water storage and leaf shedding: Drought resistance of tropical dry forest species. *Plant, Cell & Environment* **36**: 405–418.

Plavcová L, Jansen S. **2015**. The Role of Xylem Parenchyma in the Storage and Utilization of Nonstructural Carbohydrates. In: Hacke U, ed. Functional and Ecological Xylem Anatomy. Cham: Springer International Publishing, 209–234.

Pockman WT, Sperry JS. **1997**. Freezing-induced xylem cavitation and the northern limit of Larrea tridentata. *Oecologia* **109**: 19–27.

Pou A, Flexas J, Alsina M del M, Bota J, Carambula C, Herralde FD, Galmés J, Lovisolo C, Jiménez M, Ribas-Carbó M, *et al.* 2008. Adjustments of water use efficiency by stomatal regulation during drought and recovery in the drought-adapted Vitis hybrid Richter-110 (V. berlandieri × V. rupestris). *Physiologia Plantarum* **134**: 313–323.

R Core Team. **2017**. R: A language and environment for statistical computing. *R Foundation for Statistical Computing, Vienna, Austria. URL https://www.R-project.org/.*

Rehschuh R, Cecilia A, Zuber M, Faragó T, Baumbach T, Hartmann H, Jansen S, Mayr S, Ruehr N. **2020**. Drought-Induced Xylem Embolism Limits the Recovery of Leaf Gas Exchange in Scots Pine. *Plant Physiology* **184**: 852–864.

Resco V, Ewers BE, Sun W, Huxman TE, Weltzin JF, Williams DG. **2009**. Drought-induced hydraulic limitations constrain leaf gas exchange recovery after precipitation pulses in the C3 woody legume, Prosopis velutina. *New Phytologist* **181**: 672–682.

Robichaux RH, Grace J, Rundel PW, Ehleringer JR. **1987**. Plant Water Balance. *BioScience* **37**: 30–37.

RStudio Team. **2015**. RStudio: Integrated Development for R. *RStudio, Inc., Boston, MA URL http://www.rstudio.com/.*

Ryu J, Hwang BG, Lee SJ. **2016**. In vivo dynamic analysis of water refilling in embolized xylem vessels of intact Zea mays leaves. *Annals of Botany* **118**: 1033–1042.

Salleo S, Gullo MAL, Paoli D, Zippo M. **1996**. Xylem recovery from cavitation-induced embolism in young plants of Laurus nobilis: a possible mechanism. *New Phytologist* **132**: 47–56.

Salleo S, Trifilò P, Esposito S, Nardini A, Gullo MAL. **2009**. Starch-to-sugar conversion in wood parenchyma of field-growing Laurus nobilis plants: a component of the signal pathway for embolism repair? *Functional Plant Biology* **36**: 815–825.

Savi T, Miotto A, Petruzzellis F, Losso A, Pacilè S, Tromba G, Mayr S, Nardini A. **2017**. Drought-induced embolism in stems of sunflower: A comparison of in vivo micro-CT observations and destructive hydraulic measurements. *Plant Physiology and Biochemistry* **120**: 24–29.

Scholander PF, Hammel HT, Bradstreet ED, Hemmingsen EA. **1965**. Sap Pressure in Vascular Plants. *Science* **148**: 339–346.

Secchi F, Pagliarani C, Cavalletto S, Petruzzellis F, Tonel G, Savi T, Tromba G, Obertino MM, Lovisolo C, Nardini A, *et al.* 2020. Chemical inhibition of xylem cellular activity impedes the removal of drought-induced embolisms in poplar stems – new insights from micro-CT analysis. *New Phytologist* **n/a**.

Skelton RP, Brodribb TJ, McAdam SAM, Mitchell PJ. **2017**. Gas exchange recovery

following natural drought is rapid unless limited by loss of leaf hydraulic conductance: evidence from an evergreen woodland. *New Phytologist* **215**: 1399–1412.

Sperry JS, Donnelly JR, Tyree MT. **1988**. Seasonal Occurrence of Xylem Embolism in Sugar Maple (Acer saccharum). *American Journal of Botany* **75**: 1212–1218.

Sperry JS, Holbrook NM, Zimmermann MH, Tyree MT. **1987**. Spring Filling of Xylem Vessels in Wild Grapevine. *PLANT PHYSIOLOGY* **83**: 414–417.

Steudle E. **2001**. The Cohesion-Tension Mechanism and the Acquisition of Water by Plant Roots. *Annual Review of Plant Physiology and Plant Molecular Biology* **52**: 847–875.

Taneda H, Sperry JS. **2008**. A case-study of water transport in co-occurring ring- versus diffuse-porous trees: contrasts in water-status, conducting capacity, cavitation and vessel refilling. *Tree Physiology* **28**: 1641–1651.

Torres-Ruiz JM, Jansen S, Choat B, McElrone AJ, Cochard H, Brodribb TJ, Badel E, Burlett R, Bouche PS, Brodersen CR, *et al.* 2015. Direct X-Ray Microtomography Observation Confirms the Induction of Embolism upon Xylem Cutting under Tension. *Plant Physiology* **167**: 40–43.

Tyree MT. **1997**. The Cohesion-Tension theory of sap ascent: current controversies. *Journal of Experimental Botany* **48**: 1753–1765.

Tyree MT, Cochard H, Cruiziat P, Sinclair B, Ameglio T. **1993**. Drought-induced leaf shedding in walnut: evidence for vulnerability segmentation. *Plant, Cell & Environment* **16**: 879–882.

Tyree MT, Ewers FW. **1991**. The hydraulic architecture of trees and other woody plants. *New Phytologist* **119**: 345–360.

Tyree MT, Salleo S, Nardini A, Assunta Lo Gullo M, Mosca R. **1999**. Refilling of Embolized Vessels in Young Stems of Laurel. Do We Need a New Paradigm? *Plant Physiology* **120**: 11–22.

Utsumi Y, Sano Y, Fujikawa S, Funada R, Ohtani J. **1998**. Visualization of Cavitated Vessels in Winter and Refilled Vessels in Spring in Diffuse-Porous Trees by Cryo-Scanning Electron Microscopy. *Plant Physiology* **117**: 1463–1471.

Wheeler JK, Huggett BA, Tofte AN, Rockwell FE, Holbrook NM. **2013**. Cutting xylem under tension or supersaturated with gas can generate PLC and the appearance of rapid recovery from embolism: Sampling induced embolism. *Plant, Cell & Environment* **36**: 1938–1949.

Yang S-J, Zhang Y-J, Sun M, Goldstein G, Cao K-F. **2012**. Recovery of diurnal depression of leaf hydraulic conductance in a subtropical woody bamboo species: embolism refilling by nocturnal root pressure. *Tree Physiology* **32**: 414–422.

Zwieniecki MA, Holbrook NM. **2009**. Confronting Maxwell's demon: biophysics of xylem embolism repair. *Trends in Plant Science* **14**: 530–534.

Zwieniecki MA, Melcher PJ, Ahrens E. **2013**. Analysis of spatial and temporal dynamics of xylem refilling in Acer rubrum L. using magnetic resonance imaging. *Frontiers in Plant Science* **4**.

Chapter 4: The role of hydraulic failure in a massive mangrove die off event

In prep as: Gauthey, A., Backes, D., Balland, J., Alam, R., Maher, D.T., Cernusak, L.A., Brendan Choat

4.1. Abstract

Between late 2015 and early 2016, more than 7000 ha of mangrove forest died along the coastline of the Gulf of Carpentaria, in northern Australia. This massive die-off was preceded by a strong 2015/2016 El Niño event, resulting in lower precipitation, a drop in sea level and higher than average temperatures in northern Australia. In this study, we investigated the role of hydraulic failure in the mortality and recovery of one of the most dominant species, *Avicennia marina*, two years after the mortality event. We measured predawn water potential (Ψ_{pd}) and percent loss of hydraulic conductivity (PLC) in surviving individuals across a gradient of impact. We also assessed the vulnerability to drought-induced embolism (Ψ_{50}) for the species. Areas with severe canopy dieback had higher native PLC (39%) than minimally impacted areas (6%), suggesting that hydraulic recovery was ongoing. The high resistance of *A. marina* to drought-induced embolism (Ψ_{50} = -9.6 MPa), indicates that severe water stress (Ψ_{pd} < -10 MPa) would have been required to cause mortality in this species. Our data indicate that severe water stress was a causal factor in the mass die-off event, with the formation of embolism leading to hydraulic failure and mortality in *A. marina*. It is likely that lowered sea levels and less frequent inundation by seawater, combined with lower inputs of fresh water,

high evaporative demand and high temperatures, led to the development of hyper-salinity and extreme water stress during the 2015/16 summer.

4.2. Introduction

To support photosynthesis, woody plants must extract water from the soil and transport it to the leaves. Water is transported through the xylem conduits under tension and is prone to cavitation, leading to the formation of gas emboli that block the conduits and reduce hydraulic conductivity. As drought intensifies, tension in the xylem increases, increasing the probability of cavitation. This phenomenon can eventually lead to systemic failure of the water transport system and death by hydraulic failure (McDowell et al., 2008; Brodribb and Cochard, 2009). As a result, xylem vulnerability to cavitation, often represented as Ψ_{50} (i.e. water potential at which 50% of the xylem conductivity is lost), is considered to be an important component of drought tolerance in trees and the capacity of different plant species to survive during extreme drought events (Choat et al., 2012; Choat, 2013).

Many woody ecosystems are already highly vulnerable due to changes in land use and climate change. In Australia, estuarine ecosystems and coastal wetlands, including mangroves and saltmarshes, are listed as one of the most vulnerable ecosystems (Laurance et al., 2011; Dixon et al., 2016). Their distribution is fragmented and narrow, making them more vulnerable to environmental stress that could lead to local extinctions (Duke et al., 2007; Laurance et al., 2011). Increased temperature and heatwaves frequency as well as reduced rainfall can raise the vapor pressure deficit (VPD) and contribute to higher rates of plant water loss through transpiration. Mangroves are highly responsive to VPD as maintaining high water use efficiency in saline environment is essential for their survival (Reef and Lovelock, 2015). Reduced rainfall can also limit water availability in groundwater and lead to local droughts, resulting in a decrease in mangrove survival and a reduced biomass (Mafi-Gholami et al., 2020).

From a physiological perspective, mangroves are fascinating, with a range of adaptations that allow them to grow in saline, anoxic substrates and cope with frequent tidal inundation (Ball, 1988a). An important consequence of growing in a high salinity substrate is having to overcome an enormous osmotic pressure gradient in order to extract water necessary for transpiration and growth. At the salinity of seawater, this pressure exceeds 2.5 MPa, which is physiologically equivalent to growth in extremely dry soils. Leaf water potential in mangroves is therefore consistently low, ranging from -2.7 to -5.7 MPa (Scholander, 1968). To cope with increased salinity, mangroves exclude and filter the salt in sea water. Some species secrete salt via salt glands situated at the leaf level, whereas others filter salt directly at the root level (Scholander, 1968; Tomlinson, 2016). Similarly to species living in xeric environment, mangroves are resistant to water-stress (e.g. Ψ_{50} ranging from -4 MPa to -8.5 MPa) and can tolerate low water potentials without experiencing significant cavitation (Melcher et al., 2001; Jiang et al., 2021). Thus, while mangroves are effectively exposed to continuous and extreme water stress, they form a highly productive ecosystem (Bouillon et al., 2008). However, despite adaptions to growth at low water potentials, mangrove species are still impacted by drought and salinity stress (Ball and Pidsley, 1995; Mafi-Gholami et al., 2020).

Mild or moderate drought events have been reported to reduce photosynthetic capacity of leaves (in *A. germinans*; Sobrado, 1999; Sobrado, 2006); increase salt secretion rates and decrease stomatal conductance (in *A. germinans*; Sobrado, 2002); lower growth rate (*Sonneratia alba*; Krauss et al., 2007); and cause a loss of canopy (*A. marina* and *Rhizophera mucronate*; Mafi-Gholami et al., 2017). While mangrove ecosystems are known for being resilient to short-term drought periods (Galeano et al., 2017; Andrieu et al., 2020; Mafi-Gholami et al., 2020), more extreme drought events have been associated with mass dieback of mangrove vegetation (Duke et al., 2017; Lovelock et al., 2017).

In the tropics, many drought events are related to El Niño Southern Oscillation (ENSO) anomalies, leading to extensive tree mortality (Rice et al., 2004). In North-East Australia, El Niño is responsible for short-term drops in sea level, increased temperatures and reduced rainfall, which play a crucial role in mangrove dieback (Duke et al., 2017; Galeano et al., 2017). During the El Niño event of 2015-2016, northeast Australia experienced persistent and extreme high temperatures as well as severe drought due to an unusually long dry season over the previous year and below average rainfall. These conditions were coincident with a massive dieback event in mangrove forests growing along the Gulf of Carpentaria coastline. Over 1000km of coastline was effected, with a total area of more than 7400 ha of mangrove forest impacted by dieback from late 2015 to early 2016 (Duke et al., 2017; Sippo et al., 2018). Another factor associated with the dieback was the extreme variation in sea level (20 - 30 cm lower) caused by weak winds and cool water (Hamlington et al., 2016; Harris et al., 2017). The drop in sea level affected tides, resulting in less inundation of upper areas of mangroves and increased water-stress. Although it is difficult to attribute direct causality for the dieback event, previous analyses of environmental data suggest that severe moisture deficit derived from high temperatures, low input of freshwater, and less frequent tidal inundation, was likely to be a central factor causing mass mortality of mangroves (Duke et al., 2017).

Mass dieback of mangroves associated with extreme heatwaves and drought suggests that there are hard limits to the level of water stress that mangroves can survive and that these limits may be more frequently encountered with increasing global temperatures and more extreme drought events (Duke et al., 2017). The dramatic El Niño event of 2015/16 provided a unique opportunity to study drought-induced mortality in mangrove species and evaluate hydraulic vulnerability and thresholds of mortality. Despite their exposure to drought and salinity stress, very few studies have investigated the vulnerability of xylem to embolism in mangrove species (Sperry et al., 1988; Tyree and Sperry, 1989; Melcher et al., 2001; Ewers et al., 2004) or the

role of hydraulic failure in mangrove dieback events. In this study, we focused on the dominant species found in the Gulf of Carpentaria, in north Queensland, *Avicennia marina,* in order to assess its vulnerability to water stress induced mortality. We determined Ψ_{50} using a non-invasive (optical technique) method and provided an estimation of the impact of drought on plants growing along a natural gradient of water-stress. As *A. marina* is a resilient species, we expected to find it to be particularly resistant to drought and that the dieback was caused by intense climatic events.

4.3. Materials and methods

Site and plant material

The study site was located in Karumba (Kuthant and Kurtjar countries), in the southern part of the Gulf of Carpentaria (north-west Queensland, Australia; 17° 28'S, 140° 48' E). This site was chosen because of the gradient of tree mortality from seaward to landward zones observed after the 2015-16 dieback event. Trees growing on the landward zone fringing the saltpan, approximately 250 m from the ocean edge, displayed high rates of mortality, while trees growing on the ocean front exhibited no sign of impact and green canopies (Duke et al., 2017; Sippo et al., 2020). While mortality was not explicitly assessed in this study, the impact gradient was clearly visible based on satellite images (Fig. 1; mortality data also available from http://wiki.auscover.net.au/wiki/Mangrove) and was also assessed by Sippo et al. (2020).

Avicenna marina (Forssk.) Vierh. var. *eucalyptifolia* (Zipp. ex Miq.) N. C. Duke, commonly known as the grey mangrove, is one of the most widely distributed mangrove species in the Gulf of Carpentaria, occurring between 30°N and 38°S (Duke, 1990). Its latitudinal range covers a wide spectrum of habitats, and its growth form is highly plastic, ranging from a shrub

(1-3m) to tall trees (5-10m) in the tropics. It has lanceolate glossy leaves with salt glands, and aerial roots (pneumatophores), which allow the plant to excrete salt from the sap and absorb oxygen, respectively.

Three transects were established from the saltpan to the oceanfront. Three zones were defined along these transects: severe impact (landward adjacent to saltpan, SI), intermediate impact (II) and minimal impact (seaward fringe, MI) (Fig. 4-1). The impact severity was directly related, and increased with, the distance of the trees from the waterfront. Trees from MI zone did not show any sign of visible past or present impact whereas trees from SI zone had more than 75% of their branch dead or heavily impacted. Trees from II zone had between 25% and 75% of their branch dead or impacted. All measurements were done in August 2018, two and a half years after the dieback event that occurred in the summer of 2015/2016. During these two years between the dieback event and sampling, annual precipitation for this region fluctuated (970mm in 2017 and 536mm in 2018), while mean annual temperatures (34°C in 2017 and 33.8°C in 2018) remained above the mean of the past 15 years (33.6°C) (data extracted from Australian Government Bureau of Meteorology, bom.gov.au).

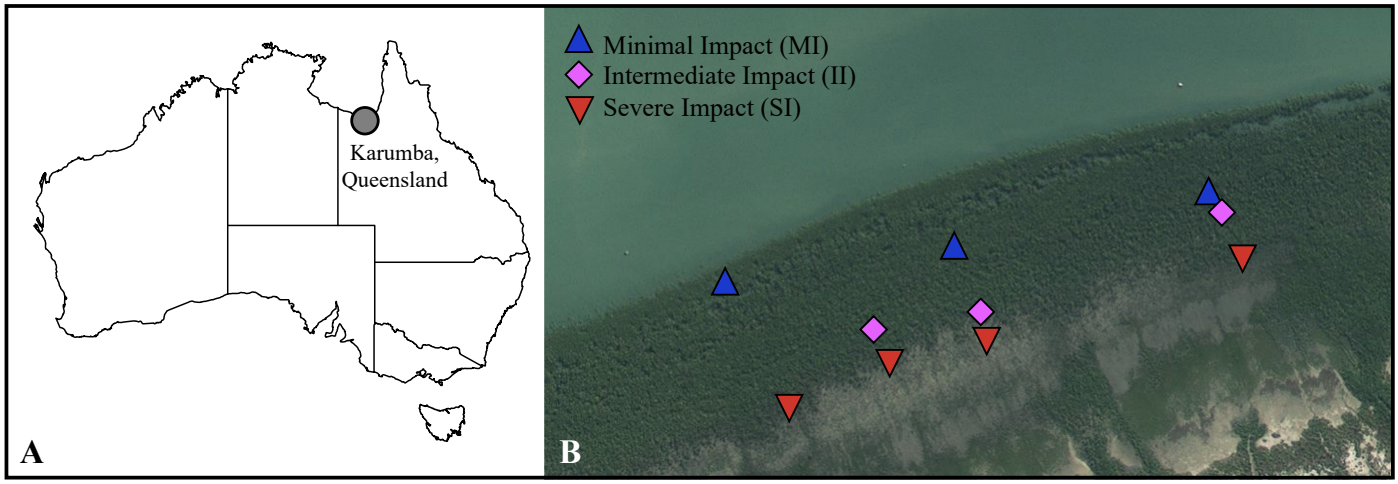

Figure 4-1 Map showing the field site in Queensland (A) and a detail of transects and sampling sites (B) (in blue sites with minimal impact, in magenta with intermediate impact and in red with severe impact). The satellite image was sourced from the Queensland Government (https://qldglobe.information.qld.gov.au/) and dated from 2018 (April to November 2018).

Native embolism

Three branches from different trees were collected per zone per transect (i.e. 30 branches total as an additional SI sampling point was added) for native embolism measurements. We harvested branches from adult trees (i.e. >2.5 m tall). Branches that were collected from SI and MI zones had part of their canopy damaged from the previous die-back event but also exhibited regrowth.

Branches over 1.5 m long (maximum vessel length ~ 20cm; from unpublished data) were collected prior to dawn to avoid hydraulic stress associated with the establishment of the transpiration stream occurring after sunrise. Branches were sealed in black plastic bags containing moist paper towels and transported to a temporary laboratory in Karumba. All measurements were undertaken within two hours after harvesting. One segment of approximately 10cm long per branch was measured (n=30).

Native embolism was assessed by measuring percent loss of conductivity (PLC) of each branch as:

$$PLC = \frac{K_{max} - K_{ini}}{K_{max}} \times 100$$

where K_{ini} is the initial hydraulic conductivity and K_{max} is the maximum hydraulic conductivity (both, kg s^{-1} m^{-1} MPa^{-1}).

Segments of the branches were cut under water and left with the cut end submerged for approximately 20 min in order to release xylem tension and avoid introducing gas bubbles into the segment while cutting (Wheeler et al., 2013). The initial hydraulic conductivity (K_{ini}) was measured by connecting the sample to a perfusing solution (deionised water and 20 mM NaCl)

and attached to a flow meter (LiquiFlow L13-AAD-11-K-10S; Bronkhorst High-Tech B.V., Ruurlo, the Netherlands). The maximum hydraulic conductivity was obtained by measuring the same sample after it was flushed. Flushing was carried out using a syringe filled with degassed perfusing solution that was pressurized using a calking gun. Segments were flushed at a pressure of ~ 100 kPa until K_{max} measurements showed no further increase in conductivity (minimum of 20 minutes).

Predawn water potential

For each native embolism value (i.e. for each branch), predawn stem water potential (Ψ_{pd}) was measured and averaged on 2 to 3 leaves. Measurements were conducted using a Scholander pressure chamber (PMS Instrument Company, Albany, OR, USA). Branches were kept in plastic bags for at least 1h before measurements, to ensure that leaf and stem water potential were equilibrated.

Vulnerability curve

Five healthy-looking branches (i.e. full canopy with intact green leaves) were collected for the vulnerability curve (VC). In order to avoid measuring branches with high native embolism that would yield misleading results (i.e. curves shifted towards more negative water potentials), branches were only collected from MI zones. Branches (~1.5m long) were harvested at predawn from adult trees and measured. The VC was obtained using the optical vulnerability technique (Brodribb et al., 2017).

Segments ranging from 0.5 to 1.2 cm in diameter were selected for each branch and a small section of bark was carefully removed to expose the xylem. An 8-megapixel camera with a

magnified 20x lens and with light-emitting diodes (LEDs) was placed on the bare xylem and a Raspberry Pi board computer (Raspberry Pi Foundation, http://www.raspberrypi.org) was set to take pictures every 10 minutes. A PSY1 Stem Psychrometer sensor coupled with a microvolt data logger (ICT International**,** Armidale, NSW, Australia) was used to automatically log measurements of xylem water potential (Ψ_x) during dry down. The psychrometer was set up on the base of the stem, at least 40 cm apart from the camera in order to minimise the effect of its installation. Bark was removed gently, and the xylem washed with Milli-Q (deionised and filtered water). Once the sensor was installed on the xylem, it was wrapped with parafilm to seal the chamber. Measurements were taken every 10 minutes to match the camera settings.

Samples were left to dry under plastic bags, in order to limit excessive transpiration, until no embolism events were observed for at least 10 hours. Images were downloaded and analysed using ImageJ (Schneider et al., 2012) following established protocols (https://github.com/OpenSourceOV). After image subtraction, embolism events were clearly revealed, and the area of embolism was calculated for each sample. The percentage of embolism, or percentage of loss of area, was determined as:

$$\%\ loss\ of\ area = \frac{A_{cav}}{A_{max}} \times 100$$

where A_{cav} is the cumulative area of cavitated xylem at time t and A_{max} is the maximum area of cavitated xylem at the end of each sample dehydration.

Each embolism event was coupled with water potential measurements, and vulnerability curves were obtained for every sample (n=5).

Data analysis

For native embolism, results of PLC and Ψ_{pd} were averaged for each zone (SI, II and MI). After testing for normality, we tested for variation in PLC and Ψ_{pd} among zones with one-way analysis of variance (ANOVA).

Vulnerability curves were fitted to a Weibull function using the fitplc package (Duursma and Choat, 2017) with branch incorporated as a random effect as the OV technique allows a series of repeated measurements on a single individual. Points of interest (Ψ_{12}, Ψ_{50} and Ψ_{88}; i.e. water potential corresponding to 12, 50 and 88% of embolism, respectively) and their 95% confidence intervals were extracted from the VC using a standard profiling method.

All statistical analyses were conducted with R 3.1.2 (R Core Team, 2017) using RStudio (RStudio Team, 2015).

4.4. Results

Native embolism

Predawn water potential differed significantly between sites SI (-7.5 MPa ± 0.2), II (-5.6 MPa ± 0.5) and MI (-3.4 MPa ± 0.6) (all *p-values* < 0.05). While Ψ_{pd} values were highly variable at the MI sites (-0.45 to -5.7 MPa), Ψ_{pd} on the SI sites was less variable (-5.65 to -8.2 MPa) but indicated a high degree of plant water stress.

PLC significantly differed between SI (38.8% ± 9.6) and MI sites (5.9% ± 3.1) (*p-value* = 0.01), but not with II sites (16.2% ± 7.8). On SI sites, PLC values were distributed in a wide range (0 to 89.4%), whereas the distribution of the PLC values on MI sites was narrower (0 to 27.8%) and indicated less hydraulic stress (Fig. 4-2).

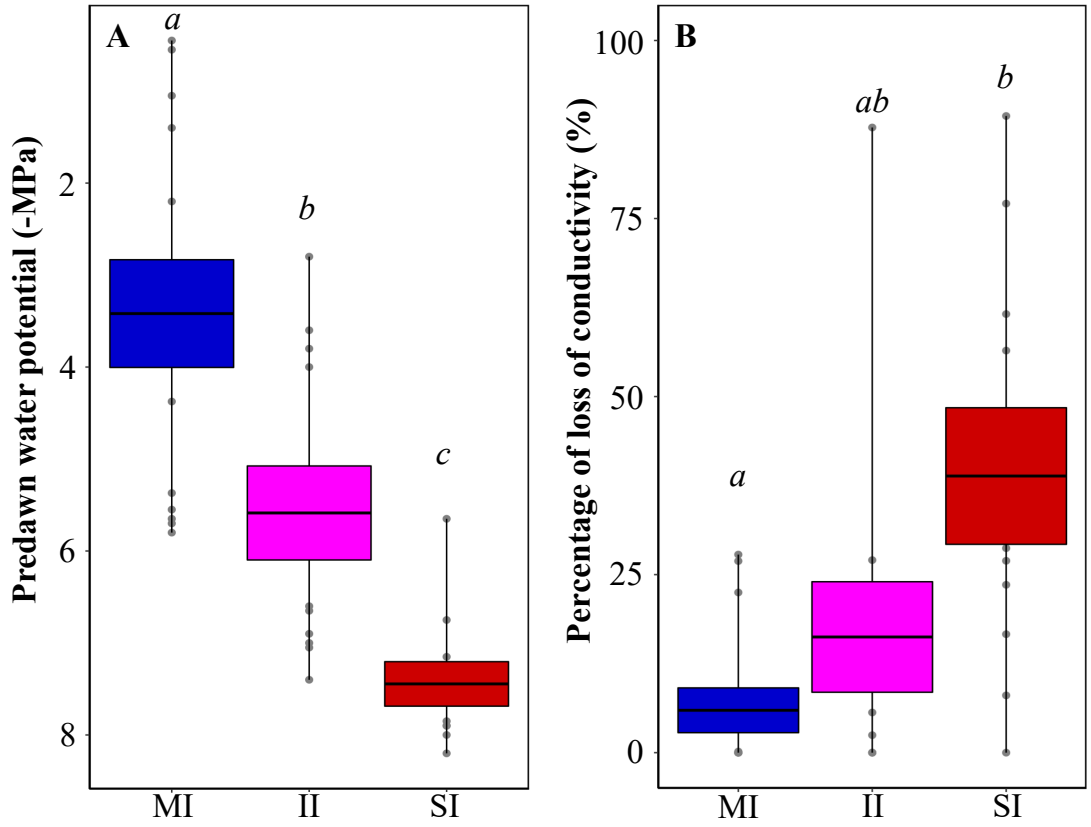

Figure 4-2 Effect of the degree of impact (MI minimal impact, II intermediate impact and SI severe impact) on predawn water potential (-MPa) (A) and percentage loss of area (B). The black horizontal lines represent the means and the edges of the boxes represent the standard errors. Whiskers extend to the maximum and minimum values and dark grey dots represent single measurements. Letters indicate significant differences from the ANOVA (*p-value* < 0.05) between the sites.

Vulnerability curves

A. marina trees from the MI zone exhibited low vulnerability to embolism (Ψ_{12} -8.87 ± 0.93 MPa; Ψ_{50} -9.59 ± 1.02 MPa; and Ψ_{88} -10.1 ± 1.71 MPa) (Fig. 4-3), indicating a capacity to withstand extremely low water potentials.

Figure 4-3 Vulnerability curve (VC) from *A. marina* trees sampled on the sites of minimal impact showing the percentage of loss of area (PLA, %) against the water potential (Ψ_x, -MPa). The average VC (blue) was built from 5 individual VCs (black). The vertical line shows Ψ_{50} and the dotted lines the intervals of confidence (95%).

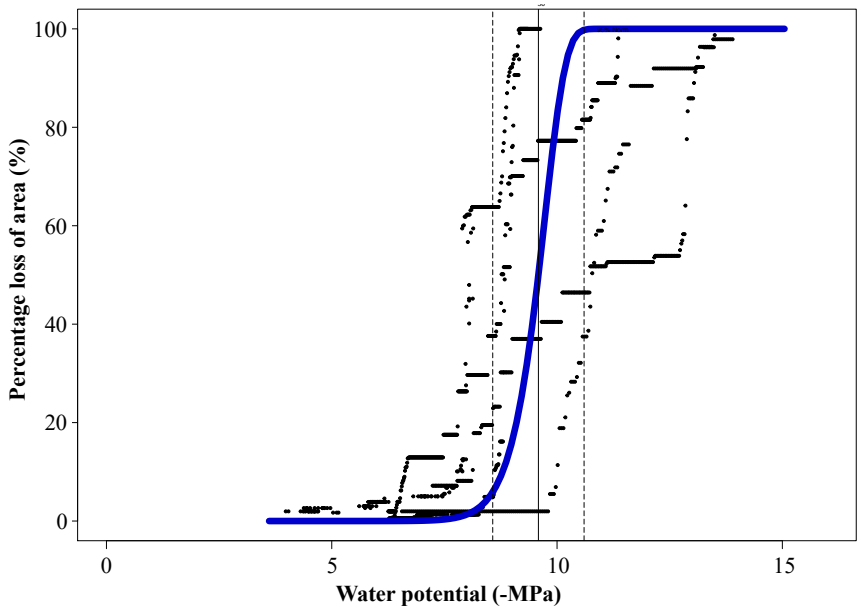

Comparison of native embolism and Ψ_{pd} with the vulnerability curve (Fig. 4) provided a good opportunity to study hydraulic thresholds that were reached by *A. marina* on each impact zones. Although, the average Ψ_{pd} for SI sites was very low at the time of measurements (Aug. 2018), when compared to the VC, mean values of Ψ_{pd} for SI sites (-7.5 MPa ± 0.2) were just under the onset of cavitation (on VC, embolism starts at ~ -7.1 MPa), thus causing minimal cavitation. Due to intraspecies variation, it should be noted that some individuals collected to build the VC started embolising before this water potential (Fig. 4-3) and therefore low Ψ_{pd} on SI sites could potentially cause embolism up to 13% in these individuals. The maximum native PLC measured at the time of the experiment (~89%) corresponded to a Ψ_x of ~-10 MPa on the VC (Fig. 4-4).

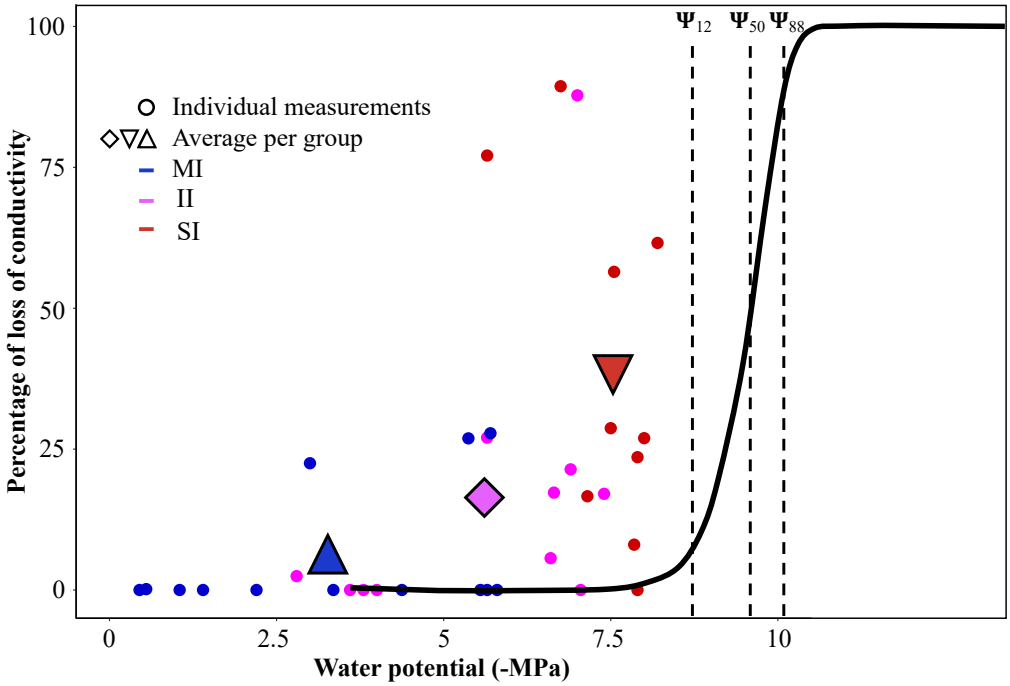

Figure 4-4 Native embolism measurements with percent loss of conductivity as a function of the water potential in branches sampled at sites of different impact (blue minimal impact, magenta intermediate impact and red severe impact). The black sigmoidal curve represents the VC. Points represent an individual measure; triangles and diamond are the average of these points for each impact class. The dotted lines represent, from left to right, values of Ψ_{12}, Ψ_{50}, Ψ_{88}, extracted from the VC.

4.5. Discussion

Mangroves growing adjacent to the saltpan (SI) exhibited higher values of native embolism (PLC) and lower predawn water potentials compared to mangroves growing on the seaward fringe (MI) (Fig. 4-2), indicating that SI individuals were more water-stressed than MI individuals. The vulnerability curve for *A. marina* (Fig. 4-3) exhibited low values of Ψ_{50}, suggesting that this species was highly resistant to drought-induced embolism. We propose that the high PLC observed in SI plants was caused by severe water-deficit and high VPD associated with the previous intense climatic event (i.e. El-Niño). The high resistance to drought induced

embolism observed for this *A. marina* population, indicates that extreme levels of water stress would have been required to cause hydraulic failure in these plants. It is likely that individuals growing furthest from the waterfront and adjacent to the salt pan would have been subjected the highest levels of water stress during this time due to the development of hyper salinity in the soil.

The strong El-Niño event of 2015 resulted in local drops of sea level and high temperatures, leading to increased soil porewater salinity while lower rainfall resulted in an absence of flushing of the substrate with fresh water and lower groundwater availability (Lovelock et al., 2017; Wang et al., 2020). Consequently, mangroves experienced increased salinity, extreme soil water stress as well as high VPD.

Significant differences in native embolism in *A. marina* along a transect of water-stress, approximately three years after the ENSO event, suggest that hydraulic failure played a central role in the dieback in 2015 in the Gulf of Carpentaria. Due to their distance to the waterfront, individuals that were found on the saltpan (SI) were expected to encounter higher water and salinity stress than individuals found on the oceanfront (MI). However, the difference in native embolism could not be explained by these gradients. Although SI individuals experienced very low water potentials, even prior to dawn, this level of water stress (~ -7.5 MPa), was not sufficient to cause significant cavitation, with vulnerability curves showing that embolism started at a mean Ψ_x of -7.1 MPa. However, SI individuals exhibited high native embolism values (mean ~ 40% PLC) that corresponded to water potentials close to -8.6MPa, with the highest native embolism values corresponding to a water potential of -10MPa (maximum native PLC was 89%). This indicates that the high PLC values measured in SI individuals were likely caused by drought rather than by the normal range of water stress that the plants are exposed to. Therefore, the native embolism measured, and impact on surviving individuals observed, would most likely have been caused by a previous stress event such as the strong ENSO that

caused the mangrove dieback in 2015-2016. While the natural gradient may have accentuated the effect of this event, it was not the cause of the high embolism values measured in this study. In contrast, *A. marina* growing on the oceanfront (MI) experienced minimal stress as indicated by the high-water potential and low native embolism.

The Ψ_{50} of *A. marina* was estimated at -9.6 MPa, with no embolism formation detected before -7.1 MPa (from the average VC). Low Ψ_{50} is correlated with high resistance to drought (Blackman et al., 2010; Corcuera et al., 2011; Nardini and Luglio, 2014) and often found in species growing in water limited environment (Nardini and Luglio, 2014; Trueba et al., 2017; Oliveira et al., 2019). *A. marina* is widely distributed in tropical and sub-tropical Oceania, and able to grow in areas with contrasting frequency of inundation, solar irradiation and rainfall patterns. *A. marina* is also known to be tolerant to changes in salinity (Ball, 1988b). While high concentrations of salt often negatively impact the plant by reducing photosynthesis (Li et al., 2008), growth rate and stomatal conductance (Parida et al., 2004), *A. marina* can maintain constant water use efficiency with increasing salinity by reducing water loss in proportion to photosynthetic rate (Ball and Farquhar, 1984; Ball, 1988b; Patel et al., 2010). The high tolerance of *A. marina* to abiotic stresses and high adaptability to its environment (Dahdouh et al., 2004), in addition to a high variability of Ψ_{50} found across latitudinal gradient (Jiang et al., 2021), may therefore explain the low Ψ_{50} found in this region.

Our results are in agreement with previous studies showing that, among plant species, mangroves have been found to be relatively tolerant to drought-induced embolism (Sperry et al., 1988; Choat et al., 2012; Jiang et al., 2017; Zhu et al., 2018). Although *A. marina* was highly resistant to drought-induced embolism, the vulnerability curve exhibited a very steep slope after Ψ_x reached Ψ_{50}. The difference between Ψ_{50} and Ψ_{88} (0.51 MPa) was smaller than the

difference between Ψ_{50} and Ψ_{12} (0.72 MPa) indicating that the embolism spread accelerated after 50% of embolism was reached.

The comparison of native embolism measurements with the vulnerability curve provided insights regarding the thresholds reached during the 2015-16 drought. In order to estimate this threshold of survival, we focused on branches where native embolism was highest (over 75%, n=3). As previously mentioned, the native embolism measured in SI sites was most likely caused by hydraulic failure from a past stress event, rather than by baseline stress resulting from their location adjacent to the saltpan. While SI individuals experienced significantly greater water-stress than plants in II and MI plots, the Ψ_{pd} values were not low enough to generate the native embolism values measured here. These measurements were undertaken two years after the drought, so we assumed that the surviving individuals that were impacted by water stress would have recovered some proportion of xylem conductance lost during the 2016 dieback event. Recovery can occur by either refilled (Ewers et al., 2004; Schmitz et al., 2012) or growth of new functional vessels in order to restore hydraulic conductivity through the branch. We therefore assumed that PLC values measured two years after the event were lower than at the time of the mortality event. Based on this assumption, we speculated that mangroves reached values of embolism that exceeded 75% (i.e. highest native embolism measured in SI branches). Studies investigating thresholds for drought induced mortality in woody plants indicate that water potentials causing 88% of loss of conductivity are a point of no-return for angiosperm species (Choat, 2013; Urli et al., 2013; Delzon and Cochard, 2014; Anderegg et al., 2015). *A. marina* survives higher stress than most plants due to high resistance to drought-induced embolism (Ψ_{12}, Ψ_{50}) and tolerance of high levels of embolism (Ψ_{88}) before recovering. A higher resistance to drought-induced mortality would indicate that this species can endure extreme hydraulic stress.

In order to maintain a positive water balance, the leaf osmotic potential must be lower than the soil (Dixon and Joly, 1894). Despite this mechanism, some *A. marina* individuals in the seaward fringing plots experienced predawn water potentials higher than the water potential of the seawater (approximately -2.5 MPa). One explanation may be the existence of foliar water uptake during precipitation or when droplets of dew form on the leaves (Steppe et al., 2018). This phenomenon has been documented to improve leaf water status in a range of species and environments (Boucher et al., 1995; Yates and Hutley, 1995; Limm et al., 2009; Gerlein-Safdi et al., 2018). Mangrove species could also use foliar water uptake as a strategy to raise leaf water potential. The capacity of salt crystals located on the surface of the leaf to attract liquid and facilitate its entrance into the leaf has been discussed, although it seems unlikely due to the potential uptake of salty water through the stomata (Reef and Lovelock, 2015). However, *A. marina* is capable of taking up water from the leaf, which induces reverse sap flow through the plant and results in the restoration of favorable plant water balance and stem diameter growth (Steppe et al., 2018; Coopman et al., 2021). Leaf water uptake would also restore leaf hydraulic conductance and could help prevent hydraulic failure during drought (Fuenzalida et al., 2019; Coopman et al., 2021).

Mangroves growing on the saltpan were at a higher elevation (~1 m to 1.5 m) than those growing on the edge of the water (Sippo et al., 2020) and this difference in elevation may partly drive the difference in water availability along the transect. With the drop in sea level and lower rainfall observed during El Niño, it is possible that the soil water in SI areas was not sufficient to meet demand of water by these trees (Xia and Li, 2012; Sippo et al., 2020). Differences in native embolism through this gradient suggest that drought-induced mortality, enhanced by the effects of El Niño, was driven by hydraulic failure. With low sea level and low rainfall, the geochemistry of the sediment was also observed to change from reducing to oxidising ions such as iron (Fe). Fe levels in mangrove wood were reported being 30 to 90 higher in dead mangroves

than baseline Fe (prior dieback) (Sippo et al., 2020). Although *A. marina* may tolerate high concentrations of Fe (Johnston et al., 2016), Fe toxicity may still contribute to mangrove mortality during this event (Sippo et al., 2020). As changes in sediment biogeochemistry and drought were concomitant, it is possible that low water availability and Fe toxicity both contributed to the *A. marina* dieback.

Conclusion

Mangrove species are found in tropical and estuarine regions, so they often face major climate disturbances. In this study, our results suggest that water stress and hydraulic failure may have played an important role into the massive mangrove dieback that followed an intense El-Niño event. The impact was more important on trees that were growing further from the seafront, suggesting that the degree of mortality was dependant from water accessibility location. Most mangrove trees show the ability to recover within a few years after an extreme climatic event (Sherman et al., 2001; Alongi, 2008; Long et al., 2016), although recovery speed and efficiency is different between species and sites (Snedaker et al., 1992; Imbert et al., 2000). Even though this species was highly resistant to drought-induced embolism, low predawn water potentials, found at high impact sites, indicated that individuals growing on the saltpan were constantly exposed to more water stress because the higher substrate salinity (compared to trees growing on the oceanfront). However, since these values could not explain the high PLC measured in some individuals, native embolism was considered a good marker to identify hydraulic failure from the drought event.

4.6. References

Alongi DM (2008) Mangrove forests: Resilience, protection from tsunamis, and responses to global climate change. Estuarine, Coastal and Shelf Science **76**: 1–13

Anderegg WRL, Flint A, Huang C, Flint L, Berry JA, Davis FW, Sperry JS, Field CB (2015) Tree mortality predicted from drought-induced vascular damage. Nature Geoscience **8**: 367–371

Andrieu J, Lombard F, Fall A, Thior M, Ba BD, Dieme BEA (2020) Botanical field-study and remote sensing to describe mangrove resilience in the Saloum Delta (Senegal) after 30 years of degradation narrative. Forest Ecology and Management **461**: 117963

Ball MC (1988a) Ecophysiology of mangroves. Trees **2**: 129–142

Ball MC (1988b) Salinity Tolerance in the Mangroves Aegiceras corniculatum and Avicennia marina. I. Water Use in Relation to Growth, Carbon Partitioning, and Salt Balance. Functional Plant Biology **15**: 447

Ball MC, Farquhar GD (1984) Photosynthetic and Stomatal Responses of Two Mangrove Species, *Aegiceras corniculatum* and *Avicennia marina* , to Long Term Salinity and Humidity Conditions. Plant Physiology **74**: 1–6

Ball MC, Pidsley SM (1995) Growth Responses to Salinity in Relation to Distribution of Two Mangrove Species, Sonneratia alba and S. lanceolata, in Northern Australia. Functional Ecology **9**: 77–85

Blackman CJ, Brodribb TJ, Jordan GJ (2010) Leaf hydraulic vulnerability is related to conduit dimensions and drought resistance across a diverse range of woody angiosperms. New Phytologist **188**: 1113–1123

Boucher J-F, Munson AD, Bernier PY (1995) Foliar absorption of dew influences shoot water potential and root growth in Pinus strobus seedlings. Tree Physiology **15**: 819–823

Bouillon S, Borges AV, Castañeda-Moya E, Diele K, Dittmar T, Duke NC, Kristensen E, Lee SY, Marchand C, Middelburg JJ, et al (2008) Mangrove production and carbon sinks: A revision of global budget estimates. Global Biogeochemical Cycles. doi: https://doi.org/10.1029/2007GB003052

Brodribb TJ, Carriqui M, Delzon S, Lucani C (2017) Optical Measurement of Stem Xylem Vulnerability. Plant Physiology **174**: 2054–2061

Brodribb TJ, Cochard H (2009) Hydraulic Failure Defines the Recovery and Point of Death in Water-Stressed Conifers. Plant Physiology **149**: 575–584

Choat B (2013) Predicting thresholds of drought-induced mortality in woody plant species. Tree Physiology **33**: 669–671

Choat B, Jansen S, Brodribb TJ, Cochard H, Delzon S, Bhaskar R, Bucci SJ, Feild TS, Gleason SM, Hacke UG, et al (2012) Global convergence in the vulnerability of forests to drought. Nature **491**: 752–755

Coopman RE, Nguyen HT, Mencuccini M, Oliveira RS, Sack L, Lovelock CE, Ball MC

(2021) Harvesting water from unsaturated atmospheres: deliquescence of salt secreted onto leaf surfaces drives reverse sap flow in a dominant arid climate mangrove, Avicennia marina. New Phytologist. doi: 10.1111/nph.17461

Corcuera L, Cochard H, Gil-Pelegrin E, Notivol E (2011) Phenotypic plasticity in mesic populations of Pinus pinaster improves resistance to xylem embolism (P50) under severe drought. Trees **25**: 1033–1042

Dahdouh F, Bondt RD, Abeysinghe PD, Kairo JG, Cannicci S, Triest L, Koedam N (2004) COMPARATIVE STUDY OF THE DISJUNCT ZONATION PATTERN OF THE GREY MANGROVE AVICENNIA MARINA (FORSK.) VIERH. IN GAZI BAY (KENYA). BULLETIN OF MARINE SCIENCE **74**: 16

Delzon S, Cochard H (2014) Recent advances in tree hydraulics highlight the ecological significance of the hydraulic safety margin. New Phytologist **203**: 355–358

Dixon HH, Joly J (1894) On the Ascent of Sap. [Abstract]. Proceedings of the Royal Society of London **57**: 3–5

Dixon MJR, Loh J, Davidson NC, Beltrame C, Freeman R, Walpole M (2016) Tracking global change in ecosystem area: The Wetland Extent Trends index. Biological Conservation **193**: 27–35

Duke NC (1990) Phenological Trends with Latitude in the Mangrove Tree Avicennia Marina. Journal of Ecology **78**: 113–133

Duke NC, Kovacs JM, Griffiths AD, Preece L, Hill DJE, van Oosterzee P, Mackenzie J, Morning HS, Burrows D (2017) Large-scale dieback of mangroves in Australia. Marine and Freshwater Research **68**: 1816

Duke NC, Meynecke J-O, Dittmann S, Ellison AM, Anger K, Berger U, Cannicci S, Diele K, Ewel KC, Field CD, et al (2007) A World Without Mangroves? Science **317**: 41b–42b

Duursma R, Choat B (2017) fitplc - an R package to fit hydraulic vulnerability curves. Journal of Plant Hydraulics **4**: 002

Ewers FW, Lopez-Portillo J, Angeles G, Fisher JB (2004) Hydraulic conductivity and embolism in the mangrove tree Laguncularia racemosa. Tree Physiology **24**: 1057–1062

Fuenzalida TI, Bryant CJ, Ovington LI, Yoon H-J, Oliveira RS, Sack L, Ball MC (2019) Shoot surface water uptake enables leaf hydraulic recovery in Avicennia marina. New Phytologist **224**: 1504–1511

Galeano A, Urrego LE, Botero V, Bernal G (2017) Mangrove resilience to climate extreme events in a Colombian Caribbean Island. Wetlands Ecol Manage **25**: 743–760

Gerlein-Safdi C, Gauthier PPG, Caylor KK (2018) Dew-induced transpiration suppression impacts the water and isotope balances of Colocasia leaves. Oecologia **187**: 1041–1051

Hamlington BD, Cheon SH, Thompson PR, Merrifield MA, Nerem RS, Leben RR, Kim K-Y (2016) An ongoing shift in Pacific Ocean sea level. Journal of Geophysical Research: Oceans **121**: 5084–5097

Harris T, Holbrook N, Duke N, Pearce K, Braganza K, Bindoff N (2017) Climate drivers

of the 2015 Gulf of Carpentaria mangrove dieback. 34

Imbert D, Rousteau A, Scherrer P (2000) Ecology of Mangrove Growth and Recovery in the Lesser Antilles: State of Knowledge and Basis for Restoration Projects. Restoration Ecology **8**: 230–236

Jiang G-F, Goodale UM, Liu Y-Y, Hao G-Y, Cao K-F (2017) Salt management strategy defines the stem and leaf hydraulic characteristics of six mangrove tree species. Tree Physiology **37**: 389–401

Jiang X, Choat B, Zhang Y-J, Guan X-Y, Shi W, Cao K-F (2021) Variation in Xylem Hydraulic Structure and Function of Two Mangrove Species across a Latitudinal Gradient in Eastern Australia. Water **13**: 850

Johnston SG, Morgan B, Burton ED (2016) Legacy impacts of acid sulfate soil runoff on mangrove sediments: Reactive iron accumulation, altered sulfur cycling and trace metal enrichment. Chemical Geology **427**: 43–53

Krauss KW, Keeland BD, Allen JA, Ewel KC, Johnson DJ (2007) Effects of Season, Rainfall, and Hydrogeomorphic Setting on Mangrove Tree Growth in Micronesia. Biotropica **39**: 161–170

Laurance WF, Dell B, Turton SM, Lawes MJ, Hutley LB, McCallum H, Dale P, Bird M, Hardy G, Prideaux G, et al (2011) The 10 Australian ecosystems most vulnerable to tipping points. Biological Conservation **144**: 1472–1480

Li N, Chen S, Zhou X, Li C, Shao J, Wang R, Fritz E, Hüttermann A, Polle A (2008) Effect of NaCl on photosynthesis, salt accumulation and ion compartmentation in two mangrove species, Kandelia candel and Bruguiera gymnorhiza. Aquatic Botany **88**: 303–310

Limm EB, Simonin KA, Bothman AG, Dawson TE (2009) Foliar water uptake: a common water acquisition strategy for plants of the redwood forest. Oecologia **161**: 449–459

Long J, Giri C, Primavera J, Trivedi M (2016) Damage and recovery assessment of the Philippines' mangroves following Super Typhoon Haiyan. Marine Pollution Bulletin **109**: 734–743

Lovelock CE, Feller IC, Reef R, Hickey S, Ball MC (2017) Mangrove dieback during fluctuating sea levels. Scientific Reports **7**: 1680

Mafi-Gholami D, Mahmoudi B, Zenner EK (2017) An analysis of the relationship between drought events and mangrove changes along the northern coasts of the Pe rsian Gulf and Oman Sea. Estuarine, Coastal and Shelf Science **199**: 141–151

Mafi-Gholami D, Zenner EK, Jaafari A (2020) Mangrove regional feedback to sea level rise and drought intensity at the end of the 21st century. Ecological Indicators **110**: 105972

McDowell N, Pockman WT, Allen CD, Breshears DD, Cobb N, Kolb T, Plaut J, Sperry J, West A, Williams DG, et al (2008) Mechanisms of plant survival and mortality during drought: why do some plants survive while others succumb to drought? New Phytologist **178**: 719–739

Meinzer FC, McCulloh KA (2013) Xylem recovery from drought-induced embolism: where is the hydraulic point of no return? Tree Physiology **33**: 331–334

Melcher PJ, Goldstein G, Meinzer FC, Yount DE, Jones TJ, Holbrook NM, Huang CX (2001) Water relations of coastal and estuarine Rhizophora mangle: xylem pressure potential and dynamics of embolism formation and repair. Oecologia **126**: 182–192

Nardini A, Luglio J (2014) Leaf hydraulic capacity and drought vulnerability: possible trade-offs and correlations with climate across three major biomes. Functional Ecology **28**: 810–818

Oliveira RS, Costa FRC, Baalen E van, Jonge A de, Bittencourt PR, Almanza Y, Barros F de V, Cordoba EC, Fagundes MV, Garcia S, et al (2019) Embolism resistance drives the distribution of Amazonian rainforest tree species along hydro-topographic gradients. New Phytologist **221**: 1457–1465

Parida AK, Das AB, Mittra B (2004) Effects of salt on growth, ion accumulation, photosynthesis and leaf anatomy of the mangrove, Bruguiera parviflora. Trees - Structure and Function **18**: 167–174

Patel NT, Gupta A, Pandey AN (2010) Salinity tolerance of Avicennia marina (Forssk.) Vierh. from Gujarat coasts of India. Aquatic Botany **93**: 9–16

R Core Team (2017) R: A language and environment for statistical computing. R Foundation for Statistical Computing, Vienna, Austria. URL https://www.R-project.org/.

Reef R, Lovelock CE (2015) Regulation of water balance in mangroves. Ann Bot **115**: 385–395

Rice KJ, Matzner SL, Byer W, Brown JR (2004) Patterns of tree dieback in Queensland, Australia: the importance of drought stress and the role of resistance to cavitation. Oecologia **139**: 190–198

RStudio Team (2015) RStudio: Integrated Development for R. RStudio, Inc., Boston, MA URL http://www.rstudio.com/.

Schmitz N, Egerton JJG, Lovelock CE, Ball MC (2012) Light-dependent maintenance of hydraulic function in mangrove branches: do xylary chloroplasts play a role in embolism repair? New Phytologist **195**: 40–46

Schneider CA, Rasband WS, Eliceiri KW (2012) NIH Image to ImageJ: 25 years of Image Analysis. Nat Methods **9**: 671–675

Scholander PF (1968) How Mangroves Desalinate Seawater. Physiologia Plantarum **21**: 251–261

Sherman RE, Fahey TJ, Martinez P (2001) Hurricane Impacts on a Mangrove Forest in the Dominican Republic: Damage Patterns and Early Recovery1. Biotropica **33**: 393–408

Sippo JZ, Lovelock CE, Santos IR, Sanders CJ, Maher DT (2018) Mangrove mortality in a changing climate: An overview. Estuarine, Coastal and Shelf Science **215**: 241–249

Sippo JZ, Santos IR, Sanders CJ, Gadd P, Hua Q, Lovelock CE, Santini NS, Johnston SG, Harada Y, Reithmeir G, et al (2020) Reconstructing extreme climatic and geochemical conditions during the largest natural mangrove dieback on record. Biogeosciences **17**: 4707–4726

Snedaker SC, Brown MS, Lahmann EJ, Araujo RJ (1992) Recovery of a Mixed-Species

Mangrove Forest in South Florida Following Canopy Removal. Journal of Coastal Research **8**: 919–925

Sobrado M (2002) Effect of drought on leaf gland secretion of the mangrove Avicennia germinans L. Trees **16**: 1–4

Sobrado MA (1999) Drought effects on photosynthesis of the mangrove, Avicennia germinans, under contrasting salinities. Trees **13**: 125–130

Sobrado MA (2006) Differential leaf gas exchange responses to salinity and drought in the mangrove tree Avicecennia germinans (Avicenniaceae). Revista de Biología Tropical **54**: 371–375

Sperry JS, Tyree MT, Donnelly JR (1988) Vulnerability of xylem to embolism in a mangrove vs an inland species of Rhizophoraceae. Physiologia Plantarum **74**: 276–283

Steppe K, Vandegehuchte MW, Van de Wal BAE, Hoste P, Guyot A, Lovelock CE, Lockington DA (2018) Direct uptake of canopy rainwater causes turgor-driven growth spurts in the mangrove Avicennia marina. Tree Physiology **38**: 979–991

Tomlinson PB (2016) The Botany of Mangroves. Cambridge University Press

Trueba S, Pouteau R, Lens F, Feild TS, Isnard S, Olson ME, Delzon S (2017) Vulnerability to xylem embolism as a major correlate of the environmental distribution of rain forest species on a tropical island. Plant, Cell & Environment **40**: 277–289

Tyree MT, Sperry JS (1989) Vulnerability of Xylem to Cavitation and Embolism. Annual Review of Plant Physiology and Plant Molecular Biology **40**: 19–36

Urli M, Porté AJ, Cochard H, Guengant Y, Burlett R, Delzon S (2013) Xylem embolism threshold for catastrophic hydraulic failure in angiosperm trees. Tree Physiol **33**: 672–683

Wang H, Krauss KW, Noe GB, Stagg CL, Swarzenski CM, Duberstein JA, Conner WH, DeAngelis DL (2020) Modeling Soil Porewater Salinity Response to Drought in Tidal Freshwater Forested Wetlands. Journal of Geophysical Research: Biogeosciences **125**: e2018JG004996

Wheeler JK, Huggett BA, Tofte AN, Rockwell FE, Holbrook NM (2013) Cutting xylem under tension or supersaturated with gas can generate PLC and the appearance of rapid recovery from embolism: Sampling induced embolism. Plant, Cell & Environment **36**: 1938–1949

Xia YQ, Li HL (2012) A combined field and modeling study of groundwater flow in a tidal marsh. Hydrol Earth Syst Sci **16**: 741–759

Yates D, Hutley L (1995) Foliar Uptake of Water by Wet Leaves of Sloanea woollsii, an Australian Subtropical Rainforest Tree. Australian Journal of Botany **43**: 157

Zhu S-D, Chen Y-J, Ye Q, He P-C, Liu H, Li R-H, Fu P-L, Jiang G-F, Cao K-F (2018) Leaf turgor loss point is correlated with drought tolerance and leaf carbon economics traits. Tree Physiol **38**: 658–663

Chapter 5: Summary and synthesis

Decades ago, the first report on human-induced warming was released, highlighting the dangerous effects of greenhouse gases on the global climate (Hansen *et al.*, 1988). Since then, an exponential number of studies have investigated the impact of climate change on biodiversity and the environment (Legagneux *et al.*, 2018). As a result, forests have become increasingly vulnerable to extreme climatic events associated with drier and warmer future climates (Allen *et al.*, 2010; Anderegg *et al.*, 2013). The physiological mechanisms underpinning mass forest mortality events associated with drought are still poorly understood, although there is now a consensus that hydraulic failure in plant vascular systems often play a central role where plants die from water stress (Dai, 2011; Adams *et al.*, 2017). This involves a breakdown in water transport through the xylem (i.e. conductive tissue) caused by the blockage of xylem conduits by gas emboli. As such, vulnerability to drought-induced embolism is widely used as a proxy to predict plant mortality under water stress.

The aim of this thesis was to investigate the consequences of drought stress and subsequent recovery across a range of native (and few non-native) Australian tree species. To do so, a key hydraulic trait (Ψ_{50}) was measured using 3 different techniques and compared across 7 species with different xylem anatomy (chapter 2), with the objective to assess the accuracy of non-destructive techniques to detect drought-induced embolism. These techniques were also utilised to examine drought recovery in *Eucalyptus saligna*, an important native tree species distributed in the Sydney basin (chapter 3). Finally, a mass forest mortality event associated with extreme weather provided an opportunity to study the underlying causes of plant mortality and recovery of a mangrove species, *Avicennia marina* (chapter 4).

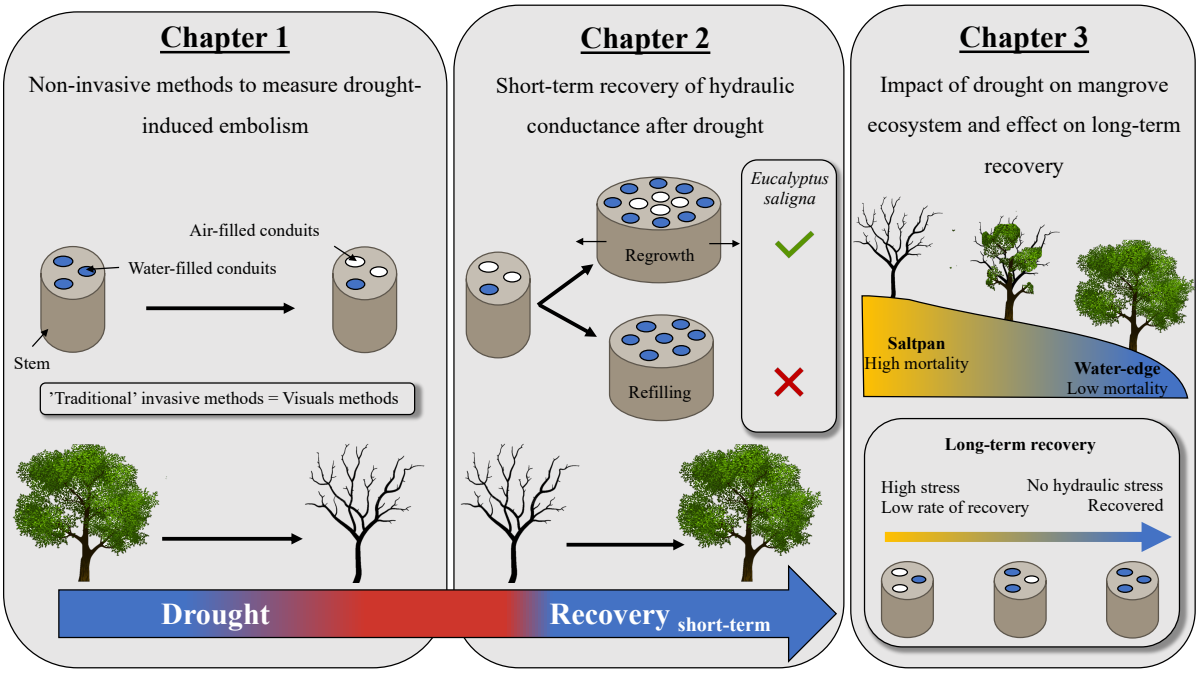

Figure 5- 1 Conceptual framework of the thesis highlighting the dynamics of xylem embolism during a cycle of drought and recovery. For each chapter, the context is presented, and the shaded boxes indicate the results.

5.1. Synthesis of experimental chapters

Non-destructive methods can be used to measure stress-induced embolism

The most common methods used to determine plant vulnerability to embolism require destructive sampling (Venturas *et al.*, 2017). As water in the xylem is transported in a metastable state, any disturbance to the water column can result in the introduction of gas bubbles (i.e. embolism). Drought often results in higher xylem tensions, leading to a greater probability of drought-induced embolism through air-seeding (Zimmermann, 2013). While this phenomenon can be limited for a certain amount of time via the closure of stomata (Domec *et al.*, 2004; Creek *et al.*, 2020) and the integrity of pit membranes (Choat *et al.*, 2008; Jansen *et al.*, 2009; Delzon *et al.*, 2010; Lens *et al.*, 2013), the spread of embolism through the xylem can lead to the complete disruption of the water transport pathway and can be fatal to the plant

(Choat, 2013). Therefore, excising stems or other plant parts in order to measure hydraulic conductivity may introduce air to the xylem and result in significant artefacts (Martin-StPaul *et al.*, 2014). Visual measurement techniques on intact plants have shown great promise as non-destructive assays of xylem vulnerability. They can also be used to resolve potential artefacts that afflict hydraulic techniques and the best manner in which these errors can be minimised. However, while visual methods can be applied non-destructively, they do not assess hydraulic conductivity directly, instead allowing quantification of embolised vessels (microCT) or of embolised area (OV), both referred to as PLV (percentage of loss of vessels), as a function of water stress. The indirect assessment of hydraulic conductivity using OV has led some authors to question the suitability of visual techniques to measurements of xylem embolism resistance.

In chapter 2, estimates of Ψ_{50} were not significantly different between hydraulic and visual methods across seven species. This suggests that while xylem network and complexity impact hydraulic conductivity, loss of vessels provide an accurate proxy to measure Ψ_{50}. These results were consistent with some previous studies (Brodribb *et al.*, 2017; Chen *et al.*, 2020) while contradicting others (Venturas *et al.*, 2019; Pratt *et al.*, 2019). The similarity between estimates of Ψ_{50} for visual and hydraulic methods observed in chapter 2 suggests that (a) errors associated with visual techniques in previous studies (presence of fluid filled, non-conductive vessels, (Pratt & Jacobsen, 2018), system level hydraulic resistance (Bouda *et al.*, 2019) or the possible damage of X-rays on the plants (Savi *et al.*, 2017)) were negligible, and (b) that hydraulic techniques can produce reliable data when the appropriate protocols are used according to species and xylem anatomical type. The differences between OV and invasive methods found by Venturas et al. (2019) and Pratt et al. (2019), could be due to imprecise implementation of the OV technique, such as the use of oil-based compounds to cover the xylem segment being observed.

The result of chapter 2 indicate that visual methods not only provide an accurate assessment of loss in xylem function associated with cavitation, but also offer advantages over hydraulic methods. MicroCT has been used to investigate xylem characteristics (e.g. vessel distribution and diameter), as well as a 3D reconstruction of the xylem that provided a more detailed picture of embolism dynamics in stems and roots (Peters *et al.*, 2020; Wason *et al.*, 2021). While both microCT and hydraulic techniques are able to detect native embolism (i.e. embolism formed before sampling), only microCT can provide the visualization of the location of this embolism as well as its possible repair (Cochard *et al.*, 2015; Choat *et al.*, 2015; Pratt *et al.*, 2020). On the other hand, the optical technique provides very high temporal resolution for development of embolism and a cost-effective method to investigate vulnerability segmentation across environmental gradients (Skelton *et al.*, 2018) or among organs (Rodriguez-Dominguez *et al.*, 2018).

Thus, we used microCT to investigate embolism dynamics through a cycle of drought and recovery (chapter 3). MicroCT was used to track embolism formation and the presence and/or absence of embolism repair in the same individual trees over a long period of time. It was essential to use this technique as it allowed the visualization of whether embolism repair was occurring, and how embolisms were distributed across treatments and in new and old xylem, during long-term recovery. In chapter 4, we used the OV technique which was more convenient for field-base study.

Embolism repair was not observed after drought

After experiencing water-stress, different recovery strategies can co-occur in many species. While two main strategies have been observed (i.e. embolism repair and regrowth of conductive tissue), the presence of embolism repair under negative pressure is still controversial (Sperry,

2013). The first response to drought is often related to the closure of stomata, as a protective role of the hydraulic system. Stomatal closure occurs before, or at the beginning of, embolism formation in plants (Martin-StPaul *et al.*, 2017; Hochberg *et al.*, 2017; Li *et al.*, 2019). Despite this preventive measure, embolism can spread inside the xylem quickly once xylem water potential reaches a critical threshold. While some plants can survive long periods of drought, it is still essential for them to recover from these events once water is restored.

In chapter 3, the first response of *E. saligna* to drought was a sharp decrease in water potential (Ψ) as well as a decline in the whole plant transpiration (E). These results suggested that mild and severe drought quickly led to stomata closure, delaying the formation of gas bubbles in the xylem. However, while mild drought did not lead to more than 20% PLV, severe drought increased PLV to approximately mortality thresholds (i.e. Ψ_{50}) (Hammond *et al.*, 2019). Leaf shedding under severe drought was likely used as a strategy to mitigate the effects of drought by minimizing any water loss that might otherwise occur from leaky stomata or cuticles (Wolfe *et al.*, 2016; Machado *et al.*, 2021).

Similar recovery strategies were observed under both types of drought. During short-time recovery (24h, 1 week or 3 weeks after rewatering), PLV did not change significantly, suggesting the absence of refilling, even under favourable conditions (low E, high water availability). Surprisingly, we observed that PLV seemed to increase slightly over time, rising to values almost three times higher (after 1 week for MD) than the ones measured at peak of the drought. This result, while unexpected, would explain the widespread forest mortality observed after a cycle of drought and rainfall, and often referred to as lagged mortality (Bigler *et al.*, 2007; Klockow *et al.*, 2018; Trugman *et al.*, 2018). This event might be due to the high amount of embolized vessels in the xylem. After a rainfall event and subsequent increased water availability, the transpiration stream is restored, but the risk of embolism spread might increase, even at lower tension.

After long-term recovery (6 months), overall PLV was found to decrease but was still high. An evaluation of the PLV in pre-drought and post-drought xylem rings showed that the new tissue, on the edge of the stem, was responsible for restoring the xylem hydraulic capacity of the plant. The older xylem was found to be almost entirely embolized, exhibiting values of PLV higher than the ones measured at the peak of the drought. The newly grown xylem tissue had PLV values that were significantly lower than those of the older xylem tissue; however, PLV values were higher than for previously measured well-water individuals. This could suggest that the presence of high numbers of embolized vessels, responsible for lagged mortality, could be a mechanism affecting long-term growth and repair in *E. saligna*.

While Choat et al. (2019) observed the accumulation of water droplets in embolized vessels of *E. saligna* after drought and rewatering, the absence of embolism repair and the slower restoration of the conductivity through the formation of new tissue suggested that refilling was not a routinely used mechanism in *E. saligna* during drought recovery. These findings agree with numerous studies that show that angiosperms are unable to refill following drought and rewatering (Cochard & Delzon, 2013; Choat *et al.*, 2015, 2019; Knipfer *et al.*, 2015).

Although recovery of hydraulic conductivity is essential for trees in order to survive after drought, the mechanisms of this recovery are not always well understood. Moreover, the mechanisms of recovery could also depend on the intensity and duration of water stress. While controlled experiments can help understand the mechanisms behind drought and recovery (chapter 3), it is often difficult to isolate these patterns of mortality in nature (chapter 4).

Drought and recovery in an extreme ecosystem

Climate change is responsible for the increased proportion and intensity of extreme climatic events (Harris *et al.*, 2018). Some natural phenomenon such as ENSO (El-Niño Southern

Oscillation) may become longer, driving more extreme events (drought, floods, hurricanes, fires) that are the principal causes of forest mortality (Granzow-de la Cerda *et al.*, 2012; Maza-Villalobos *et al.*, 2013; Duke *et al.*, 2017; Riascos *et al.*, 2018). With regards to drought-induced tree mortality, two interdependent physiological mechanisms have been proposed: carbon starvation and hydraulic failure (McDowell *et al.*, 2008). While the latter is explained by the increased xylem tension during drought, creation of embolism and disruption of the water transport pathway, the carbon starvation hypothesis proposes that stomatal closure following water stress would decrease uptake of carbon, leading to depletion of non-structural carbohydrates (NSC) and death (McDowell *et al.*, 2008). Since these two phenomena can happen concomitantly, they are difficult to separate. However, dying trees are often found with low conductivity but variable amounts of NSC (Adams *et al.*, 2017), and the threshold of mortality is often linked to water potential generating high values of PLC (Anderegg *et al.*, 2016), suggesting that hydraulic failure might be responsible for most of the forest dieback during drought.

In chapter 4, we investigated a massive mangrove die-off event in the Gulf of Carpentaria (QLD) which occurred in the summer of 2015/2016. In some areas, more dieback was observed on the saltpan than at the edge of the water, thus creating a natural gradient of impact. Even two years after the dieback occurred, native embolism and predawn water potential values measured in the dominant mangrove species, *A. marina*, varied across the gradient. Using the OV technique (chapter 2), *A. marina* was observed to be extremely resistant to drought-induced embolism, exhibiting a very low value of Ψ_{50} (-9.6 MPa). As expected, trees growing further from water were the most severely impacted, exhibiting PLC values close to mortality thresholds (i.e. Ψ_{88}). Some of these trees were also highly stressed, exhibiting predawn water potentials predicted to generate ~12% PLC. Previous studies indicate that mangrove species are relatively resistant to drought-induced embolism (Sperry *et al.*, 1988; Melcher *et al.*, 2001;

Ewers *et al.*, 2004; Jiang *et al.*, 2017), although Jiang et al. (2017) reported higher Ψ_{50} values for *A. marina* (-5.7 MPa). It was previously observed that the vulnerability of another mangrove species, *Rhizophora mangle*, was dependent on its zonal distribution, with estuarine (i.e. low salt content/less stress) trees exhibiting a higher Ψ_{50} than coastal individuals. This suggests that this species, as with many other tree species, are highly plastic, and morphological and physiological traits may depend on their environment. Therefore, it is possible that the low Ψ_{50} that we found in *A. marina* differed from that found by Jiang et al. (2017) because of plasticity in hydraulic traits.

The differences in PLC and Ψ, observed between coastal and inland *A. marina*, suggests that water was one of the main factors leading to this dieback. El-Niño caused a drop in sea level, a reduction in precipitation, and an increase in temperature, causing respectively, a decreased frequency of inundation, a reduced supply of fresh water, and higher VPD. Hence, mangroves growing on the saltpan were likely to have experienced severe water stress leading to hydraulic failure. While other factors may also have contributed to this dieback event (Sippo *et al.*, 2020), it is likely that water deficit and high evaporative demand were the main drivers of tree mortality. The high values of PLC found two years after the event also suggest that embolism repair via refilling was unlikely to have occurred in this species, consistent with our results for *E. saligna* found in chapter 3.

5.2. Conclusion and future directions

Observations of forest mortality may be accelerated by the effects of global climate change. With more extreme droughts, trees may be pushed closer to their vulnerability thresholds, given that hydraulic safety margins are already very narrow across the majority of forest biomes (Ψ_{min}-Ψ_{50}) (Choat *et al.*, 2012). Massive dieback events have been recorded in many regions

and ecosystems, generating shifts in vegetation (Gonzalez *et al.*, 2010) and longer recovery intervals (Hughes, 2003). It is therefore essential to understand the mechanisms underpinning the causes of such mortality and the dynamics of recovery, so that we can incorporate this knowledge into model-based systems to predict the future of our forests.

While species-specific vulnerability to embolism is a crucial trait to consider when assessing forest vulnerability, there is considerable debate over the reliability of different methodologies used to measure this trait. The results of this research showed that new imaging methods produce reliable estimates of species vulnerability parameters. Although some issues remain concerning their applicability to field-based studies (microCT) or the dynamics of stem embolism (OV), these techniques have the advantage, compared to flow-based techniques (BD, CA), that they can be used to measure vascular dysfunction in intact plants.

Assessment of recovery after drought is also essential in order to understand forest resilience. In many cases, lagged mortality is observed as a result of an intense event (Bigler *et al.*, 2007; Klockow *et al.*, 2018; Trugman *et al.*, 2018). Trees might die months later after intense drought even under unlimited water availability. While two non-exclusive mechanisms have been proposed to explain recovery of hydraulic capacity after drought (i.e. refilling and growth of new xylem), lagged mortality and embolism repair still require further study given the lack of long-term datasets. Our results, concentrating on one *Eucalyptus* species using microCT, adds to a growing body of evidence suggesting that embolism repair is not common. PLV values increased one week after restoration of water in the environment. The damage to vessels observed 6 months after rewatering suggests that lagged mortality could be due to a significant number of embolized vessels in the xylem, possibly leading to the expansion of embolisms at higher water potentials.

Specific mortality and recovery mechanisms are difficult to separate in the field as there are often many confounding variables. Even though controlled experimental work is essential to study mechanisms, *in-situ* studies are required to show that these mechanisms are important in mature trees exposed to natural drought. Chapter 4 followed the recovery of a mangrove forest, two years after an intense drought event, suggesting that, while this ecosystem is resilient, drought affected trees, which grew under stressed conditions. Although some gaps remain to be filled, the results of this research aimed to help resolve some issues that remain controversial.

The results presented in this study provide important advances in the field of plant hydraulics, specially concerning measurements of drought-induced embolism and investigation of the mechanisms of recovery. While this work contributes towards comprehending the causes that lead to massive dieback events, some gaps still exist and can restrict our understanding of mortality during drought stress. The methods investigated here focused on stem measurements of embolism. However, since hydraulic segmentation (i.e. difference in organ's vulnerability) can be an important strategy for drought resistance (Scholz *et al.*, 2014; Hochberg *et al.*, 2016; Zhang *et al.*, 2020), it may be essential to confirm if these imaging methods will generate accurate measurements on all plant organs, as tissues might differ anatomically. While these methods have been previously used to look at embolism dynamics in leaf midrib and secondary veins (Johnson *et al.*, 2018; Klepsch *et al.*, 2018; Losso *et al.*, 2019; Corso *et al.*, 2020; Petruzzellis *et al.*, 2020), roots and fine roots (Skelton *et al.*, 2017; Rodriguez-Dominguez *et al.*, 2018; Losso *et al.*, 2019; Peters *et al.*, 2020), the lack of comparison between techniques for these organs might induce erroneous results. This work also illuminated the potential mechanisms generating recovery of conductivity after drought. However, recovery mechanisms are known to be highly species-specific (Trifilò *et al.*, 2019) as well as environment-dependant (Zeppel *et al.*, 2019). Further work could extend the use of non-invasive techniques to investigate embolism repair, potential refilling, and long-term recovery to a larger number of

species. Finally, mechanisms leading to hydraulic failure and recovery might differ between *in-situ* and controlled conditions. Field studies are valuable, but events observed in the field are due to many uncontrolled factors, and difficult to separate from one another. Hence, there is an important role for controlled environment studies to provide insight into specific mechanisms and physiological processes that drive the observations in the field.

5.3. References

Adams HD, Zeppel MJB, Anderegg WRL, Hartmann H, Landhäusser SM, Tissue DT, Huxman TE, Hudson PJ, Franz TE, Allen CD, *et al.* 2017. A multi-species synthesis of physiological mechanisms in drought-induced tree mortality. *Nature Ecology & Evolution* **1**: 1285–1291.

Allen CD, Macalady AK, Chenchouni H, Bachelet D, McDowell N, Vennetier M, Kitzberger T, Rigling A, Breshears DD, Hogg EH (Ted), *et al.* 2010. A global overview of drought and heat-induced tree mortality reveals emerging climate change risks for forests. *Forest Ecology and Management* **259**: 660–684.

Anderegg WRL, Kane JM, Anderegg LDL. 2013. Consequences of widespread tree mortality triggered by drought and temperature stress. *Nature Climate Change* **3**: 30–36.

Anderegg WRL, Klein T, Bartlett M, Sack L, Pellegrini AFA, Choat B, Jansen S. 2016. Meta-analysis reveals that hydraulic traits explain cross-species patterns of drought-induced tree mortality across the globe. *Proceedings of the National Academy of Sciences* **113**: 5024–5029.

Bigler C, Gavin DG, Gunning C, Veblen TT. 2007. Drought induces lagged tree mortality in a subalpine forest in the Rocky Mountains. *Oikos* **116**: 1983–1994.

Bouda M, Windt CW, McElrone AJ, Brodersen CR. 2019. In vivo pressure gradient heterogeneity increases flow contribution of small diameter vessels in grapevine. *Nature Communications* **10**: 1–10.

Brodribb TJ, Carriqui M, Delzon S, Lucani C. 2017. Optical Measurement of Stem Xylem Vulnerability. *Plant Physiology* **174**: 2054–2061.

Chen Y-J, Maenpuen P, Zhang Y-J, Barai K, Katabuchi M, Gao H, Sasiwimol K, Tao L-B, Zhang J-L. 2020. Quantifing vulnerability to embolism in tropical trees and lianas using five methods: Can discrepancies be explained by xylem structural traits? *New Phytologist*.

Choat B. 2013. Predicting thresholds of drought-induced mortality in woody plant species. *Tree Physiology* **33**: 669–671.

Choat B, Brodersen CR, McElrone AJ. 2015. Synchrotron X-ray microtomography of xylem embolism in *Sequoia sempervirens* saplings during cycles of drought and recovery. *New Phytologist* **205**: 1095–1105.

Choat B, Cobb AR, Jansen S. 2008. Structure and function of bordered pits: new discoveries and impacts on whole-plant hydraulic function. *New Phytologist* **177**: 608–626.

Choat B, Jansen S, Brodribb TJ, Cochard H, Delzon S, Bhaskar R, Bucci SJ, Feild TS, Gleason SM, Hacke UG, *et al.* 2012. Global convergence in the vulnerability of forests to drought. *Nature* **491**: 752–755.

Choat B, Nolf M, Lopez R, Peters JMR, Carins-Murphy MR, Creek D, Brodribb TJ. 2019. Non-invasive imaging shows no evidence of embolism repair after drought in tree species of two genera. *Tree Physiology* **39**: 113–121.

Cochard H, Delzon S. 2013. Hydraulic failure and repair are not routine in trees. *Annals of*

Forest Science **70**: 659–661.

Cochard H, Delzon S, Badel E. **2015**. X-ray microtomography (micro-CT): a reference technology for high-resolution quantification of xylem embolism in trees: A reference method for xylem embolism. *Plant, Cell & Environment* **38**: 201–206.

Corso D, Delzon S, Lamarque LJ, Cochard H, Torres-Ruiz JM, King A, Brodribb T. **2020**. Neither xylem collapse, cavitation, or changing leaf conductance drive stomatal closure in wheat. *Plant, Cell & Environment* **43**: 854–865.

Creek D, Lamarque L, Torres-Ruiz JM, Parise C, Burlett R, Tissue D, Delzon S. **2020**. Xylem embolism in leaves does not occur with open stomata: evidence from direct observations using the optical visualisation technique. *Journal of experimental botany* **71**: 1151–1159.

Dai A. **2011**. Drought under global warming: a review: Drought under global warming. *Wiley Interdisciplinary Reviews: Climate Change* **2**: 45–65.

Delzon S, Douthe C, Sala A, Cochard H. **2010**. Mechanism of water-stress induced cavitation in conifers: bordered pit structure and function support the hypothesis of seal capillary-seeding. *Plant, Cell & Environment* **33**: 2101–2111.

Domec J-C, Warren J, Meinzer F, Brooks JR, Coulombe R. **2004**. Native root xylem embolism and stomatal closure in stands of Douglas-fir and ponderosa pine: Mitigation by hydraulic redistribution. *Oecologia* **141**: 7–16.

Duke NC, Kovacs JM, Griffiths AD, Preece L, Hill DJE, van Oosterzee P, Mackenzie J, Morning HS, Burrows D. **2017**. Large-scale dieback of mangroves in Australia. *Marine and Freshwater Research* **68**: 1816.

Ewers FW, Lopez-Portillo J, Angeles G, Fisher JB. **2004**. Hydraulic conductivity and embolism in the mangrove tree Laguncularia racemosa. *Tree Physiology* **24**: 1057–1062.

Gonzalez P, Neilson RP, Lenihan JM, Drapek RJ. **2010**. Global patterns in the vulnerability of ecosystems to vegetation shifts due to climate change. *Global Ecology and Biogeography* **19**: 755–768.

Granzow-de la Cerda Í, Lloret F, Ruiz JE, Vandermeer JH. **2012**. Tree mortality following ENSO-associated fires and drought in lowland rain forests of Eastern Nicaragua. *Forest Ecology and Management* **265**: 248–257.

Hammond WM, Yu K, Wilson LA, Will RE, Anderegg WRL, Adams HD. **2019**. Dead or dying? Quantifying the point of no return from hydraulic failure in drought-induced tree mortality. *New Phytologist* **223**: 1834–1843.

Hansen J, Fung I, Lacis A, Rind D, Lebedeff S, Ruedy R, Russell G, Stone P. **1988**. Global climate changes as forecast by Goddard Institute for Space Studies three-dimensional model. *Journal of Geophysical Research: Atmospheres* **93**: 9341–9364.

Harris RMB, Beaumont LJ, Vance TR, Tozer CR, Remenyi TA, Perkins-Kirkpatrick SE, Mitchell PJ, Nicotra AB, McGregor S, Andrew NR, *et al.* 2018. Biological responses to the press and pulse of climate trends and extreme events. *Nature Climate Change* **8**: 579–587.

Hochberg U, Albuquerque C, Rachmilevitch S, Cochard H, David-Schwartz R, Brodersen CR, McElrone A, Windt CW. **2016**. Grapevine petioles are more sensitive to drought induced

embolism than stems: evidence from *in vivo* MRI and microcomputed tomography observations of hydraulic vulnerability segmentation: Hydraulic vulnerability segmentation in grapevine. *Plant, Cell & Environment* **39**: 1886–1894.

Hochberg U, Windt CW, Ponomarenko A, Zhang Y-J, Gersony J, Rockwell FE, Holbrook NM. **2017**. Stomatal Closure, Basal Leaf Embolism, and Shedding Protect the Hydraulic Integrity of Grape Stems. *Plant Physiology* **174**: 764–775.

Hughes L. **2003**. Climate change and Australia: Trends, projections and impacts. *Austral Ecology* **28**: 423–443.

Jansen S, Choat B, Pletsers A. **2009**. Morphological variation of intervessel pit membranes and implications to xylem function in angiosperms. *American Journal of Botany* **96**: 409–419.

Jiang G-F, Goodale UM, Liu Y-Y, Hao G-Y, Cao K-F. **2017**. Salt management strategy defines the stem and leaf hydraulic characteristics of six mangrove tree species. *Tree Physiology* **37**: 389–401.

Johnson KM, Jordan GJ, Brodribb TJ. **2018**. Wheat leaves embolized by water stress do not recover function upon rewatering. *Plant, Cell & Environment* **41**: 2704–2714.

Klepsch M, Zhang Y, Kotowska MM, Lamarque LJ, Nolf M, Schuldt B, Torres-Ruiz JM, Qin D-W, Choat B, Delzon S, *et al.* 2018. Is xylem of angiosperm leaves less resistant to embolism than branches? Insights from microCT, hydraulics, and anatomy. *Journal of Experimental Botany* **69**: 5611–5623.

Klockow PA, Vogel JG, Edgar CB, Moore GW. **2018**. Lagged mortality among tree species four years after an exceptional drought in east Texas. *Ecosphere* **9**: e02455.

Knipfer T, Brodersen CR, Zedan A, Kluepfel DA, McElrone AJ. **2015**. Patterns of drought-induced embolism formation and spread in living walnut saplings visualized using X-ray microtomography. *Tree Physiology* **35**: 744–755.

Legagneux P, Casajus N, Cazelles K, Chevallier C, Chevrinais M, Guéry L, Jacquet C, Jaffré M, Naud M-J, Noisette F, *et al.* 2018. Our House Is Burning: Discrepancy in Climate Change vs. Biodiversity Coverage in the Media as Compared to Scientific Literature. *Frontiers in Ecology and Evolution* **5**.

Lens F, Tixier A, Cochard H, Sperry JS, Jansen S, Herbette S. **2013**. Embolism resistance as a key mechanism to understand adaptive plant strategies. *Current Opinion in Plant Biology* **16**: 287–292.

Li X, Smith R, Choat B, Tissue D. **2019**. Drought resistance of cotton (Gossypium hirsutum L.) is promoted by early stomatal closure and leaf shedding. *Functional Plant Biology* **47**.

Losso A, Bär A, Dämon B, Dullin C, Ganthaler A, Petruzzellis F, Savi T, Tromba G, Nardini A, Mayr S, *et al.* 2019. Insights from in vivo micro-CT analysis: testing the hydraulic vulnerability segmentation in *Acer pseudoplatanus* and *Fagus sylvatica* seedlings. *The New phytologist* **221**: 1831–1842.

Machado R, Loram-Lourenço L, Farnese FS, Alves RDFB, Sousa LF de, Silva FG, Filho SCV, Torres-Ruiz JM, Cochard H, Menezes-Silva PE. **2021**. Where do leaf water leaks come from? Trade-offs underlying the variability in minimum conductance across tropical savanna species with contrasting growth strategies. *New Phytologist* **229**: 1415–1430.

Martin-StPaul N, Delzon S, Cochard H. **2017**. Plant resistance to drought depends on timely stomatal closure. *Ecology Letters* **20**: 1437–1447.

Martin-StPaul NK, Longepierre D, Huc R, Delzon S, Burlett R, Joffre R, Rambal S, Cochard H. **2014**. How reliable are methods to assess xylem vulnerability to cavitation? The issue of 'open vessel' artifact in oaks. *Tree Physiology* **34**: 894–905.

Maza-Villalobos S, Poorter L, Martínez-Ramos M. **2013**. Effects of ENSO and Temporal Rainfall Variation on the Dynamics of Successional Communities in Old-Field Succession of a Tropical Dry Forest. *PLOS ONE* **8**: e82040.

McDowell N, Pockman WT, Allen CD, Breshears DD, Cobb N, Kolb T, Plaut J, Sperry J, West A, Williams DG, *et al.* 2008. Mechanisms of plant survival and mortality during drought: why do some plants survive while others succumb to drought? *New Phytologist* **178**: 719–739.

Melcher PJ, Goldstein G, Meinzer FC, Yount DE, Jones TJ, Holbrook NM, Huang CX. **2001**. Water relations of coastal and estuarine Rhizophora mangle: xylem pressure potential and dynamics of embolism formation and repair. *Oecologia* **126**: 182–192.

Peters JMR, Gauthey A, Lopez R, Carins-Murphy MR, Brodribb TJ, Choat B. **2020**. Non-invasive imaging reveals convergence in root and stem vulnerability to cavitation across five tree species (H Griffiths, Ed.). *Journal of Experimental Botany*.

Petruzzellis F, Tomasella M, Miotto A, Natale S, Trifilò P, Nardini A. **2020**. A Leaf Selfie: Using a Smartphone to Quantify Leaf Vulnerability to Hydraulic Dysfunction. *Plants* **9**: 234.

Pratt RB, Castro V, Fickle JC, Jacobsen AL. **2019**. Embolism resistance of different aged stems of a California oak species (Quercus douglasii): optical and microCT methods differ from the benchtop-dehydration standard (M Ball, Ed.). *Tree Physiology*.

Pratt RB, Castro V, Fickle JC, Madsen A, Jacobsen AL. **2020**. Factors controlling drought resistance in grapevine (Vitis vinifera, chardonnay): application of a new microCT method to assess functional embolism resistance. *American Journal of Botany* **107**: 618–627.

Pratt RB, Jacobsen AL. **2018**. Identifying which conduits are moving water in woody plants: a new HRCT-based method. *Tree Physiology* **38**: 1200–1212.

Riascos JM, Cantera JR, Blanco-Libreros JF. **2018**. Growth and mortality of mangrove seedlings in the wettest neotropical mangrove forests during ENSO: Implications for vulnerability to climate change. *Aquatic Botany* **147**: 34–42.

Rodriguez-Dominguez CM, Carins Murphy MR, Lucani C, Brodribb TJ. **2018**. Mapping xylem failure in disparate organs of whole plants reveals extreme resistance in olive roots. *New Phytologist* **218**: 1025–1035.

Savi T, Miotto A, Petruzzellis F, Losso A, Pacilè S, Tromba G, Mayr S, Nardini A. **2017**. Drought-induced embolism in stems of sunflower: A comparison of in vivo micro-CT observations and destructive hydraulic measurements. *Plant Physiology and Biochemistry* **120**: 24–29.

Scholz FG, Bucci SJ, Goldstein G. **2014**. Strong hydraulic segmentation and leaf senescence due to dehydration may trigger die-back in Nothofagus dombeyi under severe droughts: a comparison with the co-occurring Austrocedrus chilensis. *Trees* **28**: 1475–1487.

Sippo JZ, Santos IR, Sanders CJ, Gadd P, Hua Q, Lovelock CE, Santini NS, Johnston SG, Harada Y, Reithmeir G, *et al.* 2020. Reconstructing extreme climatic and geochemical conditions during the largest natural mangrove dieback on record. *Biogeosciences* **17**: 4707–4726.

Skelton RP, Brodribb TJ, Choat B. **2017**. Casting light on xylem vulnerability in an herbaceous species reveals a lack of segmentation. *New Phytologist* **214**: 561–569.

Skelton RP, Dawson TE, Thompson SE, Shen Y, Weitz AP, Ackerly D. **2018**. Low Vulnerability to Xylem Embolism in Leaves and Stems of North American Oaks. *Plant Physiology* **177**: 1066–1077.

Sperry J. **2013**. Cutting-edge research or cutting-edge artefact? An overdue control experiment complicates the xylem refilling story: Xylem-refilling artefacts. *Plant, Cell & Environment*: n/a-n/a.

Sperry JS, Tyree MT, Donnelly JR. **1988**. Vulnerability of xylem to embolism in a mangrove vs an inland species of Rhizophoraceae. *Physiologia Plantarum* **74**: 276–283.

Trifilò P, Kiorapostolou N, Petruzzellis F, Vitti S, Petit G, Lo Gullo MA, Nardini A, Casolo V. **2019**. Hydraulic recovery from xylem embolism in excised branches of twelve woody species: Relationships with parenchyma cells and non-structural carbohydrates. *Plant Physiology and Biochemistry* **139**: 513–520.

Trugman AT, Detto M, Bartlett MK, Medvigy D, Anderegg WRL, Schwalm C, Schaffer B, Pacala SW. **2018**. Tree carbon allocation explains forest drought-kill and recovery patterns. *Ecology Letters* **21**: 1552–1560.

Venturas MD, Pratt RB, Jacobsen AL, Castro V, Fickle JC, Hacke UG. **2019**. Direct comparison of four methods to construct xylem vulnerability curves: Differences among techniques are linked to vessel network characteristics. *Plant, Cell & Environment* **42**: 2422–2436.

Venturas MD, Sperry JS, Hacke UG. **2017**. Plant xylem hydraulics: What we understand, current research, and future challenges: Plant xylem hydraulics. *Journal of Integrative Plant Biology* **59**: 356–389.

Wason J, Bouda M, Lee EF, McElrone AJ, Phillips RJ, Shackel KA, Matthews MA, Brodersen C. **2021**. Xylem network connectivity and embolism spread in grapevine (Vitis vinifera L.). *Plant Physiology*.

Wolfe BT, Sperry JS, Kursar TA. **2016**. Does leaf shedding protect stems from cavitation during seasonal droughts? A test of the hydraulic fuse hypothesis. *New Phytologist* **212**: 1007–1018.

Zeppel MJB, Anderegg WRL, Adams HD, Hudson P, Cook A, Rumman R, Eamus D, Tissue DT, Pacala SW. **2019**. Embolism recovery strategies and nocturnal water loss across species influenced by biogeographic origin. *Ecology and Evolution* **9**: 5348–5361.

Zhang C, Wang M, Chen J, Gao X, Shao C, Lv Z, Jiao H, Xu H, Shen C. **2020**. Survival strategies based on the hydraulic vulnerability segmentation hypothesis, for the tea plant [Camellia sinensis(L.) O. Kuntze] in long-term drought stress condition. *Plant Physiology and Biochemistry* **156**: 484–493.

Zimmermann MH. **2013**. *Xylem Structure and the Ascent of Sap*. Springer Science & Business Media.